ABSTRACT

Title of Dissertation: HEAT TRANSFER AND PRESSURE DROP OF LIQUID COOLED OFFSET FIN HEAT EXCHANGERS

Sen Hu, Doctor of Philosophy, 1993

Dissertation directed by: Keith E. Herold
Assistant Professor
Department of Mechanical Engineering

An experimental and modeling study of heat transfer and pressure drop in liquid-cooled offset fin compact heat exchangers (cold plates) is described. Liquid coolants used in the testing are water and PAO (polyalphaolefin), for which the Prandtl number ranges from 3 to 150. Attention was focused on the Reynolds number range 10 - 2000 which spans most liquid cooled applications. From the data and from comparisons with previous air-cooled data, it was found that the Prandtl number has a significant effect on the Colburn factor of the offset fin geometry but little effect on the friction factor.

A numerical heat transfer analysis was performed to investigate the surface temperature distribution and uniformity of heat flux in the cold plates. The results demonstrate good agreement with surface temperature measurements. The model results were used to guide data reduction procedures. In particular, significant end effects are predicted. Through experience with the heat transfer model, these end effects were isolated. The numerical model predicts approximately uniform heat flux over the central section of the cold plates.

Predictive models were developed based on a surface contribution analysis of energy and momentum balances in a unit cell of the offset fin geometry. The Prandtl number effects on heat transfer can be viewed from two perspectives: fin perspective and array perspective. The fin perspective allows explanation of the Prandtl number dependence of the periodic fully developed Nusselt number. The array perspective is analogous to the usual thermal entry region in duct flow. Thermal development from the array perspective yields higher Nusselt numbers in the entry region. The surface contribution model shows significant Prandtl number effects on offset fin heat transfer performance. The models have estimated uncertainty of $\pm 20\%$. The models have been validated for heat transfer and pressure drop for Prandtl number ranging from 0.7 to 150 and Reynolds number from 10 - 2000.

HEAT TRANSFER AND PRESSURE DROP OF LIQUID COOLED OFFSET FIN HEAT EXCHANGERS

by

Sen Hu

Dissertation submitted to the Faculty of the Graduate School
of The University of Maryland in partial fulfillment
of the requirement for the degree of
Doctor of Philosophy
1993

Advisory Committee:

Assistant Professor Keith E. Herold, Chairman/Advisor
Associate Professor Michael Ohadi
Associate Professor Reinhard Radermacher
Associate Professor Tien-Mo Shih
Professor Theodore G. Smith

DEDICATION

To my parents

ACKNOWLEDGEMENTS

I would like to express my most sincere appreciation to Dr. Keith E. Herold, my research advisor, for his unfailing guidance and encouragement through the course of this work. I am also grateful for the cooperation of the committee members Dr. Michael M. Ohadi, Dr. Reinhard Radermacher, Dr Tien-Mo Shih and Dr. Theodore Smith.

I would like to express my deep gratitude to Miss Yuan Xu, my best friend and future wife, for her love, support and encouragement. I am also grateful to my family and all my friends for their constant support.

Finally, I would like to thank the Westinghouse Electric Corporation and the Grant-in Aid Program from the American Society of Heating, Refrigeration and Air-Conditioning Engineers for providing financial support for the project. Special appreciation is due to Dr. Frank Altoz and Mr. Rick Porter as grant monitors. I would also like to thank Dr. Dongsoo Jung and Dr. Michael Pecht for helping with the funding.

TABLE OF CONTENTS

LIST OF TABLES

LIST OF FIGURES

NOMENCLATURE

A : total heat transfer area in a unit cell, [m^2]
A_2 : heated area at bottom in a unit cell, $A_2=2l(s+t)$, [m^2]
A_B : leading or trailing edge area, $A_B = 2th$, [m^2]
A_c : front area of a unit cell, sh, [m^2]
A_f : frontal area of a unit cell, [m^2]
A_{fin} : fin area in a unit cell, [m^2]
A_P : fin side area, $A_P = 4lh$, [m^2]
A_T : top or bottom area, $A_T = 2ls$, [m^2]
C_D : form drag coefficient
c_P : specific heat, [J/kg-°C]
D_f : diameter of the flow channel inside the turbine flow meter, [m]
D_h : hydraulic diameter of offset fin, [m]
D_h^p : hydraulic diameter of parallel plates channel, $D_h^P=2h$, [m]
D_h^r : hydraulic diameter of rectangular duct, $D_h^r=(2sh)/(s+h)$, [m]
E : pumping power expended per unit area, [W/m^2]
f : average Fanning friction factor in offset strip fin
f_P : average Fanning friction factor on fin side
f_E : average Fanning friction factor on top and bottom surfaces
F_{unit} : total friction force in a unit cell, [N]
F_D : form drag force in a unit cell, [N]
F_E : friction force on top and bottom surfaces in a unit cell, [N]
F_h : specific heat transfer per unit temperature and per unit fin array volume, [W/m^3-°C]
F_f : pumping power expended per unit fin array volume, [W/m^2]
F_p : friction force on fin sides in a unit cell, [N]
F_α : modification factor of aspect ratio
g : acceleration gravity, [m/s^2]
Gr : Grashof number of in duct, $Gr=(g\beta_T(T_s-T_f)h^3)/\nu^2$
Gz : Graetz number of rectangular duct
h : fin height, [m]
h_0 : average heat transfer coefficient of fin array, [W/m^2-°C]
h_x : local unit average heat transfer coefficient of a unit cell, [W/m^2-°C]
h_P : heat transfer coefficient on fin sides, [W/m^2-°C]
h_E : heat transfer coefficient on top and bottom surfaces, [W/m^2-°C]
h_F : heat transfer coefficient on upstream fin end, [W/m^2-°C]
h_B : heat transfer coefficient on downstream fin end, [W/m^2-°C]
j : Colburn factor, $j=Nu_0/(RePr^{1/3})$
j^* : Colburn factor of experimental results (Brinkmann et al., 1987)
k : thermal conductivity of fluid, [W/m-°C]
k_A : thermal conductivity of the cold plate, [W/m-°C]

l : fin length, [m]
L : fin array length, [m]
L' : length of a unit cell, $L'=2l$, [m]
NTU : number of heat transfer unit of a heat exchanger
Nu_0 : average Nusselt number for a fin array, $Nu_0 = h_0 D_h/k$
Nu_x : local average Nusselt number of a unit cell, $Nu_x=h_x D_h/k$
$Nu_{x,E}$: Nusselt number on top and bottom surfaces, $Nu_E = h_E D_h^r/k$
Nu_F : Nusselt number of fin side in periodic fully developed thermal field
$Nu_{x,P}$: average Nusselt number of fin side in a unit cell at position x
Nu_x^p : local Nusselt number of parallel plates, $Nu_x^p=U_{1,x}D_h^p/k$
Nu^m_x : local Nusselt number of fin surface in thermal field development, modified from rectangular duct
Nu^r_F : fully developed Nusselt number in a rectangular duct
$Nu^r_{F,0.5}$: fully developed Nusselt number in a rectangular duct with aspect ratio of 0.5
ΔP : pressure drop across a unit cell, [Pa]
ΔP_{EE} : pressure drop due to entrance effects, [Pa]
ΔP_{EX} : pressure drop due to exit effects, [Pa]
ΔP_{FA} : pressure drop due to flow acceleration, [Pa]
ΔP_{FF} : pressure drop due to fin friction, [Pa]
ΔP_L : pressure drop of the fin array with length of L, [Pa]
Pr : Prandtl number of fluid
Pr_l : Prandtl number at fluid temperature
Pr_s : Prandtl number at surface temperature
q : heat flux, [W/m^2]
q_{conv} : heat flux of convective heat transfer, [W/m^2]
Q_{unit} : total heat transferred in a unit cell, [W]
Q_B : heat transferred on the leading and trailing ends of fins in a unit cell, [W]
Q_E : heat transferred on top and bottom surfaces in a unit cell, [W]
Q_P : heat transferred on fin sides in a unit cell, [W]
R : result parameter in the uncertainty analysis
Re^p : Reynolds number of parallel plates channel, $Re^p=uD_h^p/\nu$
Re^r : Reynolds number of rectangular duct, $Re^r=(uD_h^r/\upsilon)$
Re : Reynolds number based of offset fin, $Re=(uD_h/\upsilon)$
s : spacing between adjacent fins, [m]
t : fin thickness, [m]
ΔT_{lm} : log mean temperature difference of cold plate
T' : local temperature in cross section, [°C]
$T_{i,j}$: surface temperature at node (i,j), [°C]
T_s : average surface temperature in a unit cell, [°C]
T_f : average fluid temperature in a unit cell, [°C]
u : average fluid velocity in the area (sh), [m/s]
U : average overall heat transfer coefficient in a unit cell, [W/m^2-°C]
$U_{1,x}$: local unit average overall heat transfer coefficient of section I, [W/m^2-°C]

$U_{2,x}$: local unit average overall heat transfer coefficient of section II, [W/m^2-°C]
$U_{3,x}$: local unit average overall heat transfer coefficient of section III, [W/m^2-°C]
u' : local velocity in cross section, [m/s]
v : average fluid velocity in the area (s-t)h, [m/s]
w_R : relative uncertainty values for a parameter R
x : distance from the beginning of a fin array, [m]
x' : distance from the beginning of Section I (in Chapter 5), [m]
x^r : distance from the beginning of a rectangular duct, [m]
x^+_F : dimensionless hydraulic fin length
x_e : dimensionless hydraulic entrance length of a fin array, $x_e=x/(D_h^r\ Re^r)$
x^* : dimensionless thermal entry length for a fin array, $x^*=x/(D_h^r\ Re^r\ Pr)$
x^*_F : dimensionless thermal fin length
x^{P*} : dimensionless thermal entry length of parallel plates
x^{r*} : dimensionless thermal developing length for rectangular duct
$x^{r*}=x^r/(D_h^r\ Re^r\ Pr)$
X_{r1} : reduction factor of thermal boundary developing length on fins
X_{r2} : reduction factor of thermal field developing length on fin array

Greek

α : aspect ratio s/h
β : area density of heat transfer surface per unit volume of a fin array, m^2/m^3
β_T : thermal expansion coefficient
δ : t/l
γ : t/s
ρ : density of fluid, [kg/m^3]
ν : specific volume of fluid, [m^3/kg]
υ : kinematic viscosity of fluid, [m^2/s]
η : overall surface efficiency of one unit cell
η_{fin} : fin efficiency of unheated surfaces
η_P : fin efficiency of fin sides
η_F : fin efficiency of front and end surfaces of a fin
η_E : fin efficiency of top and bottom surfaces
τ_P : shear stress on fin side surface, [N/m^2]
τ_E : shear stress on top and bottom surfaces, [N/m^2]

CHAPTER 1

INTRODUCTION

Light-weight, space-saving and low cost features, make the compact heat exchanger widely used in some industrial applications. Compact heat exchangers have high "area density", typically from 700 m^2/m^3 up to 3300 m^2/m^3 (Shah and Webb, 1983). From comparison among many kinds of heat exchangers, brazed aluminum compact heat exchangers have lowest cost per unit area of heat transfer surface (Haselder, 1971). The result is that with the same volume or mass, compact heat exchangers have larger heat transfer surface area and higher heat transfer capability than regular heat exchangers, which make compact heat exchangers meet the requirements of many industrial situations, such as:

1) In electronic systems, highly-integrated semiconductor components can generate heat flux in the range 1-100 W/cm^2 and the heat generation from electronic chips is projected to continue growing (Bar-Cohen, 1985). To improve the reliability of microelectronic components and to allow further miniaturization, it is necessary to use compact heat exchangers for thermal management.

2) In cryogenic systems, where removal of heat at very low temperature is very difficult and expensive, there are stringent requirements for the heat exchangers to be compact to reduce the cost and the volume of fluid (Kern and Kraus, 1972).

3) In transportation systems, the small size and weight of compact heat exchangers can reduce the size and weight of the vehicles and improve their

performance.

4) In air conditioning systems, compact heat exchangers are preferred because of their good heat transfer performance and small size.

Compact heat exchangers usually employ fins as extended heat transfer surface. Typical fin geometries include plain fins, offset fins, perforated fins, wavy fins, pin fins and louvered fins (Norris and Spofford, 1942, Kays and London, 1984). High heat transfer coefficients are obtained from a combination of two effects: 1) larger heat transfer surface, 2) interrupted fin surfaces to disturb the flow. The performance should be evaluated not only by heat transfer, but also by pressure drop, heat transfer surface area and heat exchanger size. Shah (1978) summarized different methods to evaluate the performance of compact heat exchangers. The comparison methods were categorized as: 1) direct comparison of j and f values, referred to as "area goodness" by London (1964), 2) comparison of specific heat transfer as a function of fluid pumping power, called "volume goodness" by London and Ferguson (1949), 3) comparison with multiple constraints as proposed by Bergles et al. (1974), and 4) miscellaneous methods, some only applicable to special situations. For example, Larkin (1968) investigated the influence of $(\Delta P/P)/NTU$ on gas turbine cycle efficiency.

Cowell (1990) proposed an evaluation method based on transforming the performance calculation equations in different cases. These cases include: 1) comparison with fixed hydraulic diameter, 2) comparison with fixed frontal area of flow duct, 3) comparison with fixed heat exchanger volume, 4) comparison with fixed

pumping power and 5) comparison with fixed heat transfer. In the current study, the volume goodness method is used to reflect the practical tradeoff between the benefit of specific heat transfer versus the cost of pumping power. This method is used to compare the performance of different fin arrays in Chapter 6.

The offset fin geometry is one of the most commonly used fin geometries in industrial applications. In the current study, offset fins were used to construct seven compact heat exchangers, which are referred as cold plates in later discussions. Figure 1-1 is a schematic of the geometry of the offset fin, where l represents fin length, s represents fin spacing, t represents fin thickness, and h represent fin height. The fins used in the study are all symmetrical offset fins such that all the flow passages between fins have equal area. Multiple rows of offset fins are called a fin array.

Numerous studies have been published dealing with air cooled offset fin arrays, but very few publications describe studies using liquid coolants. Convective heat transfer coefficients of liquids are one or two orders of magnitude higher than that of air (Shah and Webb, 1983; Incropera and Dewitt, 1990). In electronic cooling applications, air cooling is limited to approximately 1 W/cm^2, and liquid cooling allows fluxes up to 20 W/cm^2 (Tuckerman, 1984) and higher. A key motivation of the work described here was to characterize offset fin performance with liquid coolants.

The objectives of the current study are listed as following:

1) To perform a series of heat transfer and pressure drop experiments to provide detailed data for liquid cooled applications of offset fin arrays and to understand the physics of these devices. The Prandtl number range of the liquid coolants covers from

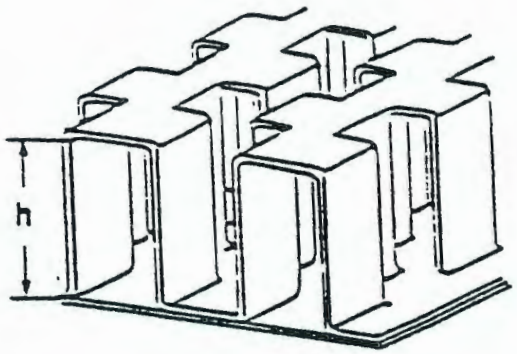

a. Perspective View

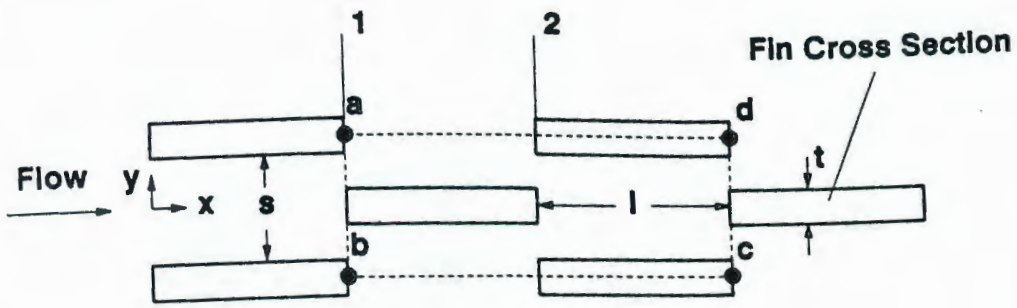

b. Cross Section View at Half Fin Height

Figure 1-1 Offset Fin Geometry

3 to 150.

2) To investigate whether air models can predict the Colburn factor in liquid applications and understand the Prandtl number effects on the Colburn factor of offset fin arrays.

3) To construct a surface contribution model to predict the heat transfer and pressure drop for offset fin arrays by considering the effects of Prandtl number and fin geometry.

4) To quantify the agreement of the surface contribution model results with experimental data.

5) To construct a numerical model to analyze the thermal spreading and end effects in the offset fin heat exchanger and evaluate their effects on the performance of offset fin arrays.

All the objectives have been accomplished during the project. In the dissertation, they are reported in the following order. Chapter 2 is a review of the research in the field of offset fin heat transfer studies, which are categorized by air-cooled research and liquid-cooled research. The liquid-cooled review includes both single-phase liquid studies and two-phase studies. Chapter 3 describes the experimental study of seven offset fin geometries using liquid coolants. The coolants, water and PAO (polyalphaolefin), have Prandtl number ranging from 3 to 150. Seven offset fin geometries were selected in order to examine geometry effects on the performance of cold plates using liquid coolants. Chapter 4 describes a laminar model to predict the heat transfer and friction factor of the offset fin geometry. The model is based on a

surface contribution approach, which models the heat transfer and friction of the fin array based on contributions from each of the surfaces in the fin structure. Chapter 5 describes a numerical conduction model used to analyze the distribution of heat flux and the surface temperatures along the heat transfer surface, which includes conduction in the heated section and end effects at the beginning and end of the heated section. Chapter 6 contains the key results of the effort. The experimental results are discussed and comparisons are made between experimental results and the models. One plate (Plate 1) had a scaling problem during testing, which led to falsely lower Colburn factor and higher friction factor. For the other six plates, the surface contribution model can predict 94% of Colburn factor and 90% of friction factor test data within a deviation of $\pm 20\%$. The comparison of Colburn factor between air and liquid demonstrates a significant Prandtl number effect on heat transfer performance. Chapter 7 summarizes the study and presents the conclusions.

CHAPTER 2

BACKGROUND

Offset fin geometry heat transfer studies have been published over the last forty years. Offset fins interrupt the boundary layer which forms on the fins, increasing the heat transfer performance of the cold plate and the pressure drop. Typical working fluids used in offset fin cold plates are air and heat transfer oils. The differences between these two types of fluids are significant but this fact has not been clearly acknowledged in the literature where the vast majority of the experimental and computational work is based on air.

2.1 Air-Cooled Offset Fin Research

Joshi and Webb (1987) and Manglik and Bergles (1990) reviewed the literature on the offset fin geometry and categorized all the past work into three approaches: empirical data and correlation; numerical and analytical solutions; qualitative observations. The following is an updated review on work done on offset fin structure, according to the three approaches.

2.1.1 Empirical Data and Correlation Studies

Numerous experimental studies using air are found in the literature. Kays (1960), Briggs and London (1961), London and Shah (1964), Mochizuki and Yagi (1977), and Dubrovsky and Vasiliev (1987) conducted experimental research on different compact offset fin geometries. Sparrow and Hajiloo (1980) performed mass

transfer testing using naphthalene sublimation to simulate heat transfer on three scaled-up offset fin arrays. Kays and London (1984) compiled experimental results of 21 offset fin arrays, which were then used as the experimental data resource for several correlation studies. Suzuki et al. (1985) conducted an experimental study on a scaled-up vertical offset fin array, where mixed convection occurred. Mochizuki et al. (1987) performed experiments on five scaled-up offset fin geometries. Joshi and Webb (1987) performed pressure drop tests on 8 scaled-up offset fin geometries. Most of the heat transfer experiments were performed with constant temperature heating, except the tests done by Dubrovsky and Vasiliev (1987), for which discrete constant power heating plates were used.

Many empirical correlations have been published based on Reynolds number and geometry ratios. Manson (1950) constructed the first correlations to predict heat transfer and pressure drop of offset fin arrays by considering the effect of Reynolds number, fin thickness ratio t/s and fin length ratio l/D_h^r. Compared with the experimental data from Norris and Spofford (1942), Joyner and Upshur (1943) and London and Ferguson (1949), "reasonable agreement" was claimed, but no specific accuracy was given. Wieting (1975) built an empirical correlation of Colburn factor, j, and Fanning friction factor, f, considering the effect of Reynolds number, the geometry ratios l/D_h^r and aspect ratio α. Compared with experimental data from Kays and London (1984), London and Shah (1968), London and Ferguson (1949) and Walters (1969), the Wieting correlation shows prediction within $\pm 10\%$ for Colburn factor and $\pm 15\%$ for friction factor. Later, Joshi and Webb (1987), Mochizuki et al.

(1987) and Dubrovsky and Vasiliev (1987) developed empirical correlations based on Reynolds number, α, l/D_h^r and t/D_h^r. Manglik and Bergles (1990) proposed empirical correlations, based on Reynolds number and three geometry ratios s/h, t/l, and t/s. Marr (1990) correlated the heat transfer of air-cooled offset fin arrays by Reynolds number, l/s and t/s. The agreement of his model with experimental data were within $\pm 20\%$. Two flow regimes were identified by these studies called laminar and nonlaminar flow, where j and f have different slopes versus Reynolds number.

2.1.2 Numerical and Analytical Studies

Kays (1972) proposed a simple analytical model for heat transfer and pressure drop. He considered the flow through an offset fin duct as similar to flow over a flat plate with velocity and temperature before each fin uniform. The Kays model does not show good prediction for heat transfer or pressure drop due, apparently, to the over-simplified assumptions. Sparrow et al. (1977) performed numerical calculations to analyze the heat transfer and pressure drop in offset fin arrays with the assumption of zero fin thickness and zero aspect ratio. They studied the temperature and velocity distribution on successive fins, which show the flow becomes periodic fully developed after a distance from the entrance of the fin array. The relationship between entrance length and Reynolds number is documented. Sparrow and Liu (1979) obtained numerical solutions considering the nonuniform velocity and temperature distribution before each fin due to the upstream fins. They employed infinite parallel plates to simulate the fin flow duct, ignoring the top and bottom surface influences.

Patankar and Prakash (1981) conducted a numerical investigation of offset fin

performance, considering finite fin thickness. They found that there are recirculation zones after fins, and the fin thickness causes higher pressure drop. Suzuki et al. (1985) conducted a numerical study on mixed convection in a vertical offset fin array concentrating on effects of fin thickness and free-stream turbulence. Joshi and Webb (1987) built a surface contribution model of heat transfer and pressure drop by considering the influence from every surface in a unit cell. They used results from Sparrow and Liu (1979) with modification for the aspect ratio. Compared with the experimental data from Kays and London (1984), the Joshi and Webb model predicts Colburn factor within $\pm 12\%$ and Fanning friction factor within $\pm 20\%$. Compared with their own experimental pressure drop data, the predictions were within $\pm 10\%$. Kelkar and Patankar (1989) studied the heat transfer, pressure drop and entrance length of the fin array, considering the effects of aspect ratio and fin length.

2.1.3 Flow Visualization Studies

Mullisen and Loehrke (1986) performed a flow visualization study on two scaled-up offset fin arrays using a Schlieren optical technique and they found that the flow becomes unsteady with increase of Reynolds number, but no specific critical Reynolds number is given. Mochizuki et al. (1988) studied vortex shedding and turbulence over staggered fins in a water channel using dye injection. They measured the turbulence intensity and pressure drop. Joshi and Webb (1987) also found a similar oscillation in the fin wake for Reynolds number larger than a critical number dependent on fin geometry. Xi et al. (1991) performed a flow visualization experiment for a five-row scaled-up offset fin array. They found that the flow becomes unsteady

and has a larger vortex generation frequency with larger Reynolds number and smaller geometry ratio s/l.

2.2 Liquid-Cooled Offset Fin Research

2.2.1 Studies of Single-Phase Liquid Cooling in Offset Fins

Compared to the work based on air, few studies have been published in liquid cooling applications. Robertson (1979) tested the heat transfer performance of an offset fin cold plate using liquid nitrogen with Prandtl number of 24. He found that there was no distinct laminar to turbulent transition and that the Colburn factor of liquids were different from that of air at the same Reynolds number. However, a detailed investigation on the Prandtl number effect was not performed. Brinkmann et al. (1988) conducted experiments on two offset fin arrays using water and dielectric fluorocarbon (FC-77), for which the Prandtl number ranges from 6 to 25. Each fin array had only 4 rows of offset fins and the thermal entrance effect on heat transfer is large. Colburn factors reported for this work are much higher than would be expected for a typical cold plate. Hou (1988) performed an experimental study on one offset fin array, using water and ethylene glycol, for which the Prandtl number ranges from 6 to 40. In the Hou study, there are 80 rows of fins in the fin array and thus the configuration is similar to the geometries considered in the present study. The cold plate was heated by constant heat flux with discrete heaters. Colburn factor, j, was found to be four times lower than what was found in the present study and the friction factor, f, is much higher than that found in the present study. One possible

explanation is mineral scale formation on the fins. In the present study, it was found that water scale formed on the fin surfaces when tap water was used. The mineral scale causes significant reduction in heat transfer and increases the pressure drop.

Marr (1990) proposed that heat transfer with a single-phase liquid can be predicted by modifying the air-cooled correlations to account for the Prandtl number effect. Marr proposed that a temperature-influenced Prandtl number factor in the form of $(Pr_l/Pr_s)^{0.25}$, where Pr_l and Pr_s are the Prandtl numbers at the liquid and surface temperatures, respectively. But no comparison between the model and experimental data is presented. An investigation of liquid coolants in an electronic cooling application was carried out by LeVasseur (1991). A SEM-E module (Standard Electronic Module - type E) was tested under 5 heating power levels and 4 flow rates, with water as the coolant. It was found that the water cooled SEM-E had significantly reduced junction temperatures, which can substantially improve the reliability of electronic components.

2.2.2 Studies of Liquid-Vapor Two-Phase Cooling in Offset Fins

Offset fins are also used in two-phase applications. Panitsidis et al. (1975) used a single-fin boiling analysis model to predict boiling inside an offset fin cold plate. From their experimental data with Freon-113, they found the single-fin model has encouraging agreement with 60% of the experimental data. However, the model results were lower than experimental data in some cases, apparently because the model was over-simplified. Robertson (1979, 1983) performed boiling tests with liquid nitrogen and Freon 11 on an aluminum offset fin cold plate. He classified the boiling

in the offset fin passage into laminar boiling and turbulent boiling heat transfer. Yung et al. (1980) numerically and experimentally studied the boiling heat transfer of ammonia in an aluminum offset fin cold plate. They built up an annular flow model for both evaporation analysis and condensation analysis by assuming that the liquid film on the fin was laminar flow and the vapor core was either laminar or turbulent. In both cases the fluid film and fins were treated separately. The model results for heat transfer coefficient are 12% higher than their experimental data.

Chen et al. (1981) modified the numerical model of Panitsidis et al. (1975) by considering the effect of velocity on heat transfer coefficient. The modified model shows better prediction of boiling heat transfer. Robertson (1982) proposed a film-flow model to analyze the experimental data of boiling with nitrogen and Freon 11. He made the assumption that the evaporating vapor-liquid mixture in a rectangular duct can be treated as a thin film of liquid flowing on the wall with vapor in the core. The correlation predicted the experimental data reasonably well, but no specific deviation was claimed. Chen and Westwater (1983) performed experiments with boiling R-113 in the offset fin geometry and constructed a model to predict heat transfer. The model is based on the local assumption, which means the local heat transfer coefficient is dependent only on the temperature difference between the metal-to-fluid temperature and the local fluid velocity.

2.3 Summary

In the current study, the liquid-cooled cold plate is investigated. Although two-phase cold plates have higher heat transfer coefficients, single-phase liquid cold plates have some advantages over two-phase cold plates, such as, lower pressure drop and smaller size. The two-phase studies are included for reference only. The studies of single-phase liquid cooling, described in section 2.2.1, are limited in scope and the mechanism of heat transfer and pressure drop dependence on fluid properties has not been fully developed. The current research is aimed at filling that gap by analyzing the Prandtl number effect on offset fin cold plate performance.

CHAPTER 3

EXPERIMENTAL STUDY

In the current research, an experimental facility has been constructed to conduct heat transfer and pressure drop testing using liquid coolants, which are water and PAO (polyalphaolefin). The system is designed to provide uniform heat flux on the test section. The measurement of heat transfer and pressure drop were performed on seven offset fin cold plates.

3.1 Experimental Facility

3.1.1 Test Section

The offset fin geometry, defined in Figure 1-1, is vacuum brazed into a cold plate assembly. The entire cold plate is made of aluminum manufactured to our specification. Aluminum has the properties of high thermal conductivity, high strength, light weight and low cost. Thus it is commonly used in the construction of cold plates. The fin array is manufactured by cold-chiseling a thin aluminum sheet to a specific fin geometry using rotating toothed dies. Seven different fin geometries were used in fabricating the cold plates tested in this effort. The fin geometry parameters, listed in Table 3-1, were selected to provide a range of fin thickness, fin length, fin height and fin spacing typical of liquid applications. The test sections used in the current study were designed to represent typical applications. The fabricated fin arrays were obtained from commercial vendors. Through inspection of the fin arrays,

Table 3-1 Cold Plate Fin Geometry

Cold Plate	Fin Thickness, t mm (inch)	Fin Length, l mm (inch)	Fin Height, h mm (inch)	Fin Spacing Distance, s mm (inch)
1	0.152 (0.006)	3.20 (0.126)	2.39 (0.094)	0.99 (0.039)
2	0.152 (0.006)	3.18 (0.125)	2.34 (0.092)	1.65 (0.065)
3	0.152 (0.006)	6.12 (0.241)	2.26 (0.089)	1.52 (0.060)
4	0.152 (0.006)	3.33 (0.131)	3.84 (0.151)	1.28 (0.050)
5	0.152 (0.006)	3.40 (0.134)	2.36 (0.093)	1.26 (0.049)
6	0.102 (0.004)	3.33 (0.131)	2.36 (0.093)	1.55 (0.061)
7	0.152 (0.006)	3.33 (0.131)	3.84 (0.151)	1.62 (0.064)

it was found that burrs exist on some fin surfaces, caused by the manufacturing process. Burrs occur at the ends of a fin and near the base. In the denser fin arrays (smaller fin spacing), the burrs block more space in the fin duct, since the burrs have a roughly uniform size of about 0.4 mm. The percentage of fin ducts blocked by burrs are called occurrence of burrs for the plate. From the inspection of the fin stock, Table 3-2 lists the occurrence of burrs for all the seven plates. The data listed in the table were obtained by examining the fin stock and counting the occurrence of burrs. Kays and London (1984), showed that burrs on fins can cause significantly increased friction factor.

The fin arrays are vacuum brazed between two aluminum cover plates. The brazing temperature is above 650 °C, with aluminum alloy (AA-4004) as the brazing material. The brazing was performed under vacuum of 9×10^{-3} mm Hg to prevent oxidation of aluminum at the high temperature. Figure 3-1 shows the structure of the

Table 3-2 Occurrence of Burrs

Plate Number	Burrs Occurrence (%)
1	40
2	15
3	10
4	8
5	10
6	14
7	10

cold plates. The fin array is arranged in the central section of the cold plate. The holes A and B are pressure taps to measure the pressure difference across the fin array in the flow direction. The pressure difference in the transverse direction is measured by holes A and C. The pressure measurement connections are made by compression tube fittings which are glued on the cover plate with a bonding epoxy. The three small holes at each end of the cold plate are used for installation of a tube fitting, which seals to the cover plate and brings the fluid in at a 90° angle to the flow direction.

As shown in Figure 3-2, the cold plate is heated on one side by an electric heater while all other surfaces are thermally insulated. The surface which contacts the heater is manufactured with flatness of 0.05 mm TIR (total indicator reading) to provide a good match between the heater and the cold plate. Two means are taken to reduce the contact thermal resistance between the cold plate and heater assembly. The first is to minimize the gap size. Six C-clamps are used to hold the two plates as close as possible. Wood pads are used between the C-clamps and the cold plate to reduce

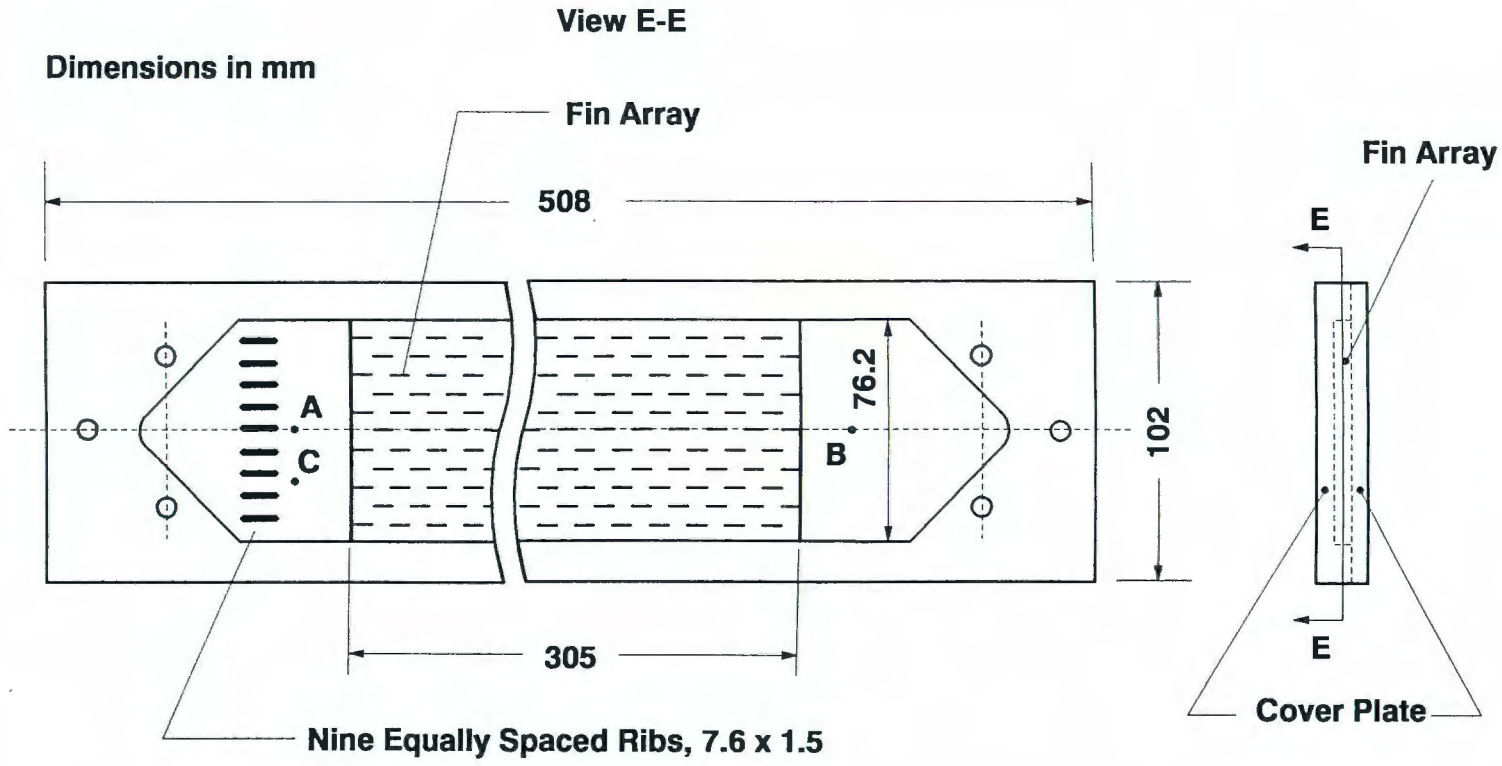

Figure 3-1 Inner Structure of Cold Plates (not to scale)

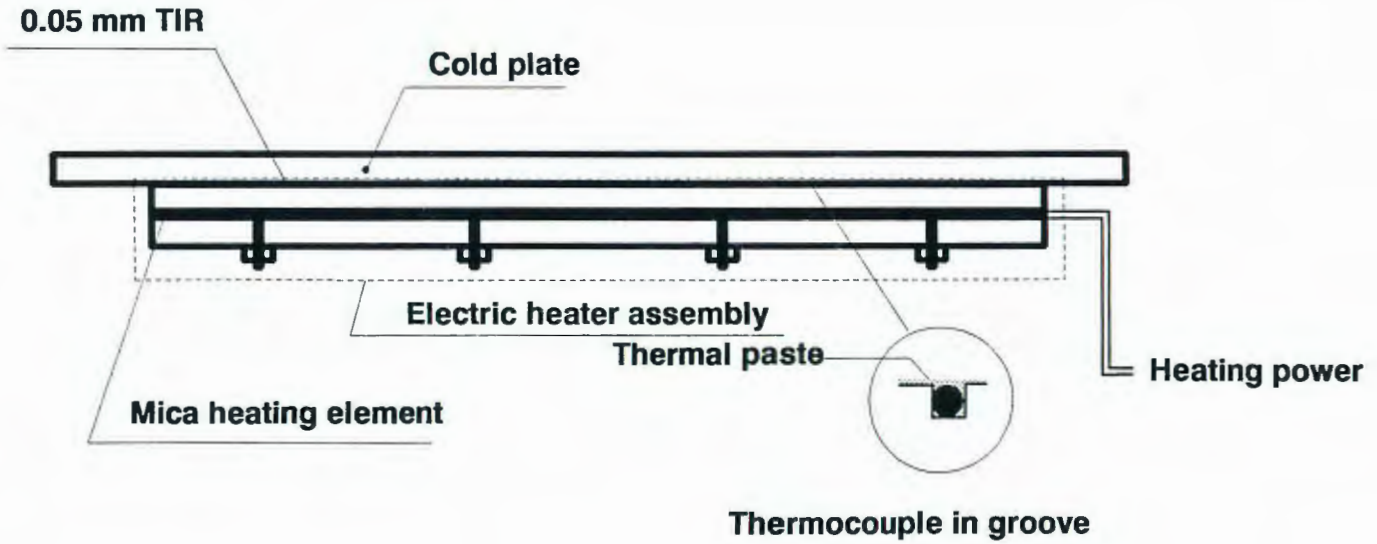

Figure 3-2 Schematic of Cold Plate and Heater Assembly (not to scale)

heat conduction through the C-clamp and to avoid deformation of the cold plate due to the force from the C-clamps. Secondly, a high thermal conductivity paste was used as a filler between the surfaces. The thermal paste is made of silver powder and conductive resins with a thermal conductivity of 4.5 W/m-K, according to the manufacturer. The electric heater, which is called the main heater in later discussion, is designed to provide uniform heat flux over the heated surface. A mica heating element was chosen because of high heating temperature. The heater is assembled by sandwiching the mica element between two aluminum plates as shown in Figure 3-2. The heater provided heat flux up to 7.5 W/cm^2 (total power is up to 1750 W).

3.1.2 Test Loop

The test loop is shown schematically in Figure 3-3. It is a recirculating liquid loop driven by a centrifugal pump (A). A shell and tube heat exchanger is employed as the system heat rejection to reject heat from the loop to a glycol chiller loop. Three filters, with pore size of 1.52 μm, are used in the system to eliminate particles in the flow.

Before the test section, there is a trim heater to control the fluid temperature. The trim heater is connected to a PID (proportional-integral-derivative) temperature controller (CHROMALOX, CN2001) and a solid state relay (SSR) element. According to the controller setting, the control system regulates the input power to the trim heater to adjust the temperature of fluid flowing to the test section. Besides the trim heater, temperature in the system was also controlled by adjusting the glycol coolant flow rate to the rejection heat exchanger. This system provided an inlet temperature

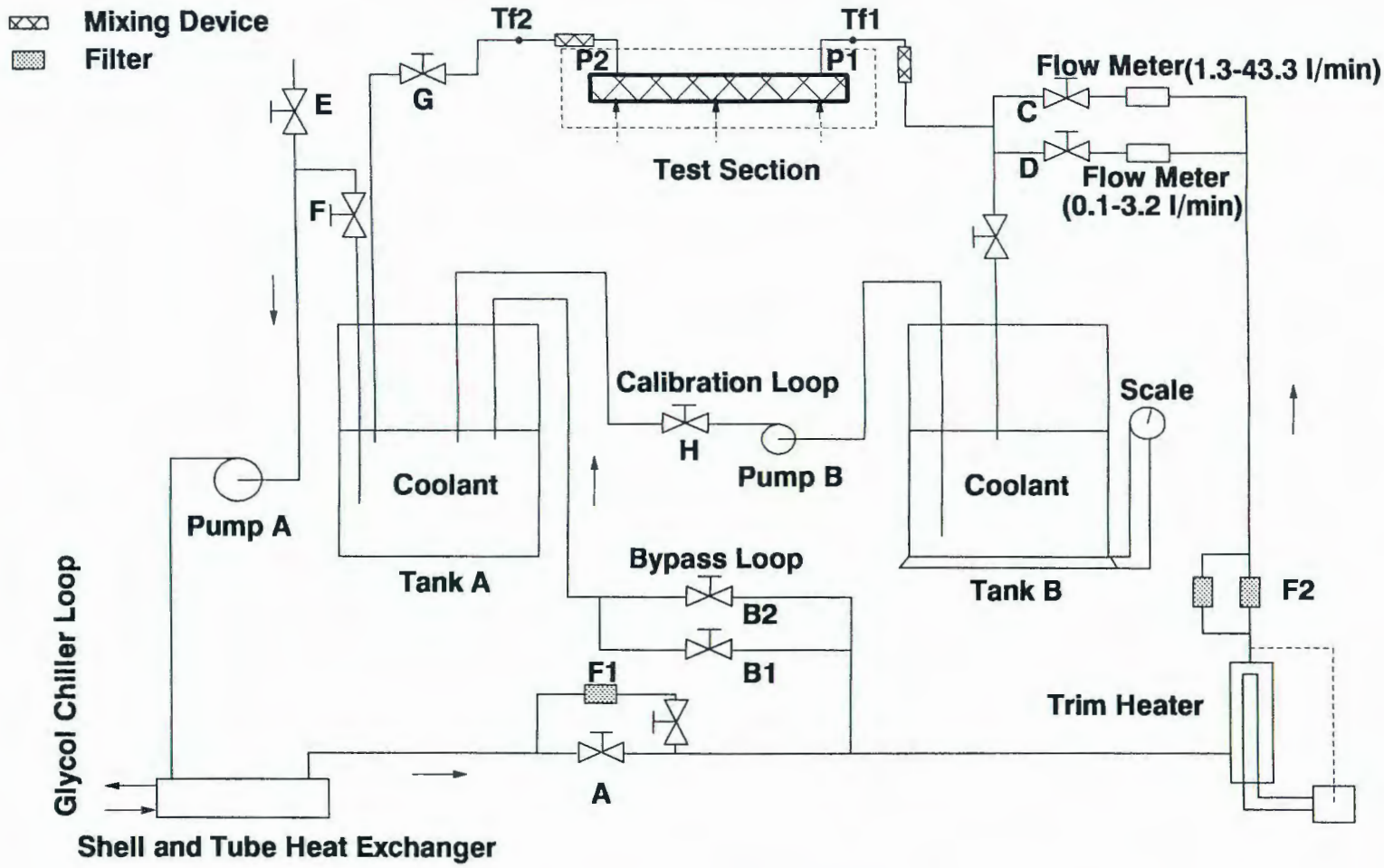

Figure 3-3 Liquid Test Loop

stable to within ± 0.2 °C during operation. The fluctuations of the fluid temperature were caused primarily by the fluctuations of the flow rate and the heating power. These fluctuations were about a stable mean temperature and their effect was minimized by averaging.

The test section flow rate was regulated by adjusting the main loop valve A, by-pass loop valves B1 and B2 and flow-meter valves C and D. For a larger flow rate, valves B1 and B2 are totally shut off and valves A and C are fully open. The full pump capacity is applied on the test section so that the largest flow rate is obtained. For a small flow rate, valves B1 and B2 should be partially open, to induce some flow to the by-pass loop.

In the system, the two-tank design allows calibration of the two turbine flow meters. Between Tanks A and B, there is a calibration loop, consisting of a small centrifugal pump B and a control valve H. Tank B takes the fluid flowing through the flow meter. Tank A is used as a buffer to hold the flowing fluid before and after the calibration. The flow meters are arranged in parallel flow paths. On-off valves are installed after each turbine meter to shift the flow from one to the other. In order to obtain reliable data from the flow meters, straight tube sections with lengths of $20 \times D_f$ and $10 \times D_f$ are installed before and after the flow meters, respectively, where D_f is the diameter of the flow channel inside the turbine flow meters.

During calibration (minimum 3 minutes), fluid flows into Tank B after valve H and C or D are shut off and the weight change of fluid in Tank B was measured. In the same period of time, the frequency from the turbine flow meter was recorded

and averaged. So the correspondence between flow rates and flow meter frequencies were obtained. Both flow meters were calibrated with each fluid and at temperatures of 20 and 60 °C.

Due to dissolved salts existing in normal tap water, serious water scale buildup on the fin structure was experienced in initial testing. Scale formation causes a significant increase in pressure drop and decrease in heat transfer in the cold plate. The scaling is caused by two factors: 1) there occurs an electro-chemical cell formed between the copper tube and the aluminum cold plate and 2) with increasing water temperature, the soluble compounds of $Ca(HCO_3)_2$ and $Mg(HCO_3)_2$ are changed to the insoluble compounds $CaCO_3$ and $MgCO_3$, which deposit on the heated plate (Kotz, 1991). To prevent scale formation, two methods were used: 1) plastic tube-fittings were installed between the copper tube and aluminum cold plate to eliminate the electro-chemical reaction and 2) deionized water with low salt concentration was used. These two measures completely eliminated the scale problems experienced in initial testing. Scale was dissolved from Plate 1 after it was detected by washing with acetic acid.

The cold plate assembly and connecting lines were insulated in order to obtain a good energy balance in the test section. To insulate the cold plate and heater assembly, fiber glass was employed, which was enclosed in an box made of polystyrene foam walls. Tube insulation is polyurethane foam. From experimental data, the energy balance on the cold plate and heater assembly shows heat loss as much as 8% at high temperature conditions. This loss does not cause a problem since

the data analysis was based on the energy added to the liquid.

3.2 Measurement Devices

3.2.1 Temperature Measurement

The heated surface temperatures of the cold plate are measured by fourteen copper-constantan thermocouples (type T) with a diameter of 0.076 mm. They are mounted between the heater assembly and the cold plate as shown in Figure 3-4. Ten grooves (0.08 mm $\times$ 0.17 mm) are machined on the heater assembly surface to carry the thermocouple lead wires. Figure 3-4 shows the thermocouple positions on the heat transfer surface. Ten thermocouples were arranged along the central line to measure the surface temperature distribution in the flow direction. Four thermocouples were mounted off-center in order to measure surface temperature symmetry. On the unheated surface, there were 5 thermocouples arranged along the center line in the flow direction (not shown on figure).

The inlet and outlet fluid temperatures were measured by type T thermocouples before and after the cold plate. Fluid mixing devices were employed upstream of the measurement locations to obtain bulk fluid temperatures. In the mixing devices, shown in Figure 3-5, the flowing fluid forms a jet through the hole of disk A, which impinges on the solid center portion of disk B. The fluid mixes strongly in the mixing chamber and goes through the holes of disk B. At the lowest flow rate used in this study, the Reynolds number for PAO (most viscous fluid) in the mixing orifice was 4000, indicating turbulent flow. The thermocouple measures the fluid temperature

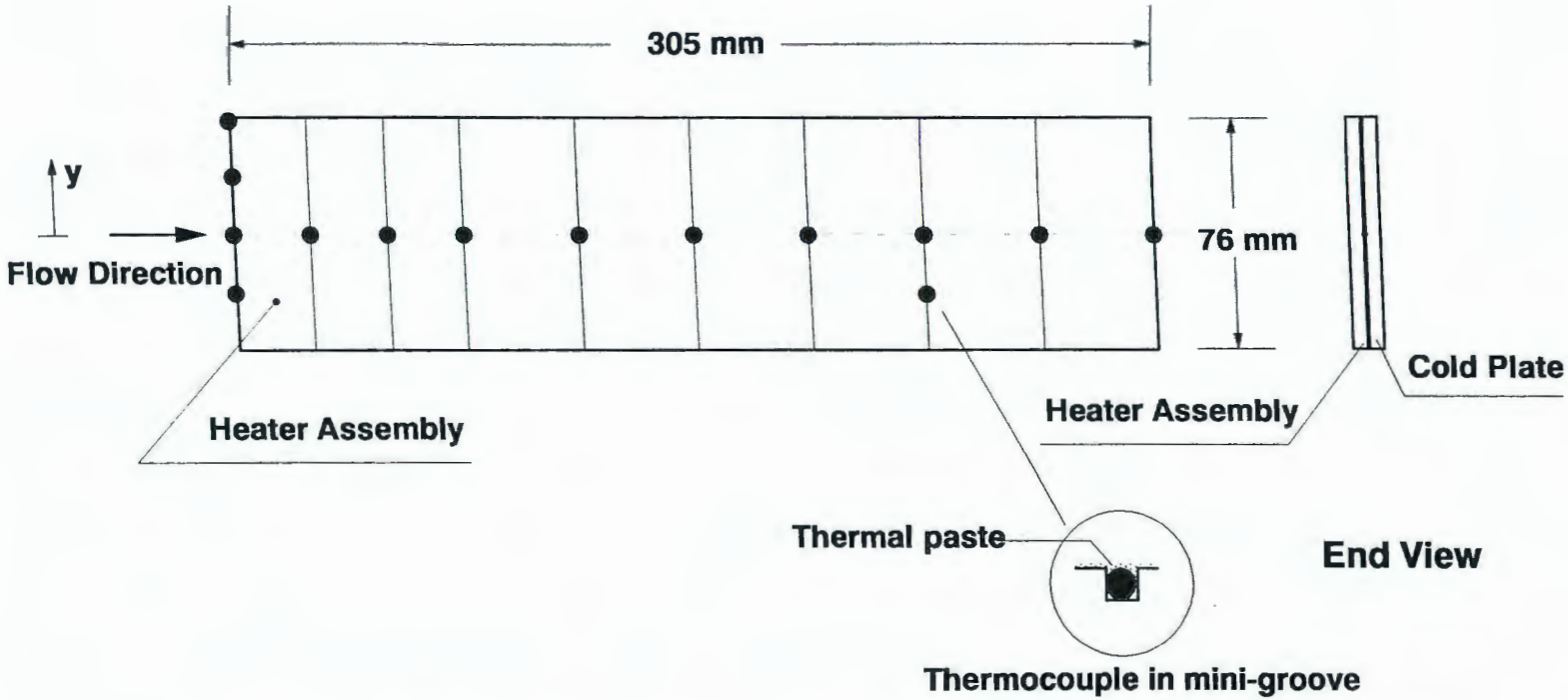

Figure 3-4 Thermocouple Arrangement on the Heater Assembly

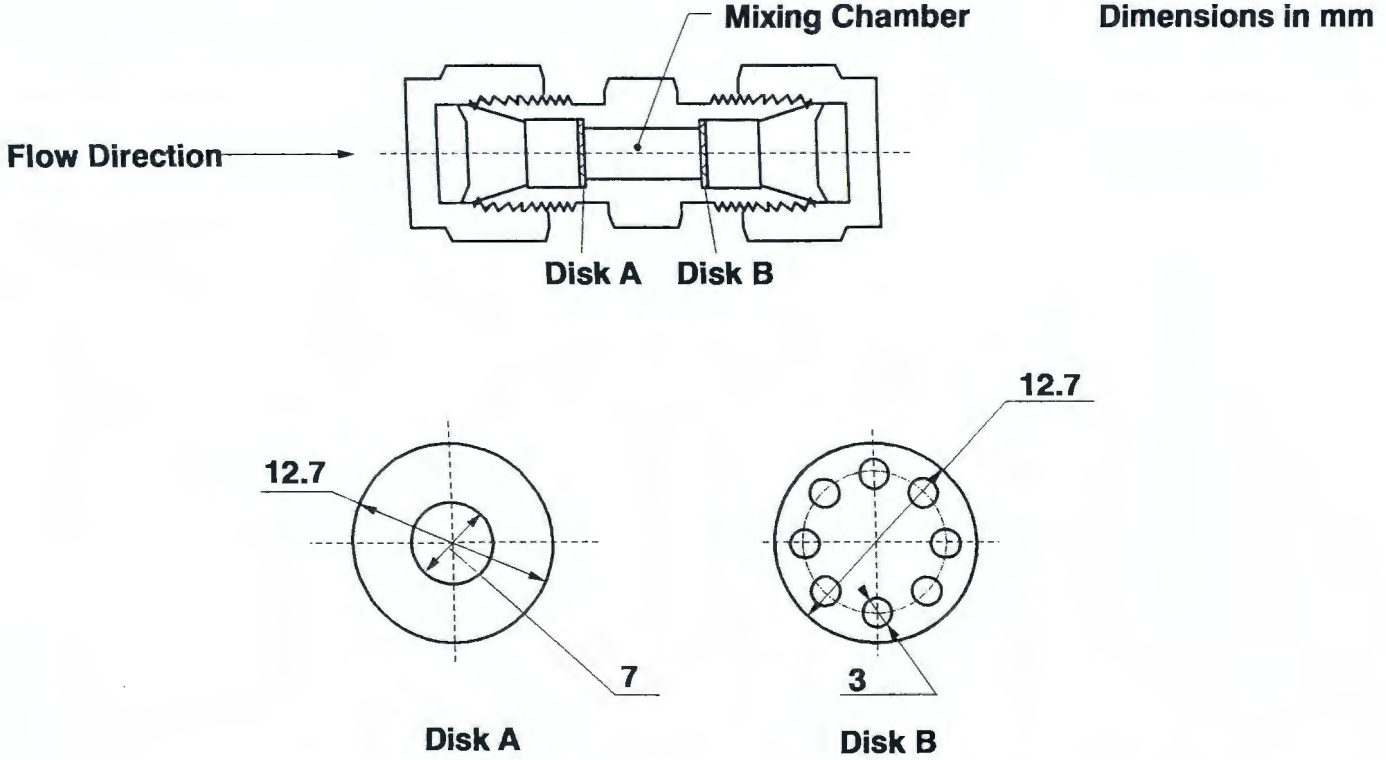

Figure 3-5 Inner Structure of Mixing Device

exiting from disk B which is designed to closely match the bulk temperature.

Thermocouples were used with an ice bath reference. The electrically-insulated reference-ends of the thermocouples were immersed in the ice bath. The ice bath was made of a vacuum thermal bottle which contained a mixture of crushed ice and water at atmospheric pressure.

3.2.2 Flow Rate, Heating Power and Differential Pressure Measurement

The coolant flow rates were measured by two turbine flow meters with different ranges. The large flow meter (Sponsler: SP-1/2) has the range of 1.3 - 43.3 liter/minute. The small flow meter (Sponsler: MF-80) has the range of 0.1 - 3.2 liter/minute. The outputs from the turbine flow meters are low-level sine-wave signals. A signal amplifier (Sponsler: SP-714) was used to convert the sine-wave to a square-wave signal and amplify the output. An electronic counter (HP 61015A) was used to record the frequency output of the turbine meter.

The power of the main heater was taken from a 208 volt single-phase power line and was adjusted with a variac (POWERSTAT, 3PN236B) by changing the voltage to the heater. The power input was closely monitored during the experiments. The power was measured by a power transducer (OSI PC5-011 CX5) which output a signal from 0 - 5 volt for a power range from 0 - 2000 W.

The pressure difference across the fin array was measured by a differential pressure transducer (SETRA, 228-1). For the input of 0 - 200 kPa pressure difference, the transducer gives 0 - 5 volt output.

3.2.3 Data Acquisition System

Figure 3-6 shows the PC based data acquisition system which is used to collect the signals from the signal transducers. In the test setup, there are 22 voltage signals and 1 frequency signal from transducers. Two multiplexer (HP 3488A and PC-MUX 61011A) units are used to choose the voltage measuring channel. A digital voltmeter (SOLARTRON 7701) is used to measure the voltage outputs and convert the analog signals to digital signals. A personal computer (HP-9000) controls all the measuring instruments as well as receives the digital data from the voltmeter and the counter. The data acquisition program, consisting of about 2000 lines written in HP-BASIC, was developed as a part of this effort.

3.3 Experimental Procedures

The primary variables investigated were fluid type, inlet fluid temperature, flow rate, heat flux and cold plate geometry. On each plate, experiments were carried out at the following conditions:

Fluid		:	PAO, water
Inlet fluid temperature	(°C)	:	10, 20, 60
Flow rate	(liter/min)	:	1 - 15
Heat flux	(W/cm^2)	:	1 - 7

The fluid temperature range spans the temperatures most commonly used in industrial applications. Within this temperature range the Prandtl number of water and PAO

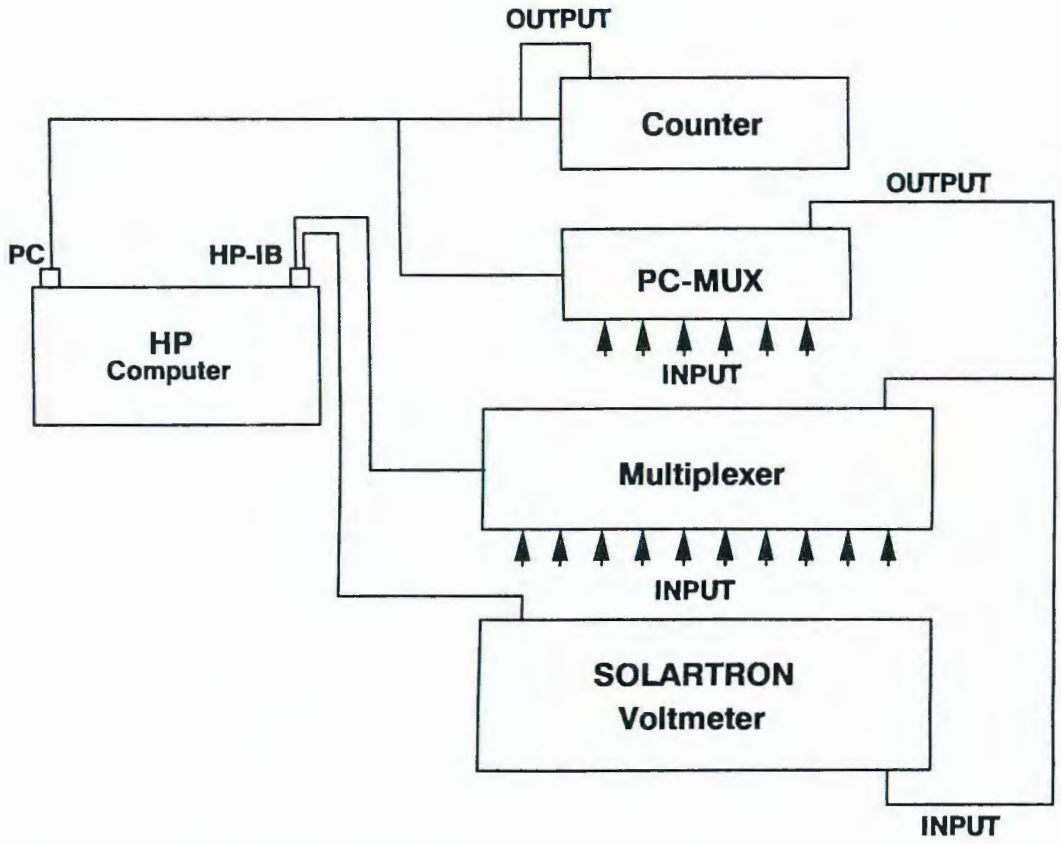

Figure 3-6 Data Acquisition System

range from 3 to 10 and 40 to 150, respectively. The maximum flow rate of the facility is limited by the pumping capacity and friction from the test rig. The largest flow rate was chosen as a test condition. At very low flow rates, the pressure drop across the fin array is small, where electromagnetic noise was found to cause large errors in the pressure measurements. So the smallest flow rate was restricted to 3 liter/min to obtain acceptable pressure measurement accuracy for water. The selection of heat flux corresponds to the flow rates in the experiment. For a large flow rate, a large heat flux is required to make the fluid temperature difference across the fin array at least 3 °C. This minimum value of difference was chosen to minimize temperature measurement error.

As a part of the facility checkout, the measuring transducers were calibrated. During the calibration, the signals from all the transducers were collected by the data acquisition system. Therefore, the calibration results include the effects from both the measuring transducers and the data acquisition system. The details of transducer calibration are described in Appendix A.

During the experiment, the following procedures were used:

1) Fluid temperature setting: With the main heater off, choose the temperature setting for the trim heater, and adjust glycol flow rate in the rejection heat exchanger. Then run the system until the fluid temperature reaches the desired temperature and maintains steady state.

2) Pressure transducer zero: Use the bleed valve to purge air out of the pressure measurement lines. After the transducer temperature reaches steady state,

shut off the flow rate to the test loop. At zero flow rate, adjust the reading of the pressure transducer to zero.

3) Adjust the main flow control valves (C or D) until the desired flow rate is obtained. Turn on the main heater.

4) Monitor the surface temperatures, fluid temperatures, heating power and flow rate versus time. When temperatures reach steady state, run the data acquisition program to collect data and save to disk.

5) Adjust the main flow control valve to attain another flow rate and change the heating power. Then follow Step 4.

6) After finishing all the tests for the fluid temperature, turn off the main heater.

7) Change the temperature setting of the trim heater, adjust glycol flow rate in the rejection heat exchanger, run the fluid through the system until the fluid temperature reaches another desired temperature. Then follow Step 2.

When the tests were finished with PAO, the system was drained completely. Ethanol was used as a solvent to clean the PAO out of the system. The system was rinsed with deionized water. After the cleaning, the system was filled with deionized water for water tests. Note: Initial tests were run with water on Plate 1 prior to the PAO tests as part of the system shakedown.

Repeatability tests were conducted as a part of the effort to examine the reliability of the experimental data. For each fluid, one test was repeated for every plate at each fluid temperature. In total forty-two repeatability tests were performed.

The results of the repeatability tests are discussed in Chapter 6.

To investigate the pressure drop distribution in the cold plates, a pressure tap hole D was made at the midpoint between A and B on Plate 2. Figure 3-7 shows the measured results for one test. Points A, B and D are the measurement points. Point E is a linear interpolation between points A and B. It is seen that the measured pressure at point D is slightly higher than the corresponding point E. This is because there is a small developing hydrodynamic region at the beginning of the fin array, which causes a little higher pressure drop from Points A and D.

Figure 3-8 shows the surface temperature distribution in the transverse direction, for Plate 3. It can be seen that the surface temperature at the center is slightly higher than the surface temperatures near the edge. This is due to transverse conduction. Since the cover plate is thin, the conduction in the transverse direction is small (about 0.6% of main heating power).

The surface temperatures on the unheated cover plate were also measured during the tests. It was found that the unheated plate was warmer than the fluid due to conduction through the fins. Thus, the unheated plate contributes to the total heat transfer area. In the analysis that follows, the unheated plate was treated as another fin.

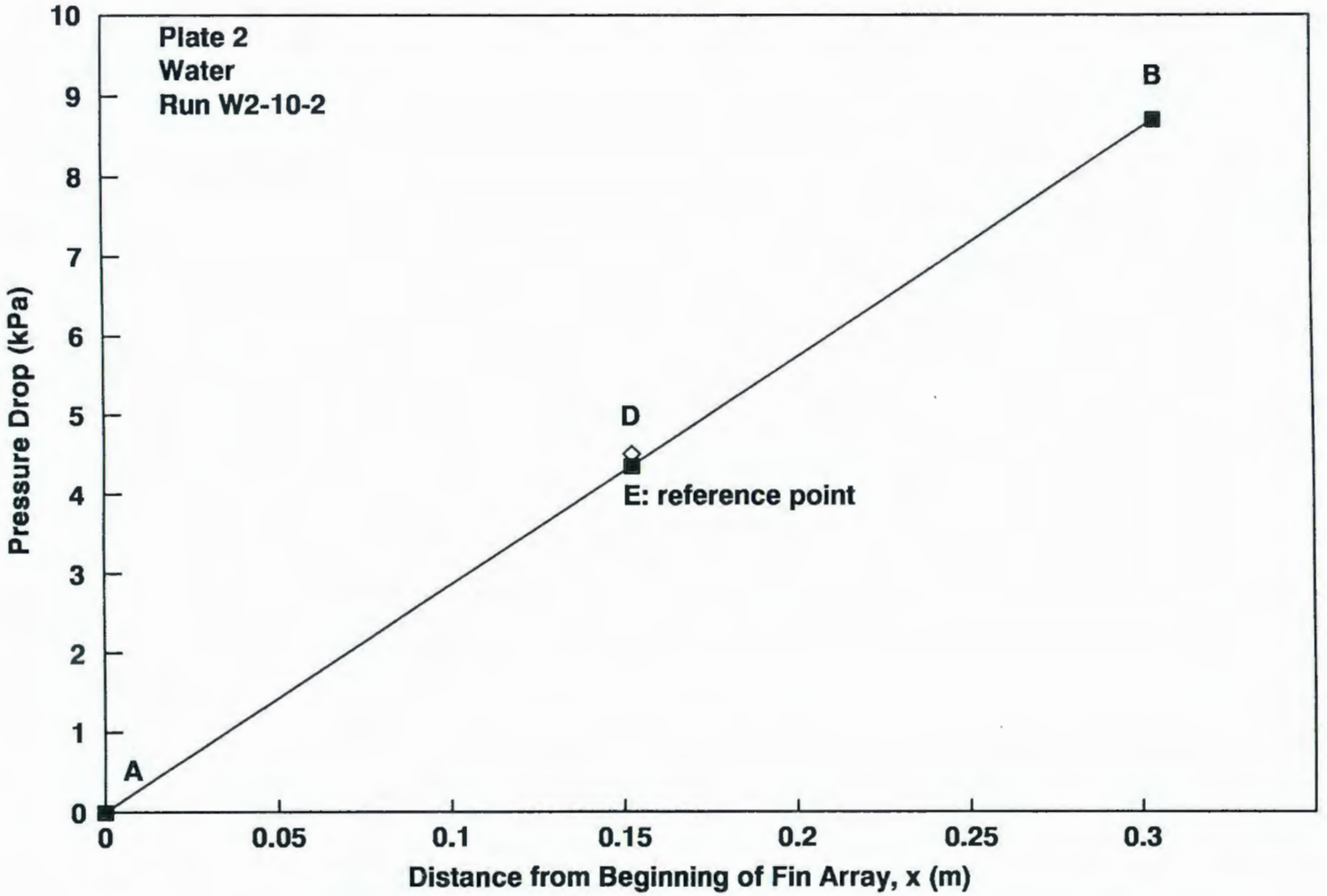

Figure 3-7 Pressure Drop Distribution in Flow Direction

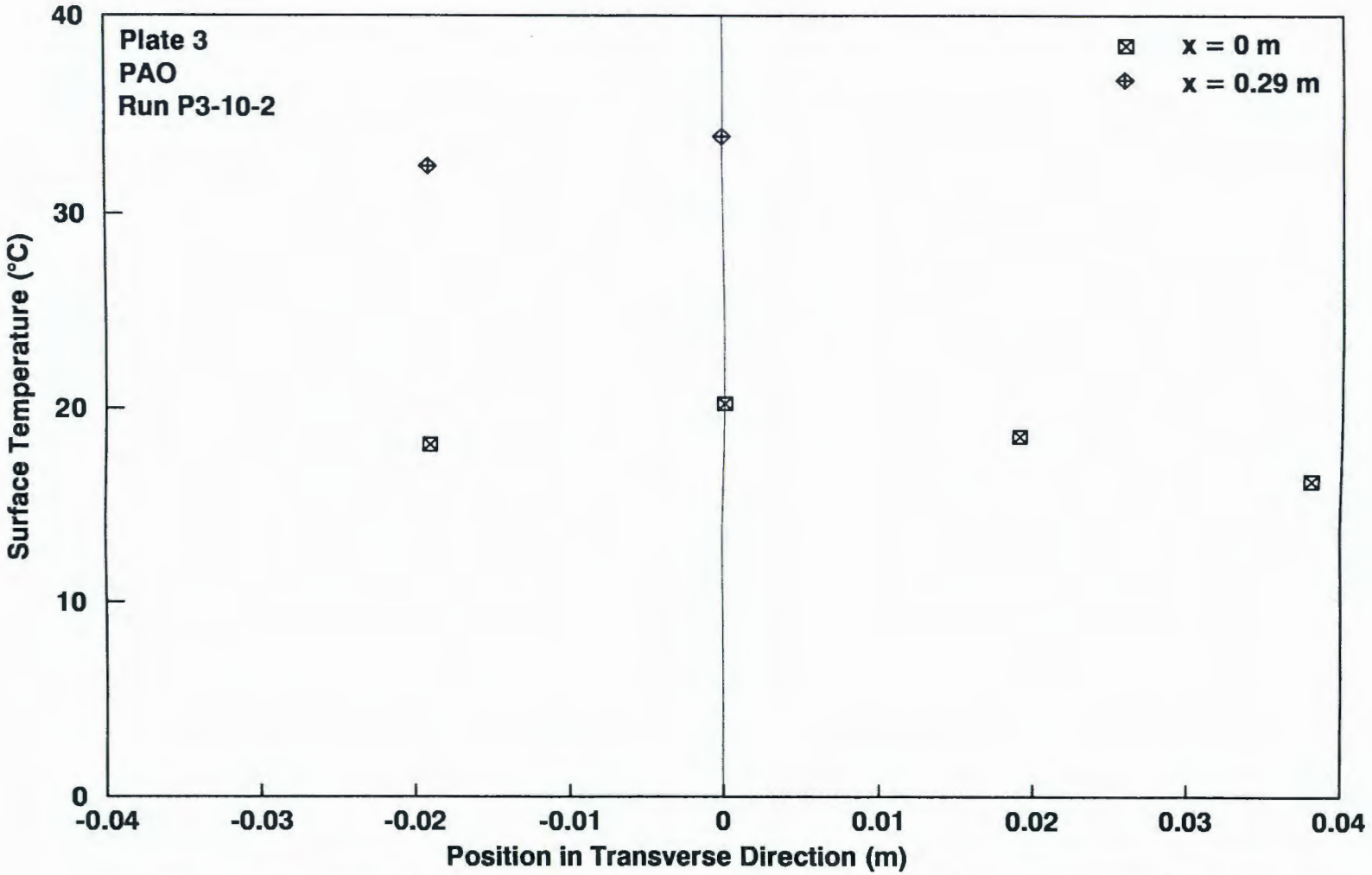

Figure 3-8 Surface Temperature Distribution in Transverse Direction

CHAPTER 4

MODEL STUDY

The liquid coolants of interest in the present study include water and a light synthetic oil called PAO (polyalphaolefin). The Prandtl number for these liquids ranges from 3 - 150 over the temperature range of interest (10 - 60 °C). In general, these liquids have higher heat transfer coefficients than air due to their combined properties (i.e. higher density, thermal conductivity and specific heat). The higher viscosity of the liquids leads to increased pressure drop as compared to air. In the present study, the fin geometry and Prandtl number effects on heat transfer and pressure drop in offset fin arrays were studied. As a part of the effort, predictive models of the heat transfer and pressure drop effects were constructed and tested against experimental data. The models are based on a surface contribution approach, similar to the approach of Joshi and Webb (1987). The models are based on the unit cell a-b-c-d, defined in Figure 1-1b. Four fin geometry parameters define the fin array: fin thickness (t), fin length (l), fin transverse spacing (s), and fin height (h). The aspect ratio of the fin geometry, α, is defined as s/h. The surfaces in the unit cell which contribute to both the heat transfer and the pressure drop include 1) the fin sides, 2) the fin ends, and 3) the top and bottom plates. For the fin geometry, the hydraulic diameter, D_h, is defined as (Kays and London 1984):

$$\frac{D_h}{L'} = \frac{4\,A_c}{A} \tag{4.1}$$

where L' is the length of a unit cell. For minimum flow area A_c and total heat transfer area A, there are several different definitions found in the literature including those listed in Table 4-1.

The definitions used by Kays and London (1956), Wieting (1975) and Mochizuki and Yagi (1977) ignore the effects of fin thickness on the hydraulic diameter. Later, Kays and London (1984) modified their definition by considering fin thickness in the heat transfer area. Joshi and Webb (1987) and Brinkmann et al. (1987) proposed a modified minimum flow area, A_c, by subtracting the fin thickness from flow area. For thin fin arrays as used in the present study, the effect of these different definitions is not particularly large. In the current study, the definition of hydraulic diameter is the same as that used by Kays and London (1984). For a unit cell, the minimum flow area of one unit cell, A_c, is

$$A_c = s\,h \tag{4.2}$$

The heat transfer area of one unit cell, A, is

$$A = 4\,(l\,h + t\,h + l\,s) \tag{4.3}$$

From Equations 4.1-4.3, the hydraulic diameter can be written as

$$D_h = \frac{2\,s\,h\,l}{s\,l + h\,l + t\,h} \tag{4.4}$$

The Reynolds number, Re, is evaluated based on the average flow velocity, u, over the minimum flow area A_c.

Boundary layer development in an offset fin cold plate can be viewed from

Table 4-1 Definition of A_c and A used in Hydraulic Diameter for Offset Fin Geometry

	A_c	A
Kays and London (1956) Wieting (1975) Mochizuki and Yagi (1977)	s h	2 (s + h)
London and Shah (1968) Kays and London (1984)	s h	4 (s h + h l + t h)
Joshi and Webb (1987)	(s - t) h	4 (s h + h l + t h)
Brinkmann et al. (1987)	(s - t) (h - t/2)	(2h+3s/2)+2t(h+s+t)-ts/2
Manglik and Bergles (1990)	s h	4 (s h + h l + t h) + 2 t s
Current study	s h	4 (s h + h l + t h)

two distinct perspectives: 1) boundary layer development at the entrance to the fin array, which is analogous to the entrance effects in a straight duct; 2) boundary layer development on each fin, which is unique to the offset fin geometry. Both of these effects are significant in predicting heat transfer. In later discussions, boundary layer development at the entrance to the fin array is also referred to as the *array perspective* and boundary layer development on each fin is called the *fin perspective*.

For the cold plates considered in the present study, the fin array dominates the pressure drop in the system. Thus, the fin array acts as an automatic flow distributor giving approximately equal flow to all sections of the fin array. For more complex cold plate geometries, uneven flow distribution contributes to more complex heat transfer characteristics. In the present study, a uniform flow distribution was assumed such that all unit cells in a row transverse to the flow are assumed to have the same

characteristics.

The pressure drop and heat transfer models in the study are based on laminar flow. Most liquid cooled offset fin applications employ laminar flow due to high pressure drops. Typical Reynolds numbers are in the range 10 - 300.

4.1 Pressure Drop Model

In the present work, it was found that the friction factor in the offset fin geometry is independent of Prandtl number but strongly dependent on Reynolds number. The model presented here predicts Fanning friction factor based on the analysis of one unit cell, a-b-c-d shown in Figure 1-1b. The flow in the fin array can be analyzed similar to the flow in a rectangular duct. The Graetz number is defined to reflect the hydraulic developing length as

$$Gz = \frac{D_h^r \, Re^r}{x} \tag{4.5}$$

where x is the distance from the beginning of the fin array. From the offset fin studies of Sparrow et al. (1977) and Kelkar and Patankar (1989), it was found that when $1/Gz > 0.005$, the flow has effectively reached a periodic hydrodynamic fully developed condition. In the current research, Reynolds numbers in the range of 10 - 2000 were considered and for the fin geometries of interest, D_h^r is approximately 0.002 m. Thus, compared to the length of a typical cold plate fin array (0.3 m), the hydraulic entrance length, x_e, is so small as to be negligible. Thus, from the array perspective, the flow is treated as hydrodynamic periodic fully developed flow.

A force balance for a unit cell takes the form

$$F_{unit} = F_P + F_E + F_D \tag{4.6}$$

where the total force on the unit cell, F_{unit}, is

$$F_{unit} = \Delta P \, A_f \tag{4.7}$$

where A_f equals (s+t)h. The viscous shear force on the fin sides, F_P, is

$$F_P = 4 \, l \, h \, \tau_P \tag{4.8}$$

The viscous shear force on the top and bottom surfaces, F_E, is

$$F_E = 4 \, l \, s \, \tau_E \tag{4.9}$$

The form drag force, F_D, is

$$F_D = \frac{1}{2} \, \rho \, v^2 \, (2 \, t \, h) \, C_D \tag{4.10}$$

Using Equations 4.7 - 4.10, Equation 4.6 can be transformed into

$$\Delta P \, A_f = 4 \, l \, h \, \tau_P + 4 \, l \, s \, \tau_E + 1/2 \, \rho \, v^2 \, (2 \, t \, h) \, C_D \tag{4.11}$$

The Fanning friction factor is defined such that

$$\Delta P = \frac{1}{2} \rho u^2 \, (\, 4 \, f \,) \, \frac{2 \, l}{D_h} \tag{4.12}$$

The shear stress on the fin sides is

$$\tau_P = \frac{1}{2} \rho u^2 \, f_P \tag{4.13}$$

The shear stress on the top and bottom surfaces is

$$\tau_E = \frac{1}{2} \rho u^2 \, f_E \tag{4.14}$$

In Equation 4.12, f represents the average friction factor in the unit cell. The friction factor for the fin sides is denoted f_P and top and bottom surfaces are denoted

f_E. Using Equations 4.12 - 4.14, Equation 4.11 can be simplified to give

$$\frac{2\,A_f f}{D_h} = f_P\,h + f_E\,s + C_D\left(\frac{v}{u}\right)^2 \frac{t\,h}{2\,l} \tag{4.15}$$

By the previous definitions of D_h and A_f, Equation 4.15 can be written as

$$f = \frac{1}{(1+\alpha+\delta)(1+\gamma)}\left(f_P + \alpha f_E + C_D \frac{t}{2\,l}\left(\frac{v}{u}\right)^2\right) \tag{4.16}$$

where δ equals t/l and γ equals t/s. Thus, the average friction factor of the offset fin array, f, can be predicted if f_P, f_E and C_D are known.

Sparrow and Liu (1979) studied the friction factor of an offset fin array with zero aspect ratio, so that they did not consider the influence from the top and bottom surfaces. In actual applications, the top and bottom surfaces do influence the pressure drop on the fin sides. The current model uses a rectangular duct model (Curr et al., 1972), which includes the effect from the top and bottom surfaces. In the model, the velocity is assumed uniform at the beginning of each fin. The hydraulic dimensionless fin length is defined as

$$x^+_F = \frac{l}{D_h^r\,Re^r} \tag{4.17}$$

From the results of Curr et al. (1972), the friction coefficient for the fin sides has the form

$$f_P\,Re^r = f\,(x^+_F\,,\ \alpha) \tag{4.18}$$

The Curr data are reproduced by the regression equations, in the form of Equation 4.18, included as Table D-1 in Appendix D. Figure 4-1 shows a comparison of the

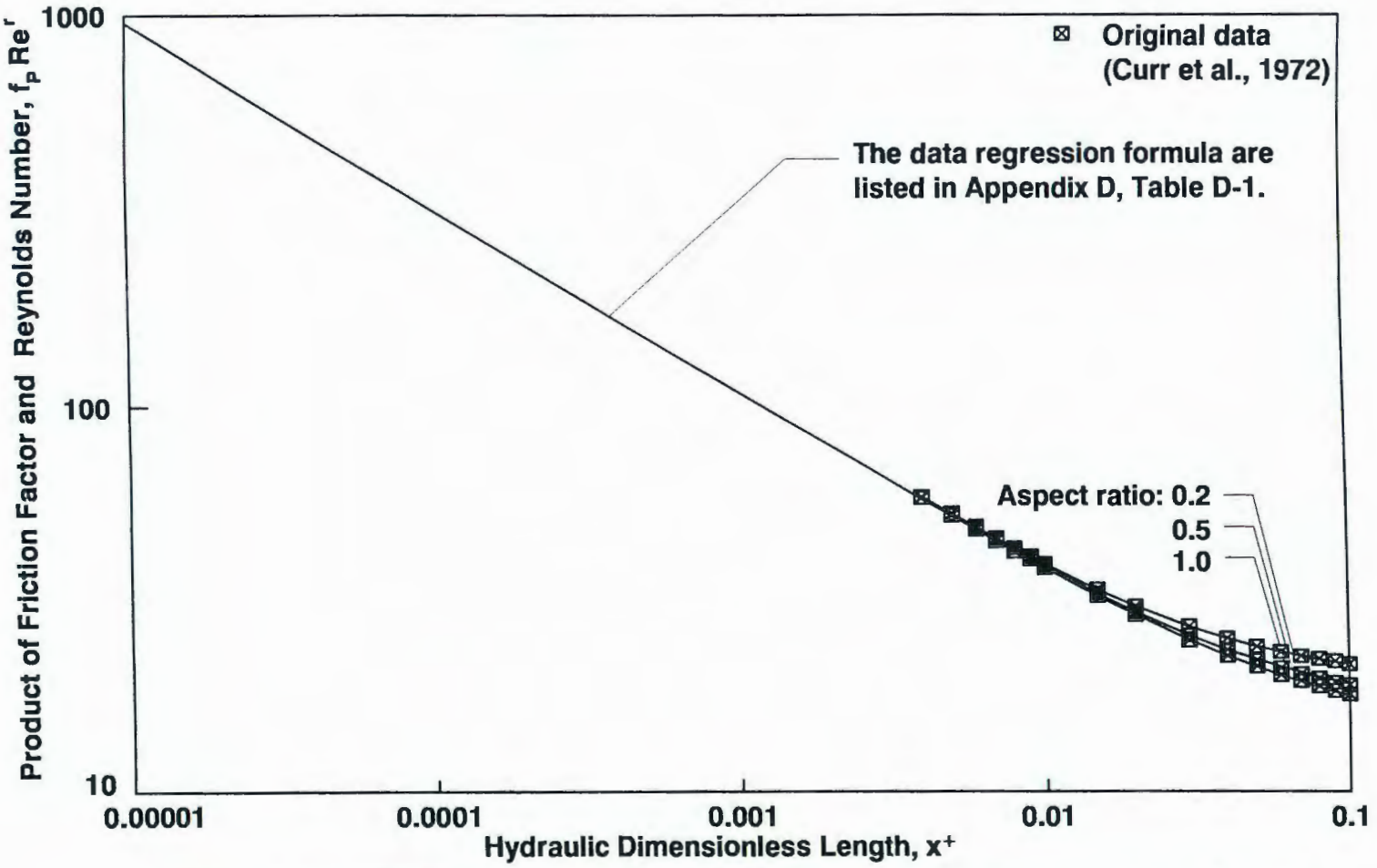

Figure 4-1 Data Regression of Friction Factor in Rectangular Ducts and Original Data

data regression results with the original data (Curr et al., 1972). The x^+_F range of Curr's results is from 0.001 to 0.1. The current model uses a linear extrapolation of the low x^+_F region data to extend the x^+_F range down to 0.00001.

Because there are no boundary interruptions on the top and bottom surfaces, the friction factor of these surfaces is assumed to be the same as the friction factor of fully developed flow in a rectangular duct. The current model utilizes the friction factor results from Shah and London (1978) for a rectangular duct, which take the form

$$f_E \, Re' = f(\alpha) \tag{4.19}$$

A regression of their data in the form of Equation 4.19 is listed in Table D-2.

Form drag is caused by fluid flowing over finite-thickness fins. The fin drag coefficient was studied by Joshi and Webb (1987), who performed pressure drop tests of offset fin arrays with water. They used a burr-free fin geometry with aspect ratio from 0.112 to 0.246. From their experimental results, they found that a constant drag coefficient C_D of 0.8 fit the data. In the current study, the constant drag coefficient of 1.0 is used to fit our experimental data. One reason that the C_D used in the present work is larger than that of Joshi and Webb (1987) is that there are burrs existing on the fins in our cold plates due to the manufacturing process. The model presented in this work has been validated against seven actual cold plates including the effects of burrs. By Equations 4.16 to 4.19, the average friction factor in a unit cell can be found. When the Reynolds number is low, the pressure drop is essentially caused by

skin friction effects. At higher Reynolds number, form drag gains more significance. For example, for Plate 3, the form drag component is approximately 10% of the skin friction component for a Reynolds number of 300. Friction factor results based on this model are discussed in Chapter 6.

4.2 Heat Transfer Model

Following the surface contribution approach, the average heat transfer coefficient in a unit cell is calculated by considering the heat transfer contribution from each of the surfaces. The surface contributions of heat transfer in the unit cell can be written as:

$$Q_{unit} = Q_P + Q_B + Q_E \tag{4.20}$$

where the total heat transferred in one unit cell, Q_{unit}, is

$$Q_{unit} = A\ \eta\ h_x\ (T_s - T_f) \tag{4.21}$$

The heat transferred from the fin sides, Q_P, is

$$Q_P = A_P\ \eta_P\ h_P\ (T_s - T_f) \tag{4.22}$$

The heat transferred from leading and trailing ends of the fin, Q_B, is

$$Q_B = A_B\ \eta_B\ (h_B + h_F)\ (T_s - T_f) \tag{4.23}$$

The heat transferred from the top and bottom surfaces is

$$Q_E = (A_E\ \eta_E\ h_E + A_E\ h_E)\ (T_s - T_f) \tag{4.24}$$

where T_s represents the average heating surface temperature and T_f represents the bulk fluid temperature in the unit cell. By using Equations 4.21 to 4.24, Equation 4.20 can be rewritten as

$$A\ \eta\ h_x = A_P\ \eta_P\ h_P + A_B\ \eta_B\ (h_B + h_F) + A_E\ \eta_E\ h_E + A_E\ h_E \qquad (4.25)$$

The overall surface efficiency in the unit cell, η, has the form

$$\eta = 1 - (1 - \eta_P)\ A_{fin} / A \qquad (4.26)$$

In each of the terms in Equation 4.25, the symbol η represents the fin efficiency of the various surfaces. Since the bottom surface is heated, the fin efficiency of the bottom surface is assigned a value of 1.0. In the current model, it is assumed for simplicity that $\eta_P=\eta_B=\eta_E$. A one-dimensional fin model is used to compute the fin efficiency. The fin efficiency, η_P, is calculated based on a one-dimensional fin model with an insulated tip. The unheated plate is lumped together with the fin area resulting in an effective fin height of (h+s). The fin efficiency expression is then

$$\eta_P = \frac{\tanh(m_P(h+s))}{m_P(h+s)} \qquad (4.27)$$

with

$$m_P = \sqrt{\frac{2\ h_P}{k_A\ t}} \qquad (4.28)$$

The fin area, A_{fin}, includes the offset fin area and the unheated top surface area

$$A_{fin} = 4\ (l\ h + t\ h) + 2\ l\ s \qquad (4.29)$$

For the liquid coolants used in the present study, fin efficiency values range from 0.6 to 0.9 as compared to values for air, for the same geometry, which are very close to 1.0. Using Equations 4.26 and 4.29, Equation 4.25 can be transformed as follows

$$4(lh + th + ls)\,\eta\, h_x = 4\,lh\,\eta_P h_P + 2\,th\,\eta_P(h_B + h_F) + 2\,ls\,\eta_P h_E + 2\,ls\,h_E \tag{4.30}$$

Assuming $h_P=h_B=h_F$, Equation 4.30 can be simplified to give

$$\eta\, h_x = \frac{1+\delta}{1+\delta+\alpha}\,\eta_P\, h_P + \frac{\eta_P + 1}{1+\delta+\alpha}\,\frac{\alpha}{2}\,h_E \tag{4.31}$$

Multiplying Equation 4.31 by D_h/k yields

$$\eta\,\frac{h_x D_h}{k} = \frac{D_h}{D_h{}^r}\left(\frac{1+\delta}{1+\alpha+\delta}\,\eta_P\,\frac{h_P D_h{}^r}{k} + \frac{\eta_P+1}{1+\alpha+\delta}\,\frac{\alpha}{2}\,\frac{h_E D_h{}^r}{k}\right) \tag{4.32}$$

or

$$\eta\, Nu_x = \frac{1+\alpha}{1+\alpha+\delta}\left(\frac{1+\delta}{1+\alpha+\delta}\,\eta_P Nu_{x,p} + \frac{\eta_P+1}{1+\alpha+\delta}\,\frac{\alpha}{2}\,Nu_{x,E}\right) \tag{4.33}$$

where k is the thermal conductivity of the fluid, Nu_x is the Nusselt number averaged over a unit cell, $Nu_{x,P}$ is the Nusselt number averaged over the fin sides in a unit cell, and $Nu_{x,E}$ is the Nusselt number averaged over the top and bottom surfaces in a unit cell. It is noted that all of these Nusselt numbers are local values in the sense that their values depend on the distance from the entrance of the fin array. The leading factor on the right hand side of Equation 4.33 comes from the different definitions of hydraulic diameter used in $Nu_{x,P}$, $Nu_{x,E}$ and Nu_x.

To model entrance effects (array perspective) on the Nusselt number in the offset fin array, the following relationship was assumed between the offset fin array and a rectangular duct, which is used to calculate $Nu_{x,P}$.

$$\frac{Nu_{x,P}}{Nu_F} = \frac{Nu^m{}_x}{Nu^r{}_F} \tag{4.34}$$

This implies that the shape of the Nusselt number profile in the entrance region is the same for both geometries. In Equation 4.34, Nu_F is the Nusselt number of the fin sides (averaged over a unit cell) in the periodic fully developed section. Also, $Nu^m{}_x$ is the local Nusselt number for thermally developing flow in a rectangular duct, which is discussed in the next section. The Nusselt number for fully developed flow in a rectangular duct, $Nu^r{}_F$, was taken from Shah and London (1978) which has the form

$$Nu^r{}_F = Nu^r{}_{F,0.5}\ F_\alpha \tag{4.35}$$

where $Nu^r{}_{F,0.5}$ is the fully developed Nusselt number in a rectangular duct with $\alpha=0.5$ ($Nu^r{}_{F,0.5}=4.11$) and F_α is a modification factor for the aspect ratio, as defined in Appendix D, Table D-3.

In the offset fin geometry, the top and bottom surfaces are continuous (not interrupted). These surfaces were modeled as if they do not experience significant periodic flow disturbances. Thus, thermal field development on the top and bottom surfaces is modeled assuming the same trend as that of a rectangular duct. The Nusselt number on the top and bottom surfaces is expressed as

$$Nu_{x,E} = Nu^m{}_x \tag{4.36}$$

Once the Nusselt number on each surface is known, the average Nusselt number of a unit cell, Nu_x, can be obtained from Equation 4.33. The heat transfer on each surface is influenced by Prandtl number. A key aspect of the present work is to investigate the effect of Prandtl number on offset fin performance.

4.3 Prandtl Number Effects On Offset Fin Performance

Normally when a fluid flows into a continuous duct, there is a developing region near the entrance of the duct, where a higher heat transfer coefficient is attained than that of the fully developed flow. The energy transfers in the entrance region are similar to boundary layer development on a plate. The transition to a fully developed condition occurs after the boundary layers forming on the walls meet in the center of the duct and the velocity and dimensionless temperature profiles become invariant in the flow direction. A fully developed velocity profile transfers less heat from a duct wall due to the convective influence of the velocity profile on the temperature profile. A fully developed temperature profile transfers less heat from a duct wall because the gradient of the temperature at the wall is reduced due to the adiabatic centerline boundary condition. The Prandtl number has a strong influence on developing heat transfer in a rectangular duct. Fluids with large Prandtl number have longer thermal development sections. At the same Reynolds number, the flow with higher Prandtl number has a larger Nusselt number in the entrance region. However, for laminar flow in a rectangular duct, the Prandtl number has no effect on the heat transfer in the thermally fully-developed section. In contrast, as will be discussed in Section 4.3.1, there is a significant Prandtl number influence on the periodic fully developed Nusselt number in an offset fin array. This is a significant difference between these geometries and can be described as Prandtl number effects from the fin perspective. These two perspectives, fin and array, are discussed separately in the following two sections.

4.3.1 Prandtl Number Effects from the Fin Perspective

For the offset fin configuration, the thermal boundary layer development on each fin has a significant effect on the heat transfer performance. An analytical investigation of developing heat transfer at the fin level was performed by Kays (1972). Later Sparrow et al. (1977), Sparrow and Liu (1979) and Kelkar and Patankar (1989) developed detailed numerical models on the fin level. In all these efforts, the working fluid is air with a Prandtl number of 0.7.

Based on the assumption that the flow through fins in the offset array is similar to the flow in a rectangular duct, the rectangular duct is used as a model to predict fin performance in the current work. Montgomery and Wilbulswas (1967) developed a numerical model of heat transfer in the thermal developing section of a rectangular duct with uniform surface heating. Their study demonstrated a significant Prandtl number influence on heat transfer in the simultaneously developing hydrodynamic and thermal regimes with velocity and temperature uniform at the entrance of the duct. For Prandtl number near unity, the temperature and velocity boundary layers develop at about the same rate. For fluids with a larger Prandtl number, such as water (Pr = 3 - 10) or PAO (Pr = 40 - 150), the velocity boundary layer is much thicker and the hydraulic entry length is much shorter than the corresponding thermal characteristics. Note that the range of Prandtl number listed is for the temperature range 10 - 60 °C.

The design concept of the offset fin geometry is to present each fin with uniform temperature and velocity fields so that the heat transfer characteristics approximate those of the entrance region of a duct. However, in practice, the fins are

closely spaced and the boundary layers which form on each fin are still present, although altered by diffusion and convection effects, when the next fin is encountered. The effect of this non-uniform boundary condition for each fin is to reduce the heat transfer from the fin as compared to an entrance region model. However, the offset fin heat transfer is still considerably greater than that for a continuous fin of the same area.

Two-dimensional predictions of the velocity and temperature fields in an offset fin geometry with zero thickness fins are plotted in Figures 4-2 to 4-4 , based on data from Sparrow et al. (1977). Figures 4-2 and 4-3 show the velocity and temperature profiles, at positions 1 and 2 in Figure 1-1, in the periodic fully developed region. Figure 4-4 shows the temperature profiles, at positions 1 and 2 in Figure 1-1, in the hydraulic and thermal entrance region. The influence of the upstream fins on the downstream fins is evident in the temperature and velocity traces. This influence tempers the heat transfer benefit of the offset fin geometry. However for real fins of finite thickness, Joshi and Webb (1987) and Mochizuki and Yagi (1988) found that small vortices are formed after each fin at sufficiently high Reynolds number. The mixing of the fluid caused by the swirling flow reduces the temperature nonuniformity seen by the downstream fin. The average Nusselt number for the entrance region of a rectangular duct was computed by Montgomery and Wilbulswas (1967). A data regression was performed on their results to yield an equation of the form

$$Nu_F = f(Pr, x^*, \alpha) \tag{4.37}$$

The data of Montgomery and Wilbulswas cover a range of dimensionless thermal

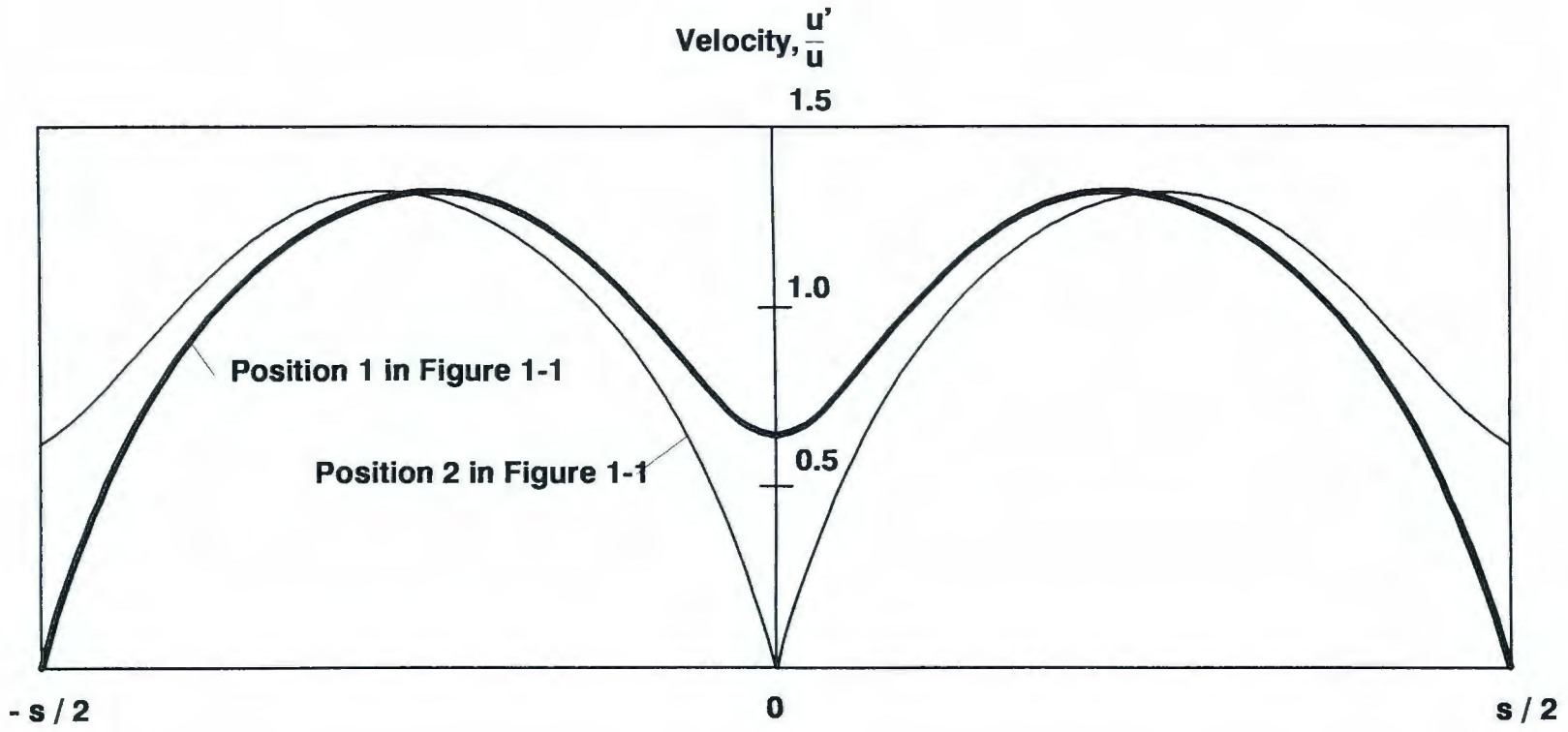

Figure 4-2 Calculated Velocity Profiles in Periodic Fully Developed Two Dimensional Flow in an Offset Fin Array, Re=1600, Pr=0.7 (Sparrow et al., 1977)

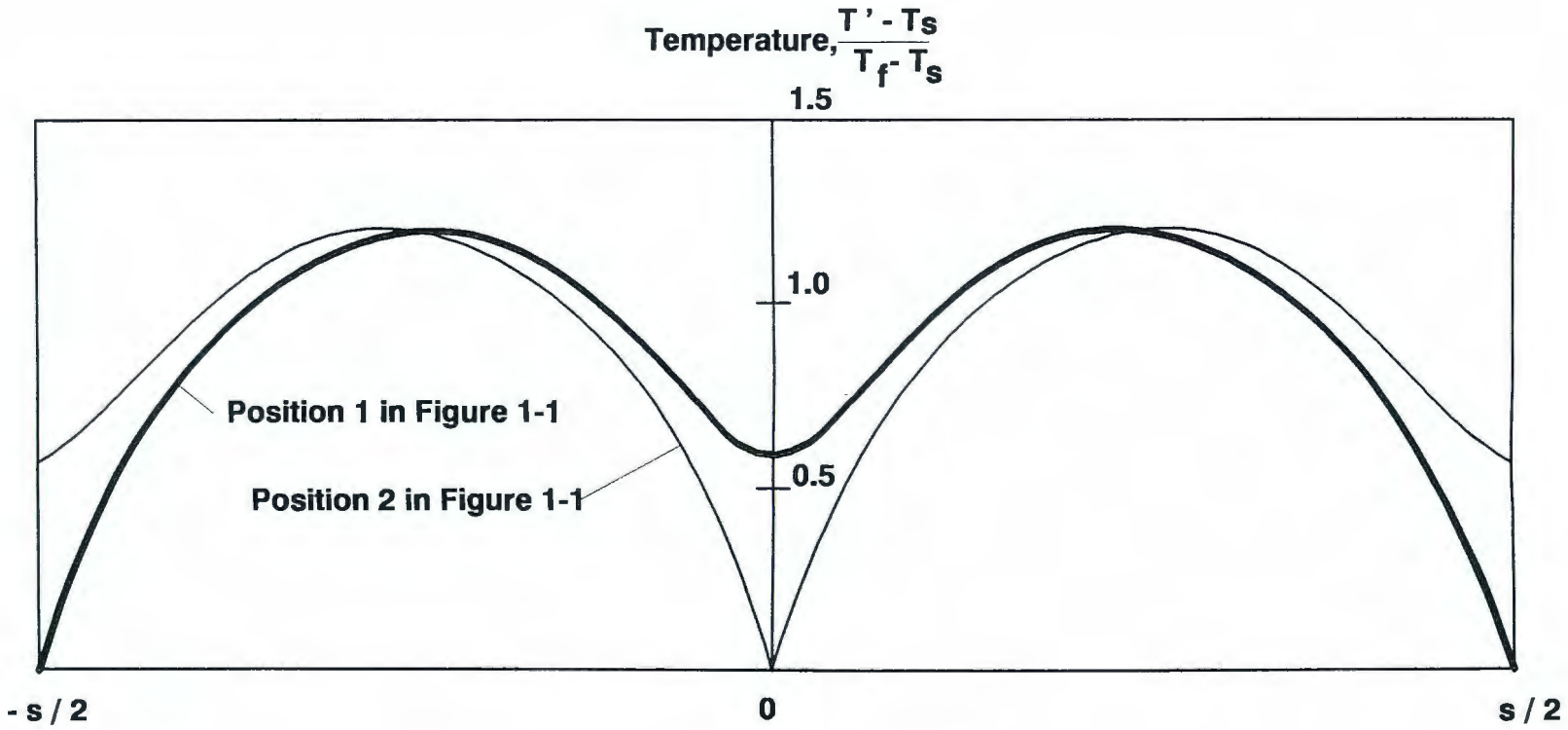

Figure 4-3 Calculated Temperature Profiles in Periodic Fully Developed Two Dimensional Flow in an Offset Fin Array, Re=1600, Pr=0.7 (Sparrow et al., 1977)

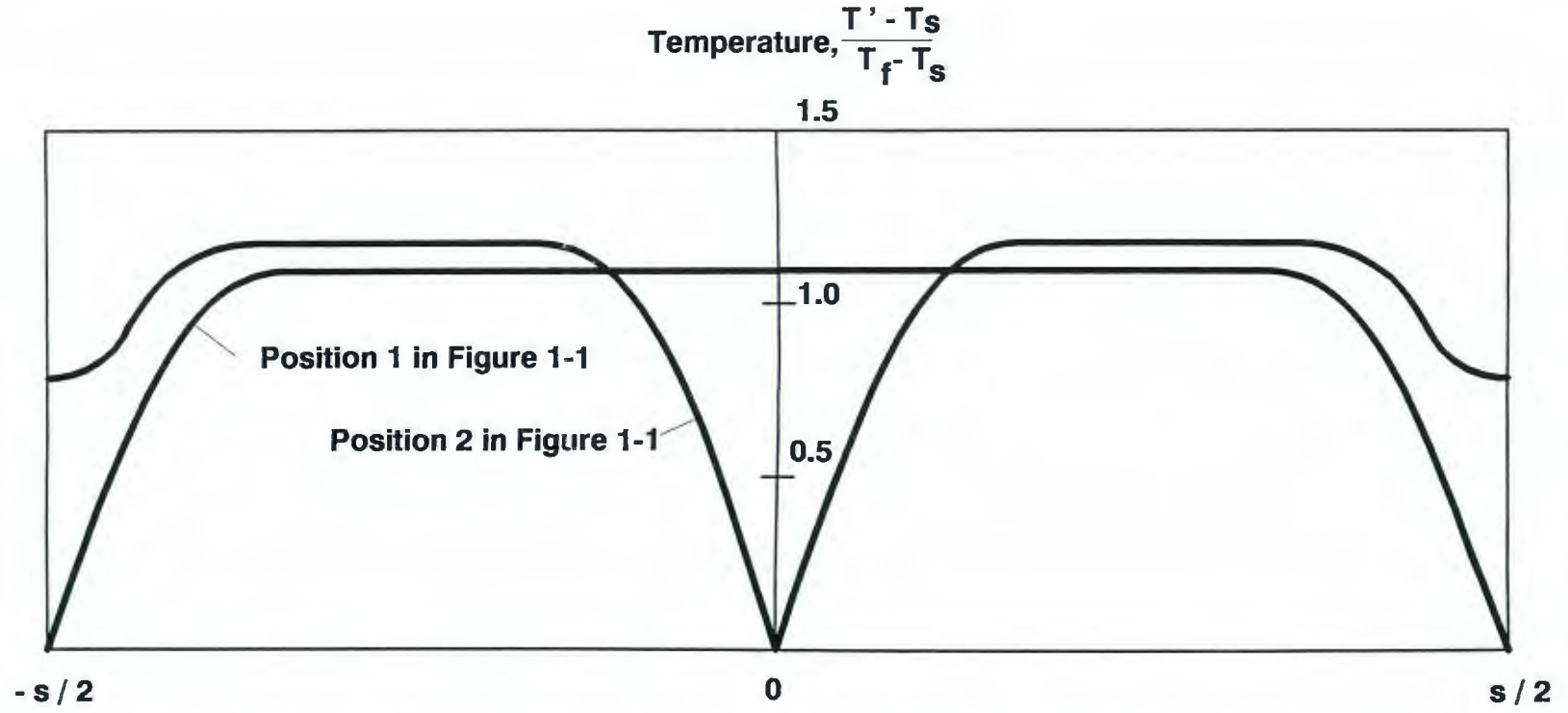

Figure 4-4 Calculated Temperature Profiles in Thermally Developing Two Dimensional Flow in an Offset Fin Array, Re=1600, Pr=0.7 (Sparrow et al., 1977)

length of 0.0025 to 0.5. The model was extended to match the fully developed characteristics and the data were linearly extrapolated down to a dimensionless length of 10^{-5}. Figure 4-5 shows the comparison of data regression results with the original data (Montgomery and Wilbulswas, 1967). Considering the influence of the nonuniform fluid temperature and velocity at the beginning of each fin, this result was modified into the form

$$Nu_F = f\,(Pr,\ x^*_F,\ \alpha,\ X_{rl}) \tag{4.38}$$

The final form of Nu_F is given in Appendix D, Table D-3. The factor X_{rl} is introduced to reduce the effective development length along a fin. This factor was determined from our experiments to have the form

$$X_{rl} = 3.63346 + 6.6725 \log_{10}\left(Pr\left(\frac{D_h}{l}\right)^{0.15}\right) \tag{4.39}$$

It is well known that for a high Prandtl number fluid, the thermal boundary layer develops much slower than the hydrodynamic boundary layer, because the thermal diffusivity is relatively low compared to the momentum diffusivity. In the offset fin geometry, a large Prandtl number causes larger temperature nonuniformities at the beginning of each row of fins. The fin geometry ratio D_h/l also influences the temperature nonuniformity. Shorter fin length and larger hydraulic diameter tend to cause larger temperature nonuniformity. In Equation 4.39, it is seen that X_{rl} increases with both Prandtl number and D_h/l. From Table D-3, it can be seen that an increase in X_{rl} means an increase in the effective dimensionless fin length, which implies decreased average heat transfer.

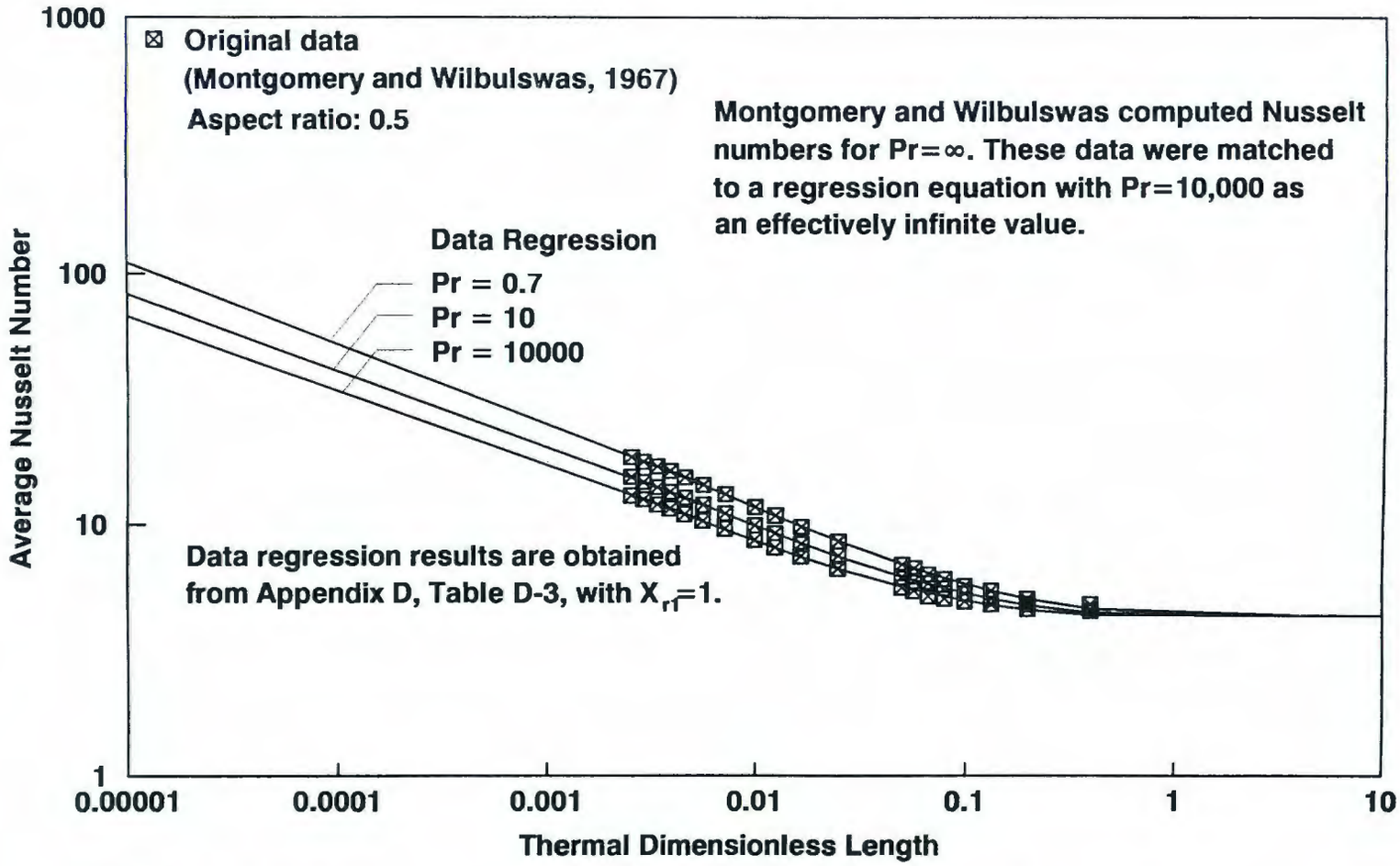

Figure 4-5 Data Regression of Average Nusselt Number in Rectangular Ducts and Original Data

In Equation 4.38, Nu_F is the average Nusselt number on the fin sides of one unit cell. This model for Nu_F applies to the periodic fully developed flow regime. Due to the interruptions of the thermal boundary layer on the fins, the periodic fully developed heat transfer is higher than that of fully developed flow in a comparable rectangular duct. Different from rectangular ducts, the Nusselt number for periodic fully developed heat transfer in an offset fin array is influenced by both Reynolds and Prandtl numbers. This point is returned to after discussion of entry length considerations from the array perspective.

4.3.2 Prandtl Number Effects from the Array Perspective

When air flows into an offset fin array with a uniform velocity profile, the flow achieves periodic fully developed velocity and temperature profiles after less than 10 fin lengths depending on Reynolds number (Sparrow et al., 1977). For a high Prandtl number fluid, however, the thermal field development occurs over a greater length. Eventually, a periodic fully developed temperature field does develop, but for high Prandtl number fluids the cold plate characteristics are significantly impacted by entry length effects when the flow is laminar.

The heat transfer in the offset fin entrance region is simulated here analogous to entrance region heat transfer in rectangular ducts. Sparrow et al. (1977) and Kelkar and Patankar (1989) used numerical calculations to simulate the thermal entrance region in an offset fin array using air. A comparison of the thermal entry length between their work and rectangular ducts is shown in Table 4-2, where the dimensionless thermal entry length of a rectangular duct is 0.05 with constant wall

Table 4-2
Comparison of Thermal Developing Length Between Offset Fin Array and Rectangular Duct (air)

	Sparrow et al. (1977)	Kelkar and Patankar (1989)
x^{r*}/x^{*}	10	9.5

temperature (Shah and London, 1978).

The comparison shows that the thermal entrance length of the offset fin geometry is about 10% of that in a rectangular duct. There are two effects causing the entry length to be shorter in the fin geometry as compared to a rectangular duct. One effect is associated with the definition of the hydraulic diameter, D_h^r, where the channel width is chosen as s. From an entry length perspective, the effective channel width is more like s/2 since the temperature boundary layers form on all fins and they meet in the middle of each channel of width s/2. This accounts for a factor of two difference in the entry length. Another factor which significantly reduces the thermal entry length for the offset fin geometry is the convection of energy associated with the transverse velocity component. Due to the periodic geometry of the fins in the flow direction, the velocity boundary layer formation causes the transverse velocity to fluctuate around zero. This transverse convection has a mixing effect which increases the transfer of energy into the bulk flow and results in a shorter entry length. Both factors make the thermal entry length shorter than that of the rectangular duct. As mentioned above, all known thermal entry length calculations for the offset fin geometry are based on air. For the high Prandtl number fluids of interest in the

current study, no entry length calculations were found in the literature. For the present model, it is assumed that the dimensionless thermal entry length is 10% of that of a rectangular duct. This effect is represented by a reduction factor, $X_{r2}=10$, in later equations.

Developing heat transfer in a rectangular duct was calculated by Montgomery and Wilbulswas (1967). These results are used in the present study, modified based on the above entry length discussion, to yield a function of the form

$$Nu_x^m = f\,(Pr,\ x^*,\ \alpha,\ X_{r2}) \qquad \textbf{(4.40)}$$

The data regression form of Nu^m_x is found in Table D-4 of the Appendix D. The Montgomery and Wilbulswas's results cover a range of x^* from 0.01 to 0.25. Similar to the average Nusselt number case of Figure 4-5, the model was extended on both ends to cover the x^* range 10^{-5} - 10. Figure 4-6 shows the comparison of the data regression results with the original data. The thermal field development from the array perspective affects the heat transfer on all fin surfaces, including fin sides and top and bottom surfaces. This point is returned to in the discussion section which follows.

4.4 Discussion of the Surface Contribution Model Results

In Figures 4-7 and 4-8, the predicted Nusselt number on the fin sides is plotted versus plate length with different Prandtl numbers at two Reynolds numbers for Plate 3 as a representative geometry. In the figures, the abscissa is the distance from the inlet of the fin array. The ordinate is the local Nusselt number of the fin sides averaged over one unit cell. From Equations 4.34, 4.35, 4.38 and 4.40, the Nusselt

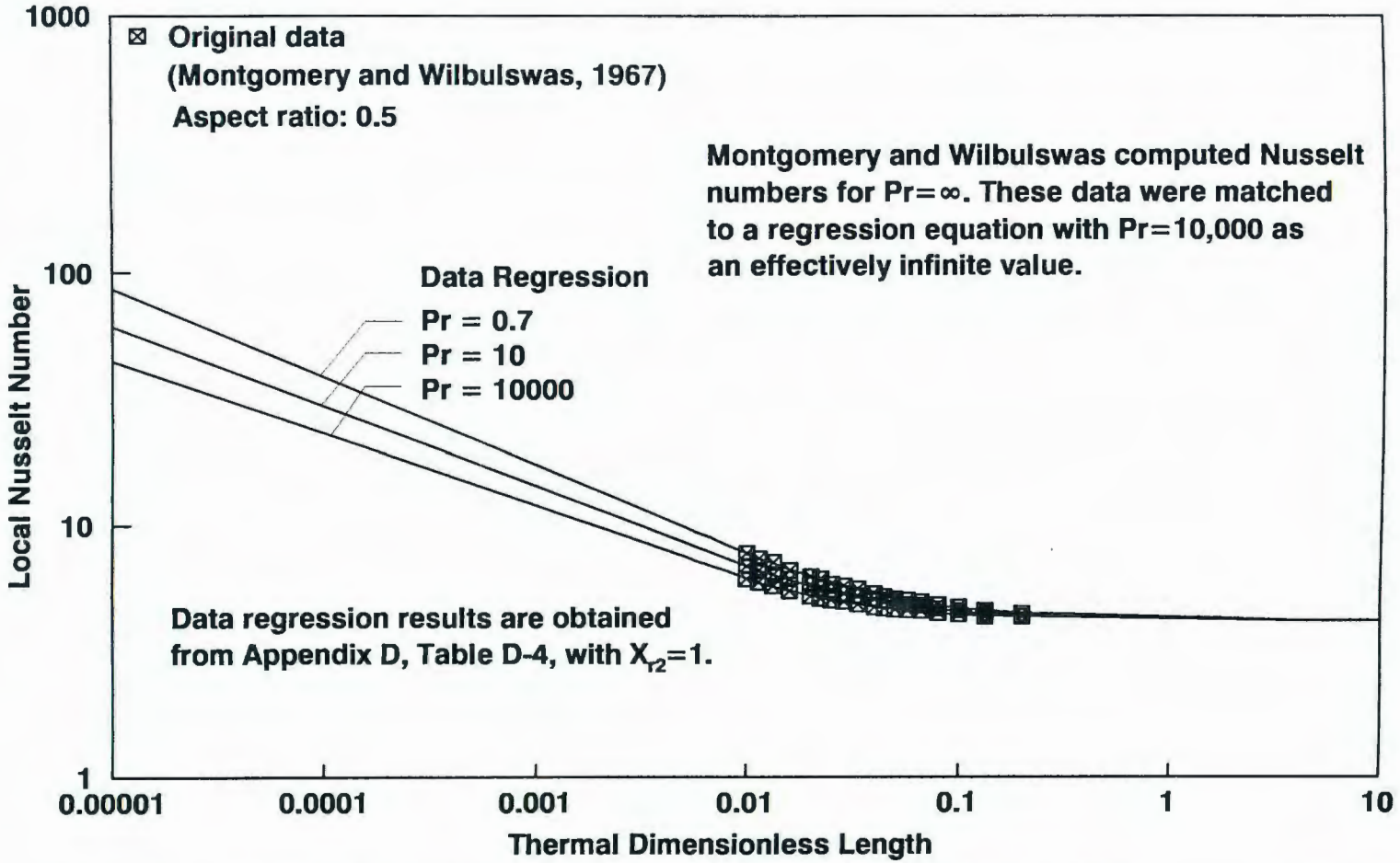

Figure 4-6 Data Regression of Local Nusselt Number in Rectangular Ducts and Original Data

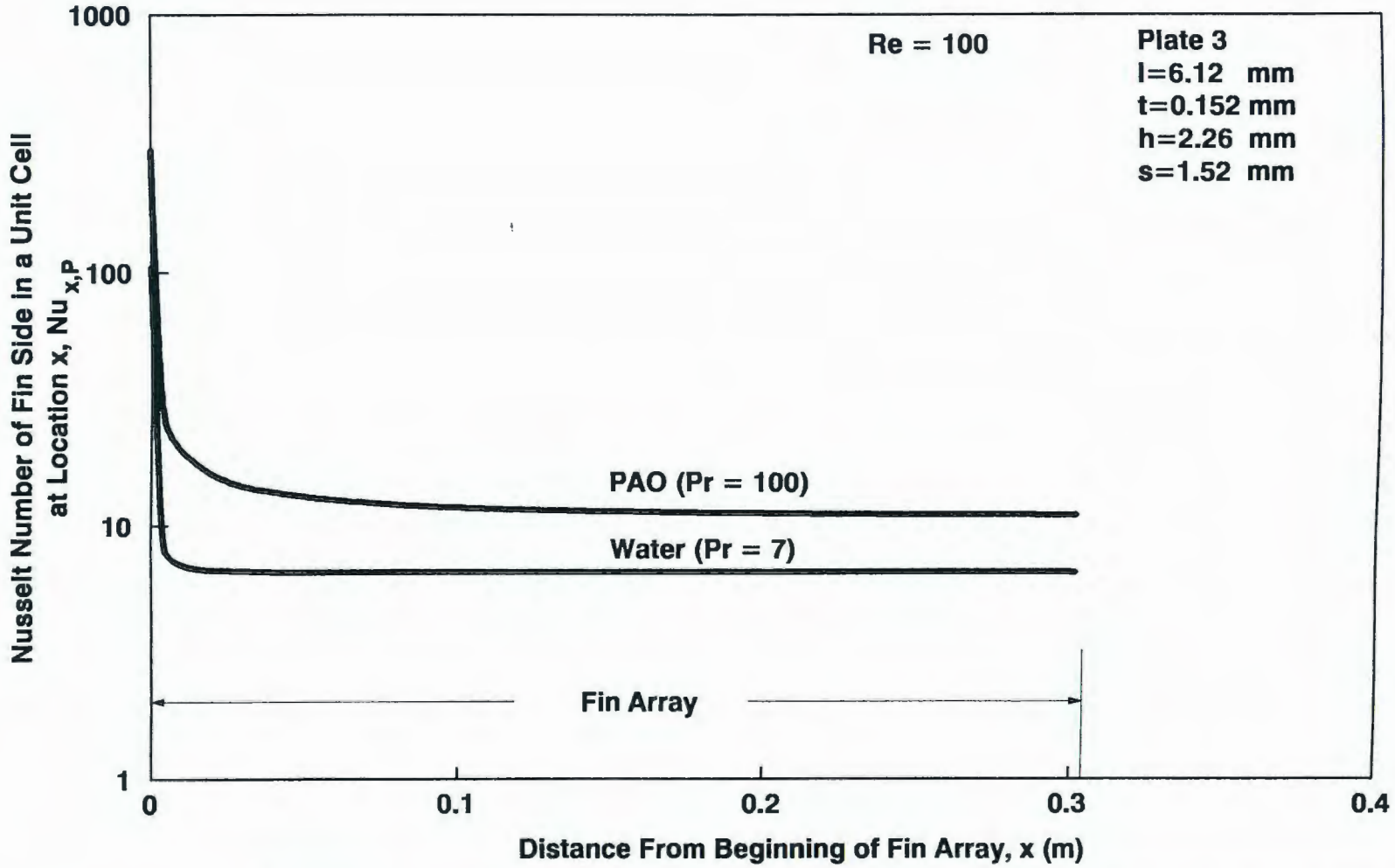

Figure 4-7 Thermal Development from the Array Perspective for Re=100

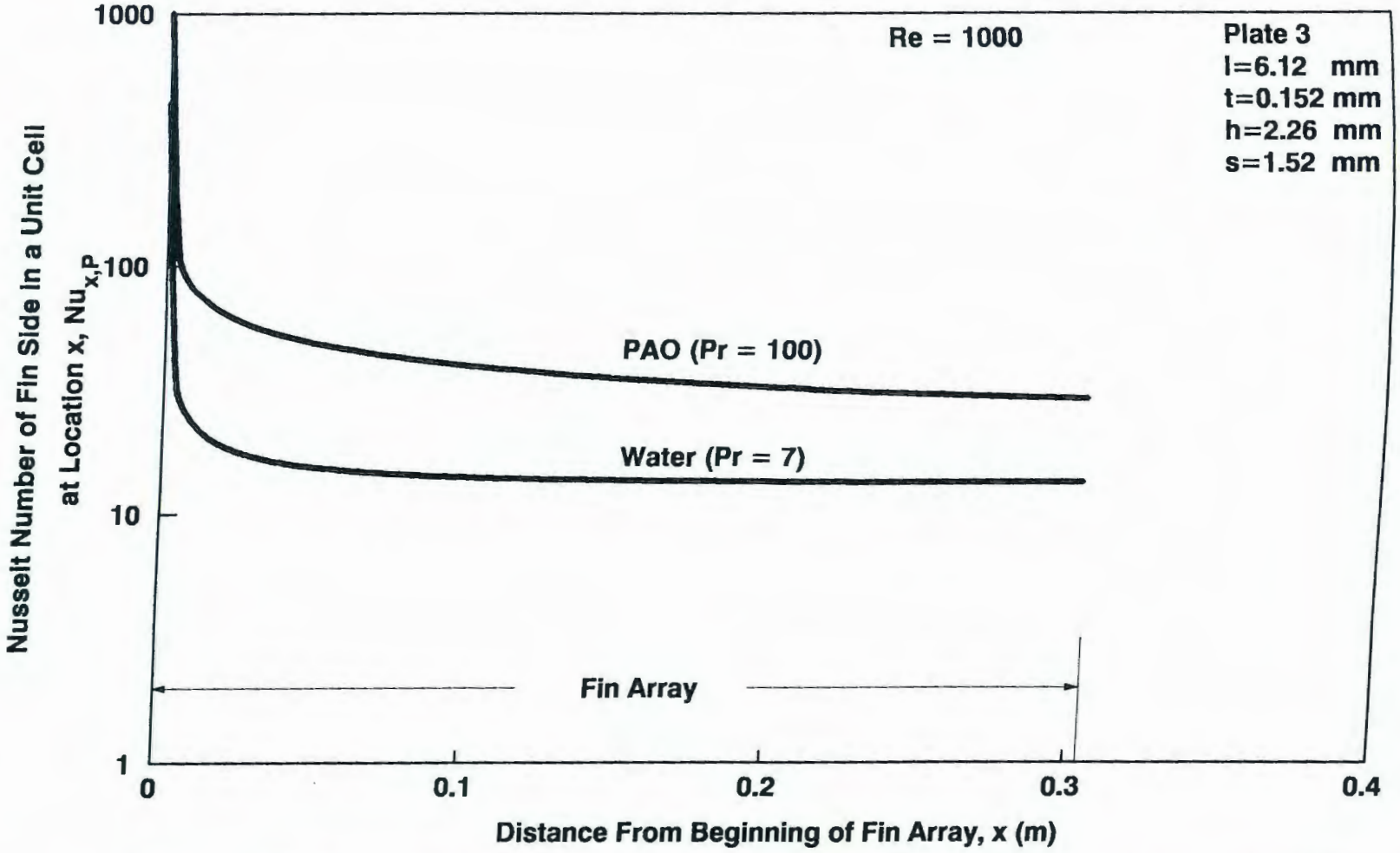

Figure 4-8 Thermal Development from the Array Perspective for Re=1000

number on the fin sides is seen to be influenced by Reynolds number, Prandtl number and fin geometry. It is observed that the array perspective effects have a significant influence on the heat transfer performance when Reynolds and Prandtl numbers are large. At the entrance of the fin array, the Nusselt number is high because of the thermal field development. Along the fin array, the thermal field develops until it reaches the periodic fully developed condition. A larger Prandtl number implies a longer distance to achieve a periodic fully developed thermal field (array perspective effects). Unlike the fully developed heat transfer in a continuous duct, the periodic fully developed Nusselt number for the offset fin geometry is dependent on Prandtl number. This is because the offset fin interrupts the flow periodically, causing a thermal boundary layer to develop on each fin. Therefore due to the periodic interruptions in the fins, the heat transfer in the periodic fully developed regime is influenced by both Reynolds and Prandtl numbers. The flow with larger Prandtl number has a longer thermal developing region on each fin, which achieves a higher average heat transfer over the fin (fin perspective effects).

Comparing Figures 4-7 and 4-8, it can be seen that a larger Reynolds number increases the Nusselt number from both the fin and the array perspectives. From the array perspective, an increase in Reynolds number extends the thermal entry length. From the fin perspective, a larger Reynolds number extends the high Nusselt number region on each fin by reducing the boundary layer thickness causing a higher periodic fully developed Nusselt number. Figure 4-7 displays a case with relatively small Reynolds and Prandtl numbers and the thermal field development from the array

perspective has a relatively small effect on overall heat transfer (bottom curve). In contrast, Figure 4-8 displays a case with large Reynolds and Prandtl numbers which is affected by thermal development from both the array and fin perspectives (top curve). These characteristics are integrated into the surface contribution model to predict the overall heat transfer.

CHAPTER 5

NUMERICAL STUDY - THERMAL SPREADING AND END EFFECTS

The experiment was designed to apply an approximately constant heat flux to the cold plate. Thus, the surface temperatures increase in the flow direction, which causes minor heat conduction in the heater assembly and cold plate. This effect is called thermal spreading in the following discussion. Conduction effects also exist in the unheated end sections, which are termed the end effects. End effects and thermal spreading in a similar geometry are discussed by Philips (1988), who applied constant heat flux on liquid cooled microchannel heat sinks. To estimate these effects, a numerical heat transfer model, called the spreading model, was created to predict system temperatures and heat flux distribution.

The spreading model is based on a two-dimensional cross section of the geometry of a cold plate as shown in Figure 5-1a. The finite difference model is designed to calculate the temperature distribution and heat transfer in the section A-B-C-D, which models the aluminum cover plate. Surface B'-C' is heated by the main heater. Surfaces A-B, C-D, B-B' and C-C' are insulated.

5.1 Principal Equation

Two dimensional conduction in the plate is modeled assuming constant thermal conductivity of the plate. For this situation, the plate temperature field obeys the Laplace equation. For the calculation, this equation was discretized using a constant

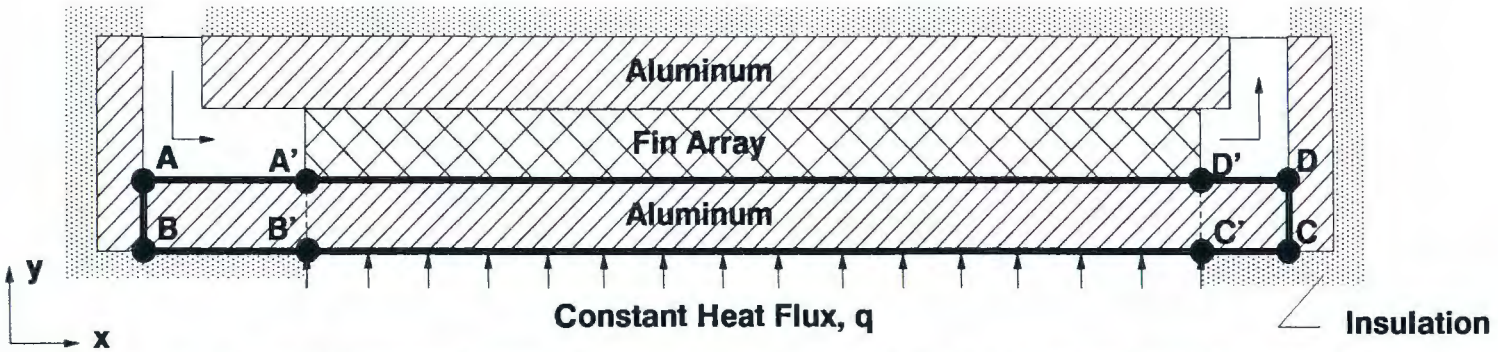

a. Two Dimensional Cross Section of Cold Plate (not to scale)

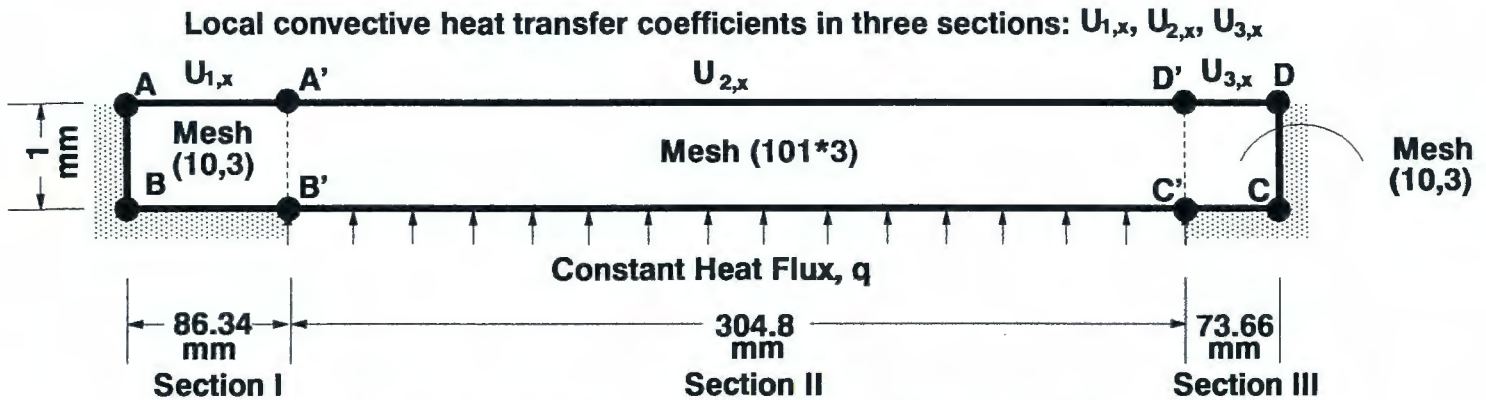

b. Simplified Calculation Domain (not to scale)

Figure 5-1 Geometry Used in Thermal Spreading Model

$$\frac{\partial^2 T}{\partial x^2} + \frac{\partial^2 T}{\partial y^2} = 0 \qquad (5.1)$$

volume formulation which is inherently conservative.

5.2 Boundary Conditions

5.2.1 Convective Boundary Conditions on Unfinned Section

Surface A-A' experiences convective heat transfer, which is treated as developing flow between two infinite parallel plates (Shah and London, 1978). The dimensionless thermal entry length at the location x' is defined as

$$x^{P*} = \frac{x'}{D_h^P \, Re^P \, Pr} \qquad (5.2)$$

where the superscript P stands for the parallel plate channel and x' is the distance from the beginning of Section I. Then the Nusselt number for the channel has the form

$$Nu_x^P = f\,(x^{P*}) \qquad (5.3)$$

Table D-5 in the Appendix D lists the formula from Shah and London (1978) used to calculate Nu_x^P. The local overall heat transfer coefficient in area A-A', $U_{1,x}$ is

$$U_{1,x} = \frac{Nu_x^P \, k}{D_h^P} \qquad (5.4)$$

In Section III, laminar developing heat transfer is also assumed as that in Section I. Therefore the local overall heat transfer coefficient in area D-D', $U_{3,x}$ can be obtained by replacing x' as x''' in Equation 5.4.

The total heat transfer from these end sections is a small fraction (less than

1.9%) of the total heat transfer in the cold plate. Thus an approximate model for these sections is adequate for the purpose of calculating the overall heat transfer.

5.2.2 Convective Boundary Condition in Finned Section

Surface A'-D' represents the fin array. The extended surface is modeled as an effective Nusselt number. The Nusselt number is influenced significantly by thermal development in the fin array. A model for the effective, local, fin-average heat transfer coefficient of the offset fin array h_x, is given by the model proposed in Chapter 4. The local fin-average overall convective heat transfer coefficient on the finned surface A'-D', $U_{2,x}$ has the form

$$U_{2,x} = \frac{h_x A \eta}{A_2} \tag{5.5}$$

where heat transfer surface efficiency η is obtained from Equation 4.26.

5.2.3 Other Boundary Conditions

Referring to Figure 5-1b, the boundary condition imposed on surface B'-C' is a uniform heat flux boundary condition

$$-k_A \frac{\partial T}{\partial y} = q \tag{5.6}$$

where q is the heat flux from the main heater. Surfaces A-B and C-D are insulated so that

$$\frac{\partial T}{\partial x} = 0 \tag{5.7}$$

and surfaces B-B' and C-C' are insulated so that

$$\frac{\partial T}{\partial y} = 0 \tag{5.8}$$

5.3 Calculation Procedure

The difference equations consist of a coupled set of linear algebraic equations in the unknown temperatures. The discretized Laplace equation has the form

$$A_1 T_{i,j} + A_2 T_{i+1,j} + A_3 T_{i+1,j+1} + A_4 T_{i+2,j+1} + A_5 T_{i+2,j+2} = C \qquad \textbf{(5.9)}$$

where i is the grid number in x direction ranging from 1 to 119 and j is the grid number in y direction ranging from 1 to 3. For the current numerical model scheme, fluid temperature is represented by the values of grids with j=4.

$$T_f(i) = T_{i,4} \qquad \textbf{(5.10)}$$

The fluid temperature distribution is obtained by an energy balance on the fluid. The Gauss-Seidel method was used to solve the coupled set of equations iteratively. During the iteration process, the temperature difference between two successive iterations is evaluated for each node. The convergence criterion for the iteration is the maximum temperature difference must be less than 10^{-10} °C. When the calculated results between two iterations is smaller than the convergence criterion, the iteration stops. In order to accelerate the convergence of the iteration, initial guess values for the temperatures are carefully selected. According to the heat input, the initial fluid temperatures are assigned a linear variation, which corresponds to uniform heat flux and constant fluid properties. Initial guess values for surface temperature are assigned equal to the fluid temperature at the same x position. Because of the large aspect ratio of the flat plate geometry, the convergence of the calculation takes about 10000 iterations, which entails approximately 25 minutes on an IBM-PC 386 running at 33 MHz.

5.4 Discussion of Spreading Model Results

Program inputs include coolant flow rate, heating power and inlet coolant temperature. In a typical analysis, data from an experimental run were input to the model in order to compare the model predictions against experimental surface temperatures. The average fluid temperature was used to calculate the fluid thermal properties. The model was run for each of the experimental runs. In the final version discussed here, the convective heat transfer coefficients for the offset fin array were obtained from the experimental data. Therefore, the numerical model predicts the surface temperature distribution quite well. The real value of the model is that it reveals the relative importance of the heat transfer mechanisms in an offset fin cold plate. In addition, the model was used to help interpret the experimental surface temperature data.

The conductive and convective heat transfer are calculated by the numerical model. The results presented here are representative of the predictions of the model. The discussion here is based on Plate 3 as a representative geometry. All the other plates have similar distribution of surface temperature and heat flux. Two cases with similar Reynolds numbers are selected to show the Prandtl number effect on the distributions of heat flux and surface temperature. Figures 5-2 and 5-3 show the heat flux distribution versus plate length in the flow direction for Plate 3. Figure 5-2 represents the case with a Reynolds number of 245 and Prandtl number of 140. Figure 5-3 represents the case with Reynolds number of 285 and Prandtl number of 3. In the figures, the abscissa is the position along the cold plate and the ordinate is the heat

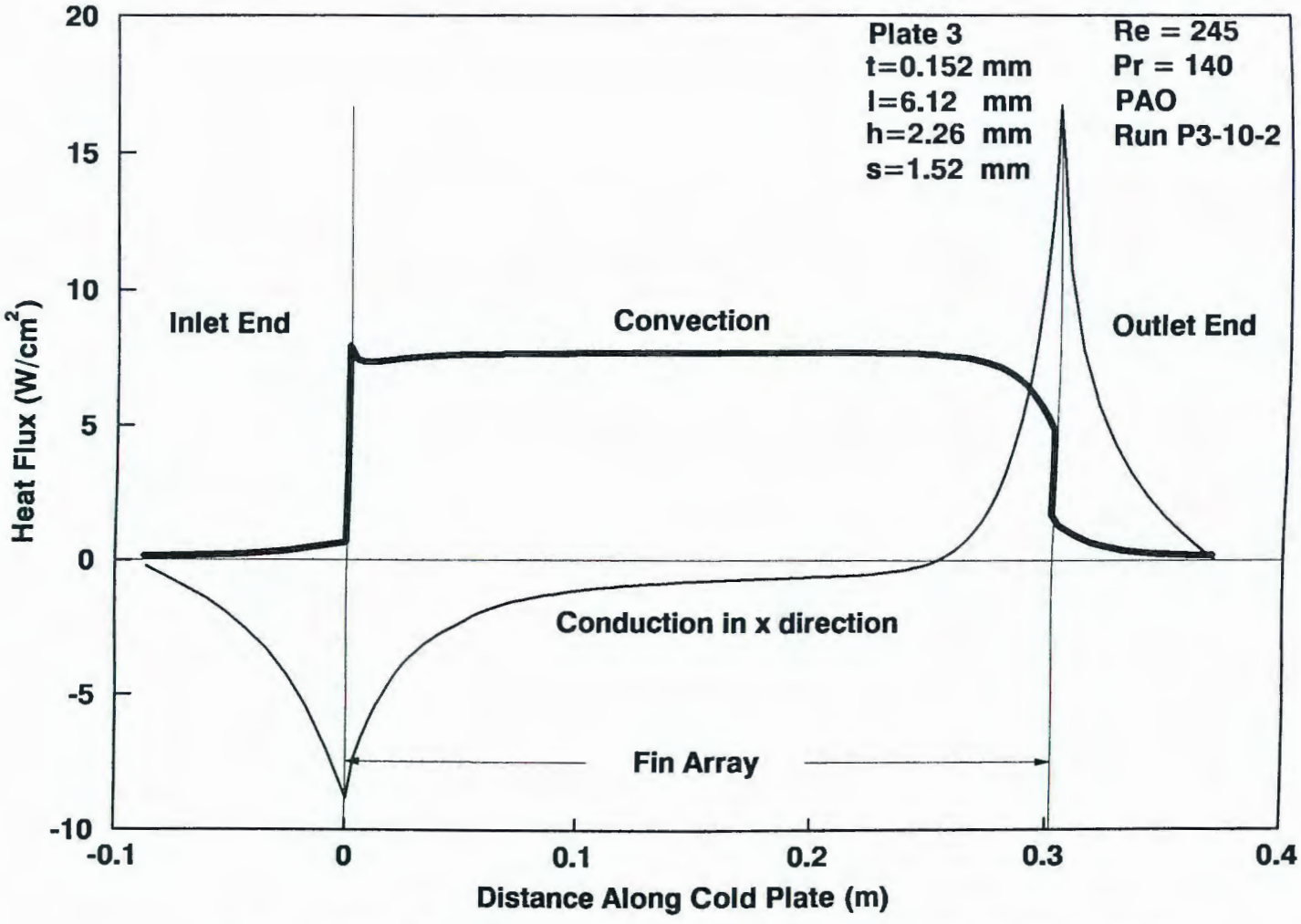

Figure 5-2 Calculated Heat Flux in Plate 3 for Pr=140

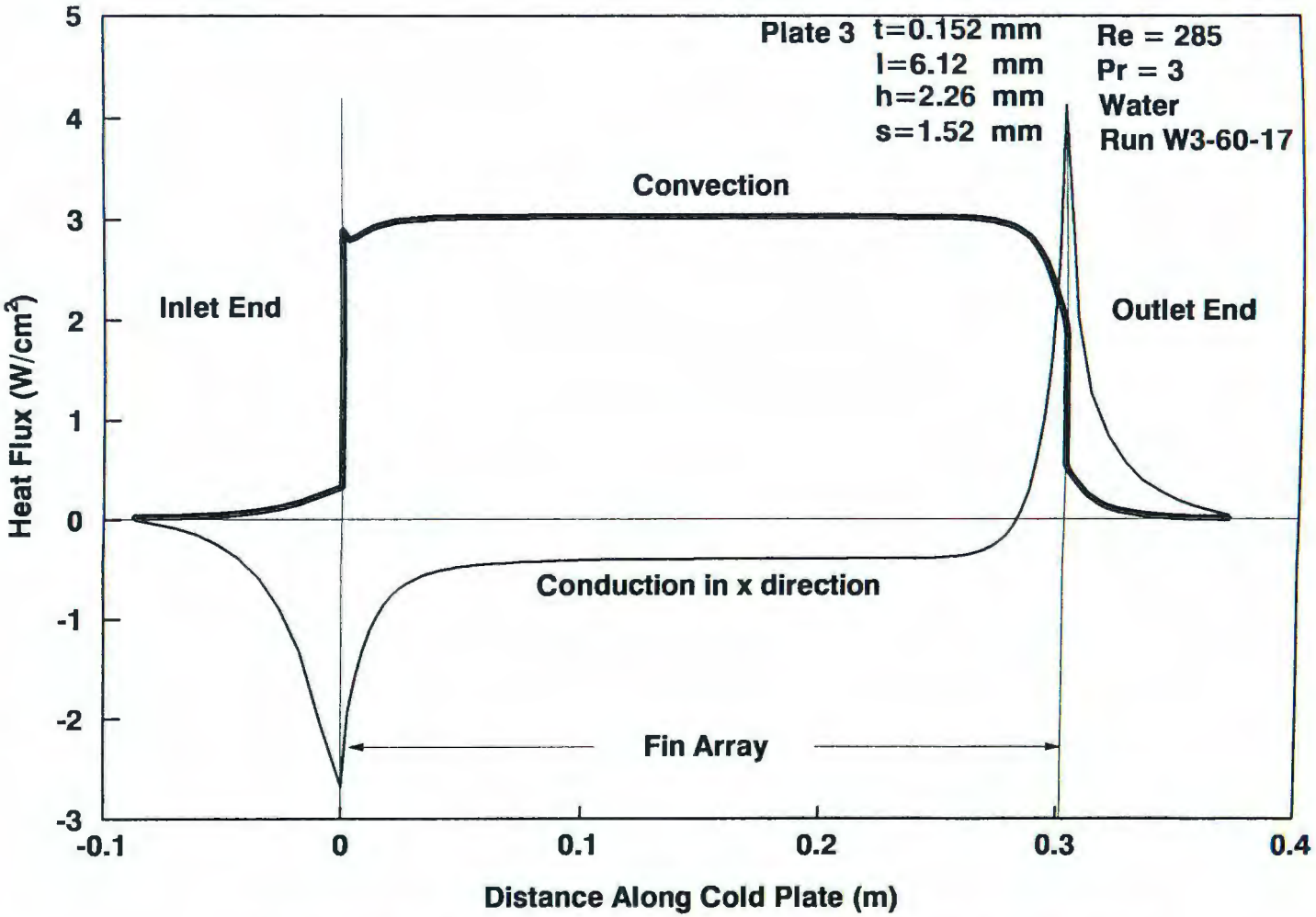

Figure 5-3 Calculated Heat Flux in Plate 3 for Pr=3

flux. The thin line represents the conductive heat flux in the x direction and thick line is the convective heat flux. It should be noted that the two fluxes are based on different areas and thus cannot be compared directly. It can be seen that conduction effects are relatively large at both ends of the heated section (which corresponds to the fin array), due to the large temperature gradients existing between the heated and unheated regions. The conduction at both ends influences the convection through the surface temperatures, causing non-uniform heat flux near the ends. The results indicate that end effects are significant for approximately 0.03 m at the inlet and 0.07 m before the exit of the fin array.

The shape of the convective curve at the inlet end of the fin array is due to two factors. The initial peak and following drop off is due to the shape of the heat transfer coefficient as the flow approaches a periodic fully developed regime. The minimum in the curve is due to conduction (end effect) transferring heat to the unheated inlet region, which decreases the surface temperatures and reduces the convective heat transfer. At the exit end of the fin array, the convective heat flux drops, which is also due to the end effect where conduction to the unheated exit region is important. Sufficiently far from both ends, the calculations indicate an essentially constant convective heat flux over the central section of the fin array.

Thermal spreading (i.e. conduction) is present in the finned region but it is not particularly important. Compared to the end effects, the effect of thermal spreading in the central section is small. At the center of the cold plate, the conduction heat transfer rate is only 0.2% of the total power input for the cases shown here.

Figures 5-2 and 5-3 show similar convective heat flux distributions along the fin array. These results support the assumption of constant heat flux used in our data analysis. The results of the model were used as a guide in isolating end effects from the data. As was already noted, the convection and conduction heat fluxes are based on different heat transfer areas. The conduction heat transfer area is the cross section area of the cold plate, which is much smaller than the convection area. Thus, the total convection heat transfer is much larger than the conduction heat transfer in the x direction. For example, for the case shown in Figure 5-2, the conduction heat transfer rate at the center of the plate is 3 W, while the convection heat transfer rate is 1500 W. However, at the outlet end, the conduction rises to a peak value of 33 W.

Comparisons between the numerical model predictions and experimental data for the surface temperatures for the same two cases are shown in Figures 5-4 and 5-5. It can be seen that the experimental surface temperatures exhibit the same trend as the model results. The lower surface temperature at the beginning of the fin array is caused by end effects due to conduction, and by the effect of developing convective heat transfer. It can be seen that the surface temperatures in the inlet and exit regions are higher than the fluid temperature, which is due to conduction from the heated area to the unheated area. This heat is then transferred to the fluid by convection. Due to the relatively low Nusselt number in the entrance and exit un-finned sections, the fluid temperature does not change significantly in these sections. In the heated section, the fluid follows closely a linear temperature distribution in the flow direction consistent with the approximately uniform heat flux. A linear fluid temperature distribution is

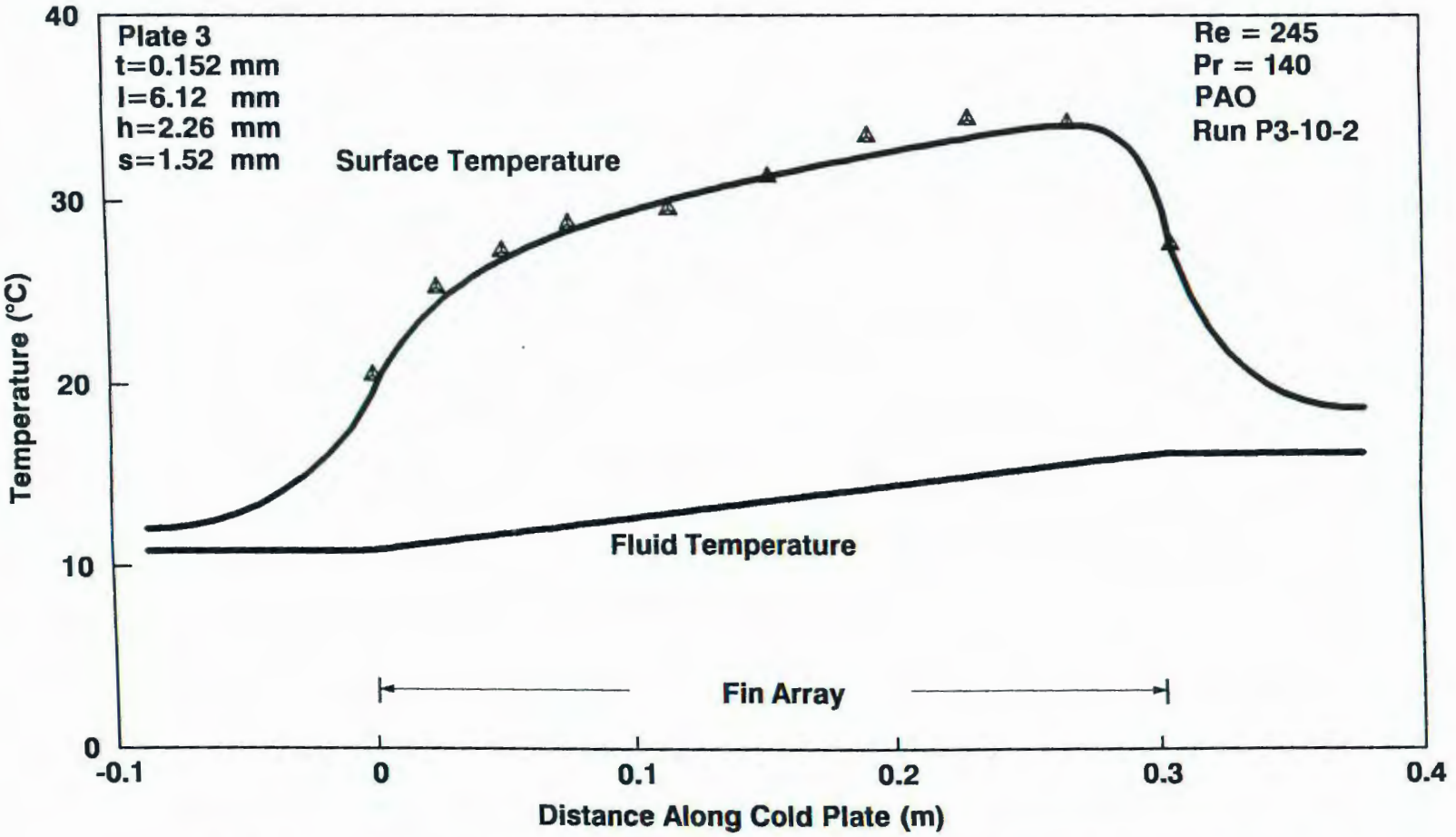

Figure 5-4 Cold Plate Temperatures from Spreading Model and Experiment (Plate 3) for Pr=140

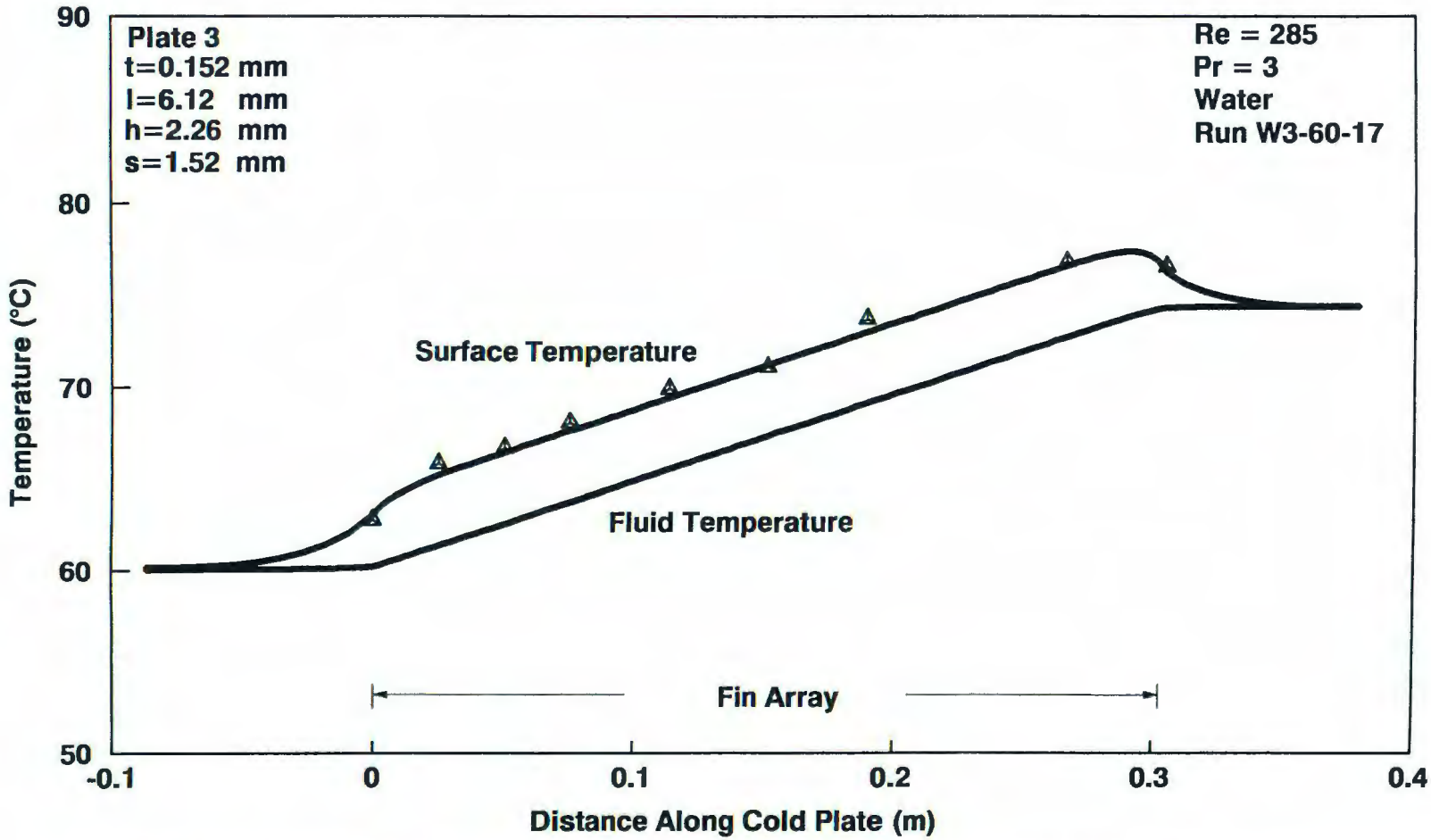

Figure 5-5 Cold Plate Temperatures from Spreading Model and Experiment (Plate 3) for Pr=3

assumed in the experimental data reduction.

Figure 5-4 represents the case with Reynolds number of 245 and Prandtl number of 140. For these Reynolds and Prandtl numbers, thermal development is important in the heat transfer in the fin array. In the entry region of the fin array, the convective heat transfer coefficient is high due to thermal development effects. In Figure 5-4, it can be seen that the difference between the surface and fluid temperatures in the developing region is smaller than that near the exit. Figure 5-5 represents the case with Reynolds number equal 285, which is similar to that in Figure 5-4, and Prandtl number of 3. The figure shows that the thermal development effect is relatively small. For this case, the temperature difference between the surface and fluid is approximately constant over the length of the fin array.

CHAPTER 6

RESULTS AND DISCUSSION

6.1 Data Reduction

The data reduction procedures to obtain heat transfer and friction factor data for the seven cold plates tested in the current study are based on the unit cell bounded by a-b-c-d, shown previously in Figure 1-1b (Page 4). The entire fin array can be considered as consisting of many such unit cells, which have the same geometry. To avoid the end effects in the fin array, the heat transfer analysis is based on a central section of fin array. For the purpose of finding the average heat transfer coefficient and friction factor in the fin array, each unit cell in the data reduction domain is assumed to have the same heat transfer coefficient and friction factor. The data reduction results of heat transfer and pressure drop are based on the hydraulic diameter defined in Equation 4.4. The hydraulic diameters of all the seven plates are listed in Table 6-1, where the fin geometry is also listed for reference. A total of 511 tests were performed on the seven cold plates with fluids water and PAO. The experimental results are summarized in Appendix E, which provides test data of the seven offset fin cold plates for the fluid Prandtl number ranging from 3 - 150.

6.1.1 Heat Transfer Data

It should be realized that in the inlet section the local cell-average heat transfer coefficient decreases along the length in the flow direction. As the flow approaches a periodic fully developed regime, the heat transfer coefficient approaches a constant

Table 6-1 Fin Geometry and Hydraulic Diameter

Cold Plate	Fin Thickness mm	Fin Length mm	Fin Height mm	Fin Spacing Distance mm	Hydraulic Diameter mm
1	0.152	3.20	2.39	0.99	1.351
2	0.152	3.18	2.34	1.65	1.881
3	0.152	6.12	2.26	1.52	1.790
4	0.152	3.33	3.84	1.28	1.849
5	0.152	3.40	2.36	1.26	1.596
6	0.102	3.33	2.36	1.55	1.836
7	0.152	3.33	3.84	1.62	2.211

value. The entry length effect is shown in Figures 4-7 and 4-8. In the current data reduction, the heat transfer coefficient obtained from measured data, h_0, is the average value over a section of the fin array, which has higher heat transfer coefficient at the beginning of the section and lower heat transfer at the end. In the comparisons between measured and predicted data in this chapter, a consistent basis is used which accounts for the entry length effects.

The data analysis to compute h_0 is based on the unit cell, where the thermal resistance of the unit cell can be written as

$$\frac{1}{U\,A} = \frac{b}{A_2\,k_A} + \frac{1}{A\,\eta\,h_0} \qquad \textbf{(6.1)}$$

In Equation 6.1, the term on the left hand side represents the total thermal resistance between the heated surface and the bulk fluid, where U is the overall heat transfer coefficient. On the right hand side of Equation 6.1, the first term is the thermal

resistance of the aluminum cover plate with thickness b, where k_A is the thermal conductivity of aluminum. The second term is the thermal resistance associated with convection from the offset fins, where η is the heat transfer surface efficiency.

Different from an air cooled application, the resistance of the aluminum cover plate cannot be ignored, since the liquid fluids have significantly higher heat transfer coefficients. For example, when water is used as the fluid, the thermal resistance of the cover plate (for the geometries considered in this study) contributes up to 15% of the total thermal resistance. From Equation 6.1, the heat transfer coefficient, h_0, has the form

$$h_0 = \frac{1}{\eta} \frac{1}{\frac{1}{U} - \frac{b\,A}{k_A\,A_2}} \tag{6.2}$$

The overall heat transfer coefficient, U, is calculated from the data according to

$$U = \frac{Q}{\Delta T_{lm}\,A} \tag{6.3}$$

where ΔT_{lm} is the log mean temperature difference between the heated surface and the fluid. For a fluid with constant specific heat, the log mean temperature difference results from integrating the local temperature difference over a finite length (Sparrow et al., 1977). The log mean temperature difference is defined as

$$\Delta T_{lm} = \frac{(T_{s1}-T_{f1})-(T_{s2}-T_{f2})}{\ln(T_{s1}-T_{f1})-\ln(T_{s2}-T_{f2})} \tag{6.4}$$

where points 1 and 2 define the region sufficiently far from both ends as to isolate end

effects. The measured surface temperatures of points 1 and 2 are represented by T_{s1} and T_{s2}, respectively. The fluid temperatures corresponding to points 1 and 2 are calculated based on an assumed linear profile between the measured fluid inlet and outlet temperatures. The overall heat transfer coefficient for that section, U, can be calculated with Equation 6.3. The heat transfer surface efficiency, η, is related to the fin efficiency according to

$$\eta = 1 - \frac{A_{fin}}{A} (1 - \eta_{fin}) \tag{6.5}$$

The calculation of η_{fin} is based on the unheated surfaces of fin array defined in Equation 4.29. For data reduction purposes, the fin efficiency of unheated surfaces is calculated based on a one-dimensional fin model with an insulated tip. The area of the unheated plate (opposite to the heated plate) is lumped together with the fin area resulting in an effective fin height of (h+s). The fin efficiency expression can be written as (Incropera and Dewitt, 1990)

$$\eta_{fin} = \frac{\tanh(m\ (h+s))}{m\ (h+s)} \tag{6.6}$$

$$m = \sqrt{\frac{2\ h_0}{k_A\ t}} \tag{6.7}$$

From Equations 6.5 to 6.7, it can be seen that η and h_0 depend upon each other. For data reduction, an iterative calculation is performed by first assigning an arbitrary value of η (η=1) and calculating h_0. Then, based the new value of h_0, η is corrected.

The iterative calculation proceeds until both η and h_0 satisfy Equations 6.5 to 6.7.

The heat transfer performance evaluation is completed by transforming the average heat transfer coefficient, h_0, into a Nusselt number, Nu_0. An alternative dimensionless heat transfer coefficient often used for offset fin studies is the Colburn factor, j, defined as

$$j = \frac{Nu_0}{Re\ Pr^{1/3}} \tag{6.8}$$

where fluid properties are calculated at the mean fluid temperature in the cold plate.

6.1.2. Pressure Drop Data

From Kays and London (1984), the pressure drop across a cold plate has the form

$$\Delta P = \Delta P_{EN} + \Delta P_{FA} + \Delta P_{FF} + \Delta P_{EX} \tag{6.9}$$

where ΔP_{EN} represents the pressure drop due to entrance loss effects, ΔP_{EN} represents the pressure drop due to exit loss effects, ΔP_{FA} represents the pressure drop due to flow acceleration and ΔP_{FF} represents the pressure drop due to fin friction. The entrance and exit effects are quite small since the flow velocities are generally small. The flow acceleration pressure drop contains the factor of (ν_2/ν_1-1), where ν represents the specific volume of the coolant. Because the liquid coolants are essentially incompressible, (ν_2/ν_1-1) is very small and the acceleration factor is negligible. Therefore the pressure drop measured across the cold plate is essentially the pressure drop across the fin array. This pressure drop can be expressed in terms of the Fanning

friction factor, f, defined as

$$f = \frac{\Delta P_L \, D_h}{2 \, \rho \, u^2 \, L} \tag{6.10}$$

where ΔP_L is the pressure drop of the fin array with length L in the flow direction.

6.1.3 Repeatability of Experimental Results

Repeatability tests were conducted as a part of the effort to examine the reliability of the experimental data. For each fluid, two repeatability tests were performed on every plate at each fluid temperature. Figure 6-1 summarizes the 41 repeatability test results in terms of Colburn factor. For Colburn factor, it is found that all the repeatability tests are within ±20% of the original tests while 80% of the repeatability results are within ±10% of the original tests. Figure 6-2 shows the 41 repeatability test results in terms of Fanning friction factor. For the friction factor, all the repeatability results are within ±20% of the original tests while 85% of the repeatability test results are within ±10% of the original test results.

The repeatability tests are affected by the stability of experimental instrumentation and test system. The experimental instrumentation consists of all measurement transducers, including thermocouples, pressure transducer, turbine flow meters and power transducer. The test system includes the controls of flow rate and heating power and inlet fluid temperature. Because of the drift in flow rate, heating power and inlet fluid temperature in the test system, the test system is the important factor affecting the repeatability results. The results of the repeatability tests led to a number of quality control procedures designed to minimize the deviations.

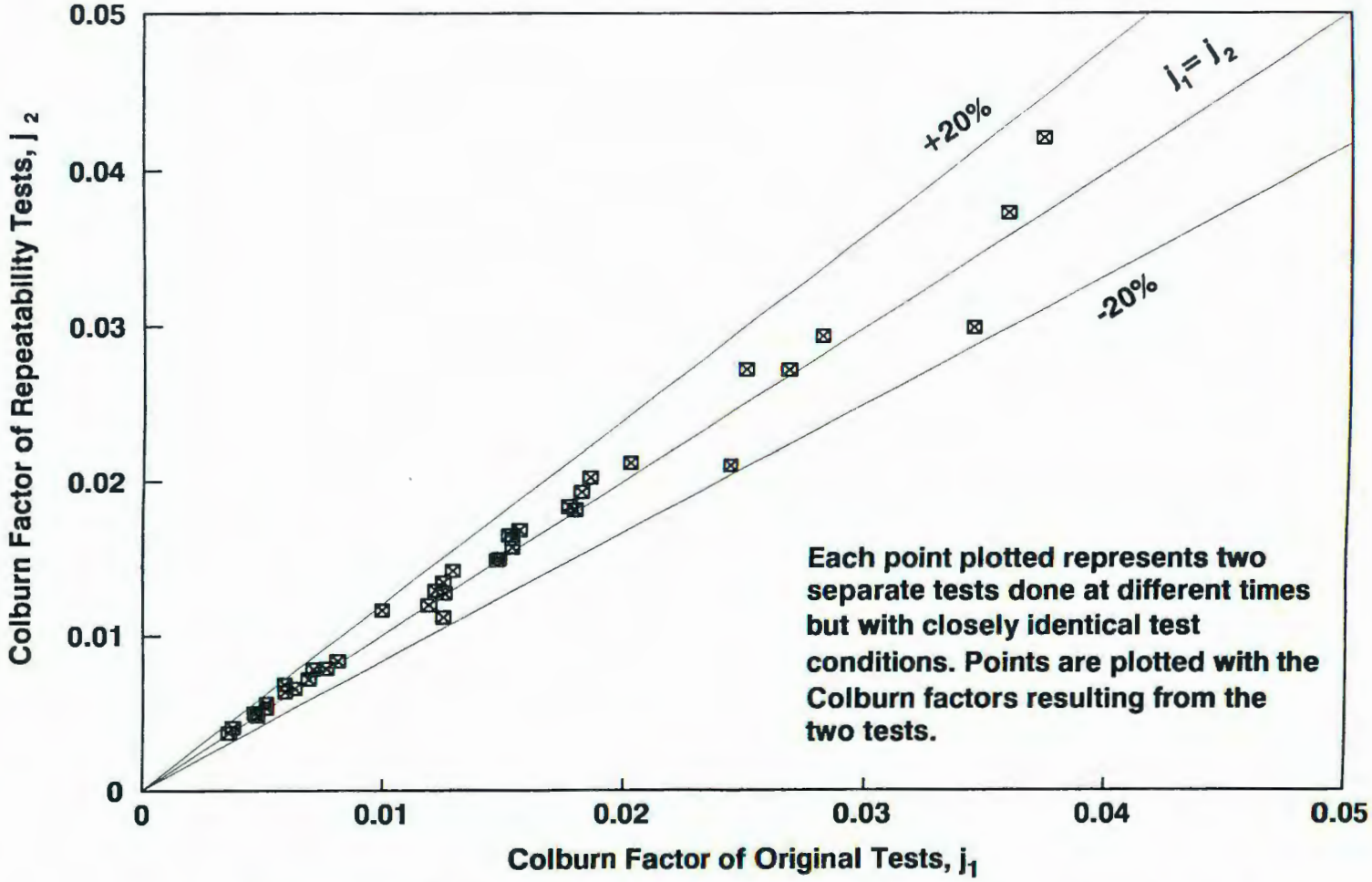

Figure 6-1 Repeatibility of Experimental Colburn Factor Data

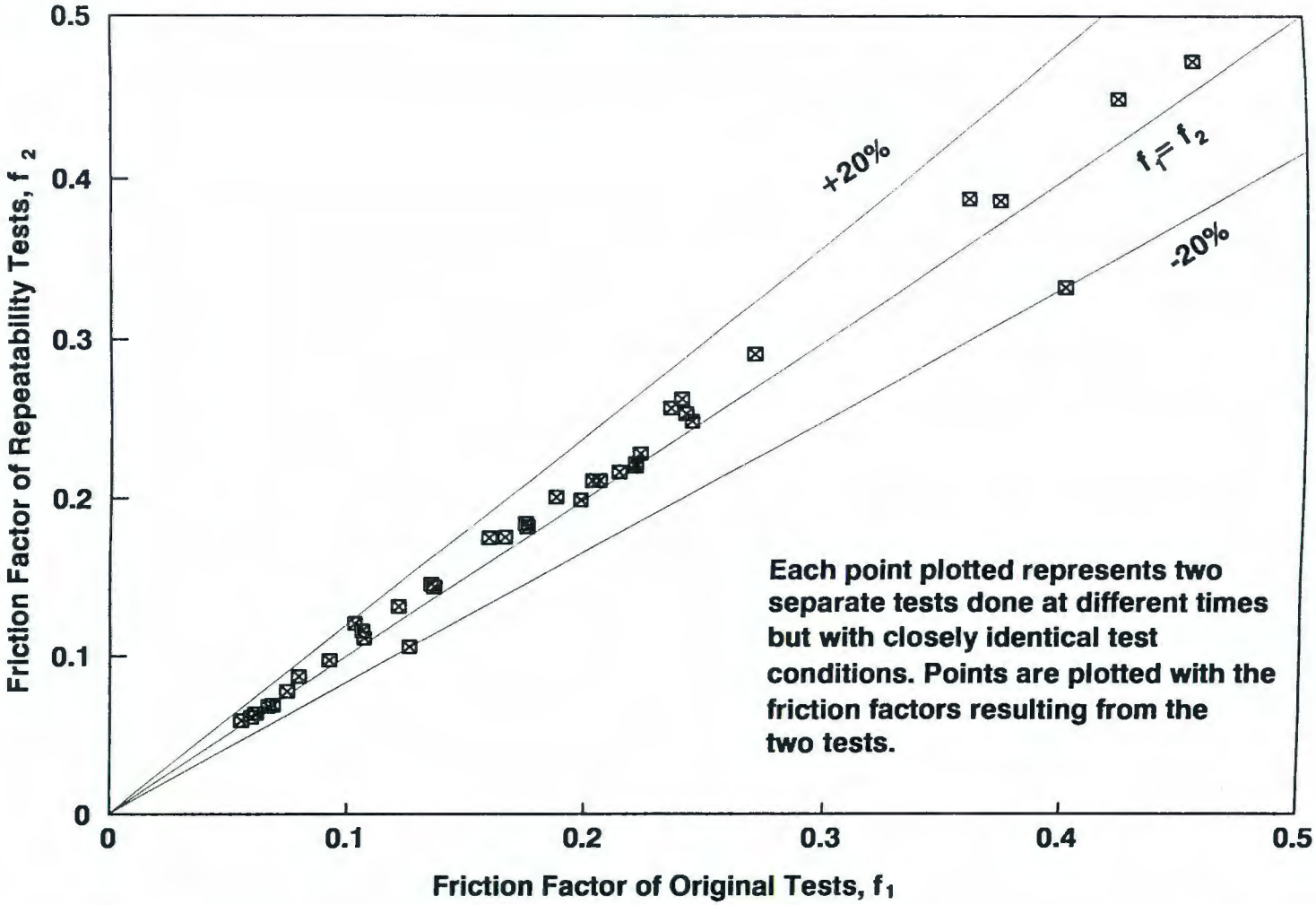

Figure 6-2 Repeatibility of Experimental Friction Factor Data

6.2 Discussion of Results

6.2.1 Geometry Effects on Performance

The compactness of the offset fin is usually evaluated by the heat transfer area density, β, which is the heat transfer surface area in a unit volume of fin array. Since different fin geometry has different heat transfer area density, hydraulic diameter and distributions of fluid velocity and temperature, the fin geometry has a strong influence on heat transfer and pressure drop of the fin array. Several heat exchanger performance evaluation methods have been described in Chapter 1. The current study employs a comparison method where heat transfer is traded off against fluid pumping power, which is described by Shah (1978). The specific heat transfer has the form of $F_h=\eta h_0\beta$, which represents the heat transfer per unit temperature and per unit fin array volume. The specific pumping power has the form of $F_f=E\beta$, where E represents the pumping power expended per unit surface area and F_f represents the pumping power expended per unit volume of fin array. The comparison between F_h and F_f is equivalent to comparing the benefit of heat transfer against the cost of pumping power. This method is recommended to compare the performance of fin geometries in applications without significant system and manufacturing constraints (Shah, 1978). The two parameters can be expressed as (Shah, 1978)

$$F_h = \eta h_0 \beta = \frac{c_p \mu}{Pr^{2/3}} \eta \frac{4A_c/A_f}{D_h^2} jRe \qquad (6.11)$$

$$F_f = E\beta = \frac{\mu^3}{2g\rho^2}\frac{4A_c/A_f}{D_h^4} fRe^3 \qquad (6.12)$$

In Equations 6.11 and 6.12, the first terms at the right hand side of each equation incorporates the fluid property effects, and the second term is related to fin geometry effects.

Performance comparisons of the seven cold plates are conducted by use of the surface contribution model for different fluids at fluid temperature of 10 °C. The fin geometry effects can be found by comparing the performance among fin arrays with the certain fluid at the same fluid temperature. The results of the geometry studies are given in Figures 6-3 to 6-5 for PAO, water and air, where the abscissa represents the specific pumping power F_f and ordinate represents the specific heat transfer F_h.

In Figure 6-3, the comparison of specific heat transfer F_h against specific pumping power F_f is made for the geometries of the seven plates using PAO. Referring to the hydraulic diameters listed in Table 6-1, it can be seen that the hydraulic diameter has a strong influence on the performance of the fin arrays. Plate 1 with the smallest D_h (D_h=1.351 mm), has the highest value of F_h. As the hydraulic diameter increases, specific heat transfer F_h decreases for a certain specific pumping power. Therefore, the performance of a fin array can be increased by decreasing the hydraulic diameter, which leads to more compact heat exchangers. The hydraulic diameter effects are consistent with the results of London and Shah (1968), in which fin arrays with smaller hydraulic diameter were found to have higher specific heat

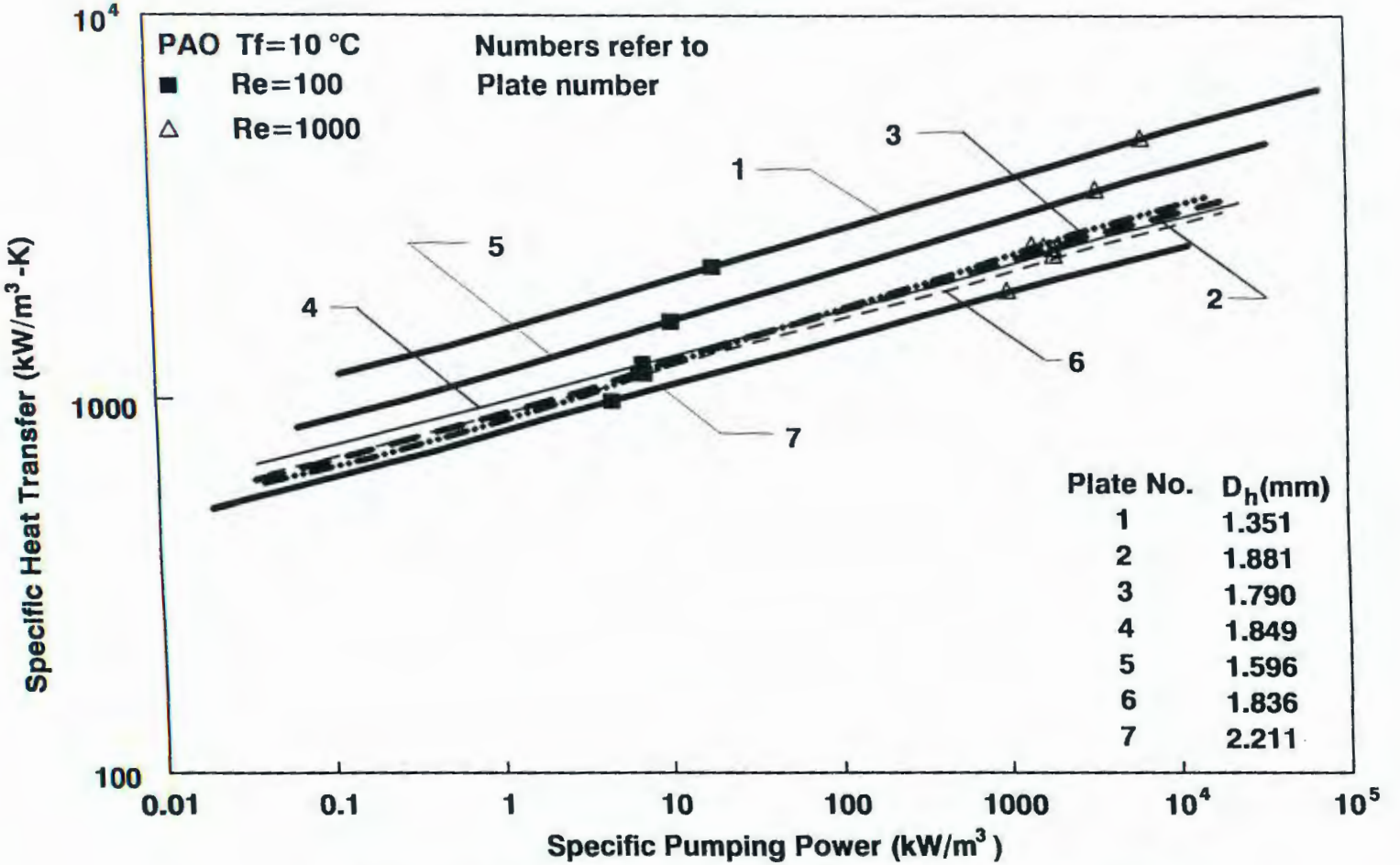

Figure 6-3 Performance Evaluation of Fin Arrays with PAO as Coolant

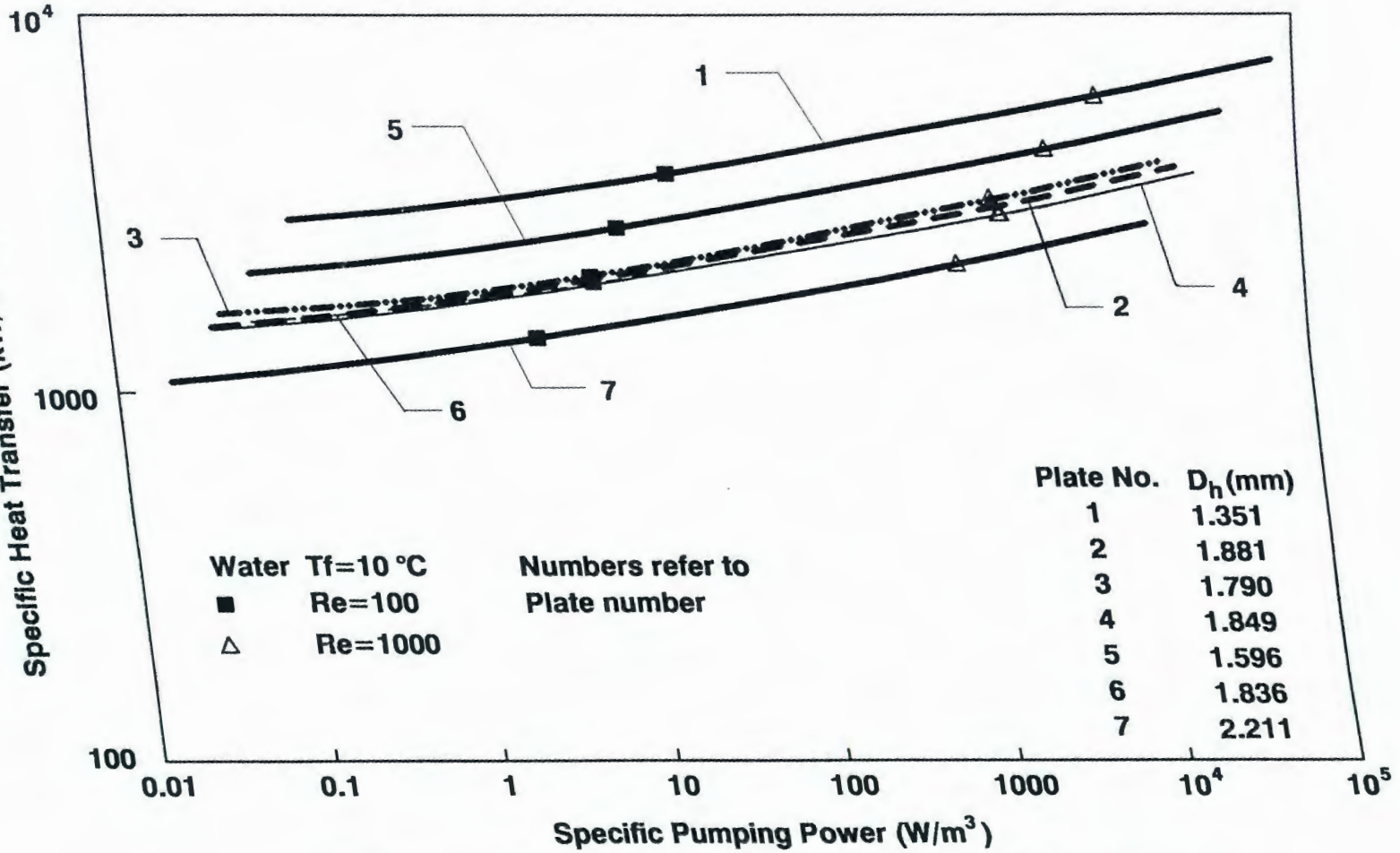

Figure 6-4 Performance Evaluation of Fin Arrays with Water as Coolant

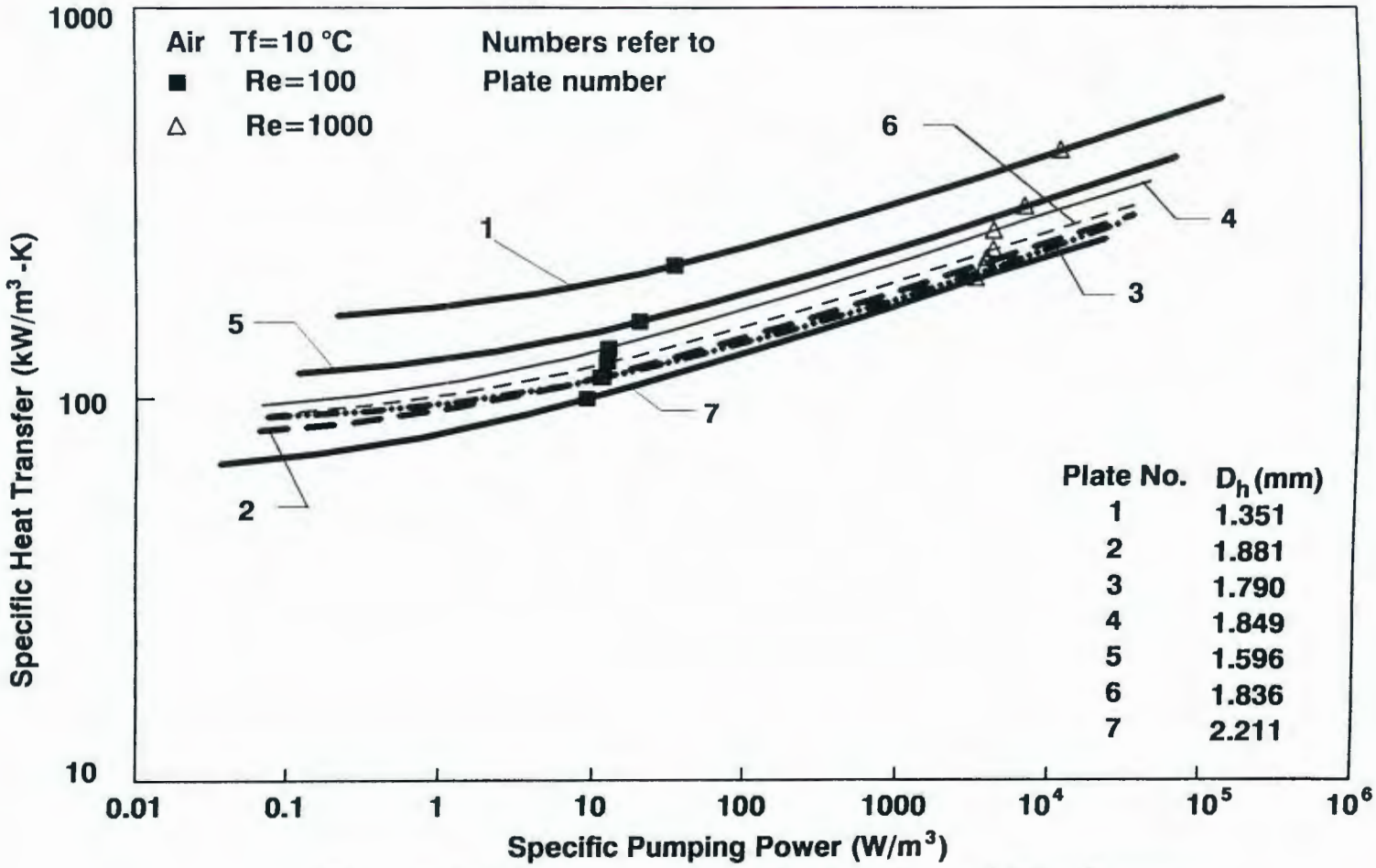

Figure 6-5 Performance Evaluation of Fin Arrays with Air as Coolant

transfer for a certain specific pumping power. In Figure 6-3, the Reynolds number of each plate is shown at two values for reference. It can be seen that fin array with smaller hydraulic diameter requires higher specific pumping power to achieve a certain Reynolds number. And for the same Reynolds number, the fin array with smaller D_h has higher values of specific heat transfer.

For fin arrays with similar hydraulic diameters, other geometry parameters also influence on the performance. Figure 6-3 shows that Plate 2 has larger specific heat transfer than Plate 6 when the Reynolds number is greater than 100, although Plate 2 (D_h=1.881 mm) has larger D_h than Plate 6 (D_h=1.836 mm). Plates 2 and 6 have similar fin geometry parameters except Plate 2 (t=0.152 mm) has larger fin thickness than Plate 6 (t=0.102 mm). From Equations 6.6 and 6.7, larger fin thickness causes higher fin efficiency, which leads to higher surface efficiency for a fin array. It is the high surface efficiency that makes the heat transfer of Plate 2 higher than Plate 6. With PAO as the fluid, the heat transfer performance of a fin array can be improved by increasing fin thickness.

The effects of fin length on performance can be seen in the comparison between Plates 2 and 3. Although Plate 2 (D_h=1.881 mm) has larger hydraulic diameter than Plate 3 (D_h=1.790 mm), Figure 6-3 shows that specific heat transfer of Plate 2 is close to that of Plate 3. Since Plate 2 (l=3.18 mm) has shorter fin length than Plate 3 (l=6.12 mm), the fins in Plate 2 interrupt the boundary layer more frequently, which causes more developing heat transfer effects on the fins and increase the entire heat transfer of Plate 2. The enhanced heat transfer of Plate 2 offsets the

possible decrease of specific heat transfer due to the larger D_h and causes Plate 2 to have similar specific heat transfer as that of Plate 3. From above discussion, it can be concluded that with PAO as the fluid, the performance of fin arrays can be enhanced by decreasing the fin length.

Similar comparisons of fin performance with water and air are given in Figures 6-4 and 6-5. Using water as fluid, the geometry effects on fin performance are similar to that found for PAO. For the cases with air as coolant, the influence of surface efficiency on performance is reduced, because the heat transfer coefficient associated with air is small, which causes the surface efficiency to be above 90% and reduces the variation of η due to the different fin geometries. In Figure 6-5, the comparison of Plates 2 and 6 for air is different from the results for PAO and water, shown in Figures 6-3 and 6-4. Because the reduction of surface efficiency effects, the heat transfer coefficient of Plate 2 does not increase significantly due to the thicker fins. The thicker fins of Plate 2 do cause higher form drag, which increases the specific pumping power of Plate 2. For a certain specific pumping power, Plate 2 has lower specific heat transfer than Plate 6. Therefore, with air as the fluid, the performance of a fin array can be improved by decreasing the fin thickness. The fin length effects on performance are minimally affected by the reduction of effects from surface efficiency. The fin length effects for air are similar to the effects for PAO and water.

From the above discussion, it can be concluded that hydraulic diameter has a significant effect on fin performance. The performance of a fin array can be increased by choosing a smaller hydraulic diameter. With similar D_h, fin thickness effects on

fin performance depend on the fluid. Using a fluid with superior heat transfer properties, such as water or PAO, thicker fins increase fin performance. However, for air, thinner fins increase the fin performance. The fin length effects for the three fluids are similar. Shorter fins lead to higher fin array performance.

From Equations 6.11 and 6.12, fluid properties are also found to influence fin array performance. Figure 6-6 is a plot of the performance comparison of Plate 3 for threes fluids at fluid temperature 10 °C. For a certain specific pumping power expended, water has the highest specific heat transfer, and air has the lowest value of specific heat transfer. Water is the best heat transfer fluid among the three fluids. If water did not have problems with scale, fouling and corrosion, water would be the heat transfer fluid of choice.

6.2.2 Comparison of the Current Surface Contribution Model and Experimental Results with Different Inlet Temperatures and Heat Fluxes

In Figures 6-7 and 6-8, the experimental results for Plate 3 with PAO and water at different fluid temperatures are compared with the model developed in this project and described in Chapter 4. From both figures, it is seen that at low Reynolds number the Colburn factor is higher at high temperature due to the temperature dependence of the Prandtl number. In Figure 6-7 where PAO is used as the fluid, the Prandtl number ranges from 150 to 40 as temperature ranges from 10 to 60 °C. These curves exhibit a significant Prandtl number effect, as shown by the intersection of the j curves for 10 and 60 °C. The high Prandtl number fluid has a higher average j at

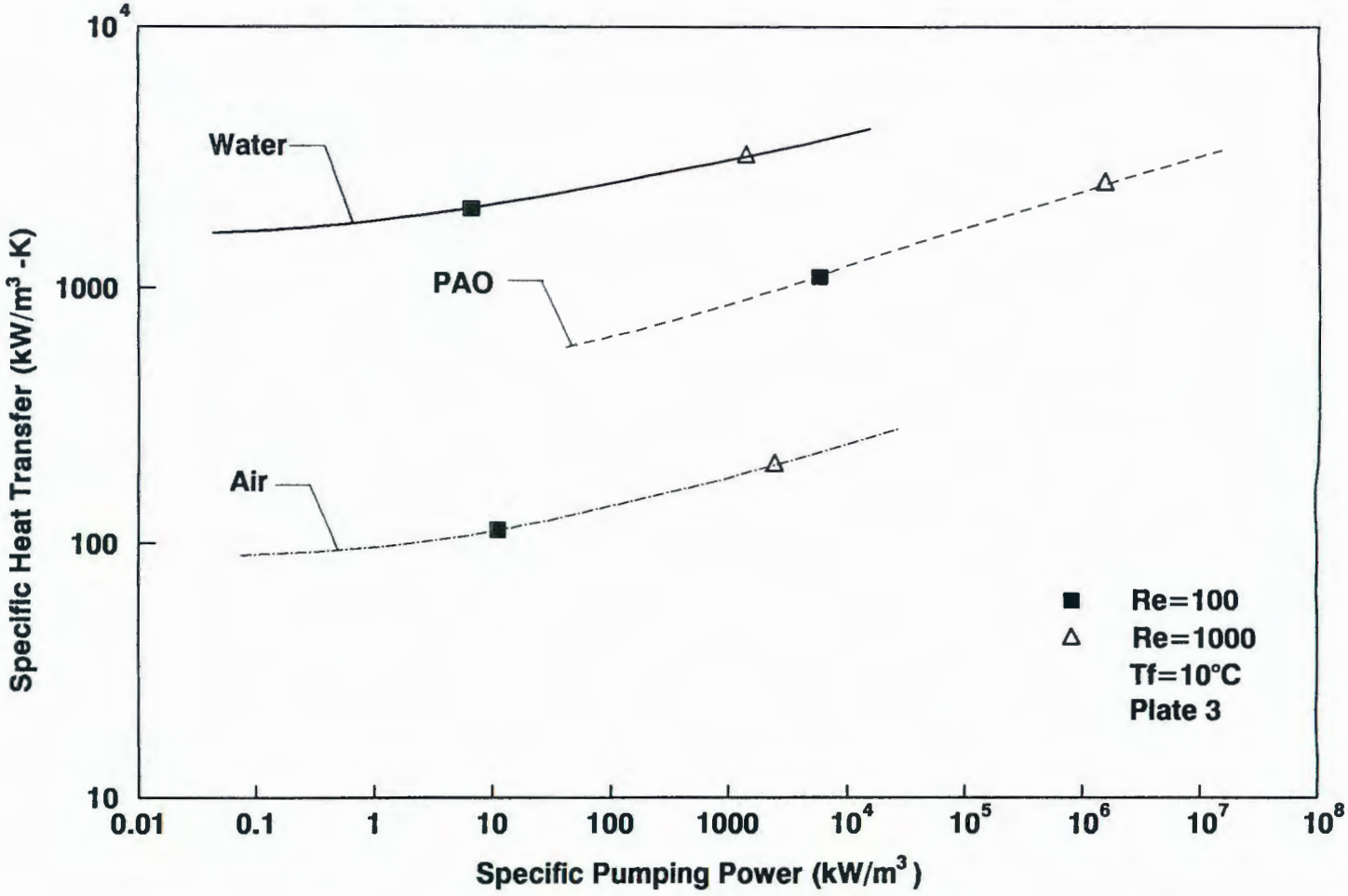

Figure 6-6 Performance Evaluation For Plate 3 with Different Fluids

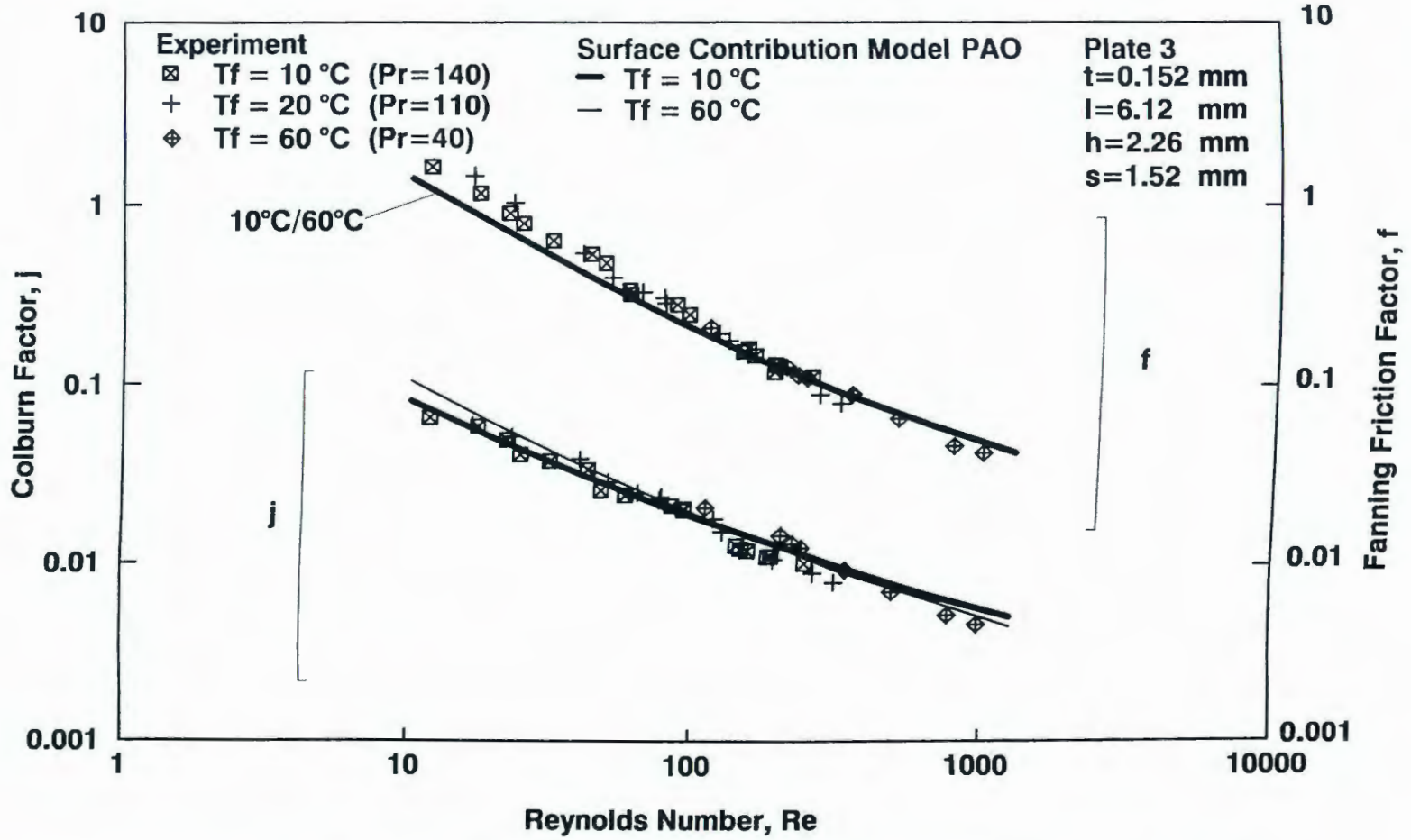

Figure 6-7 Effect of Fluid Temperature on Performance of Plate 3 with PAO as Coolant

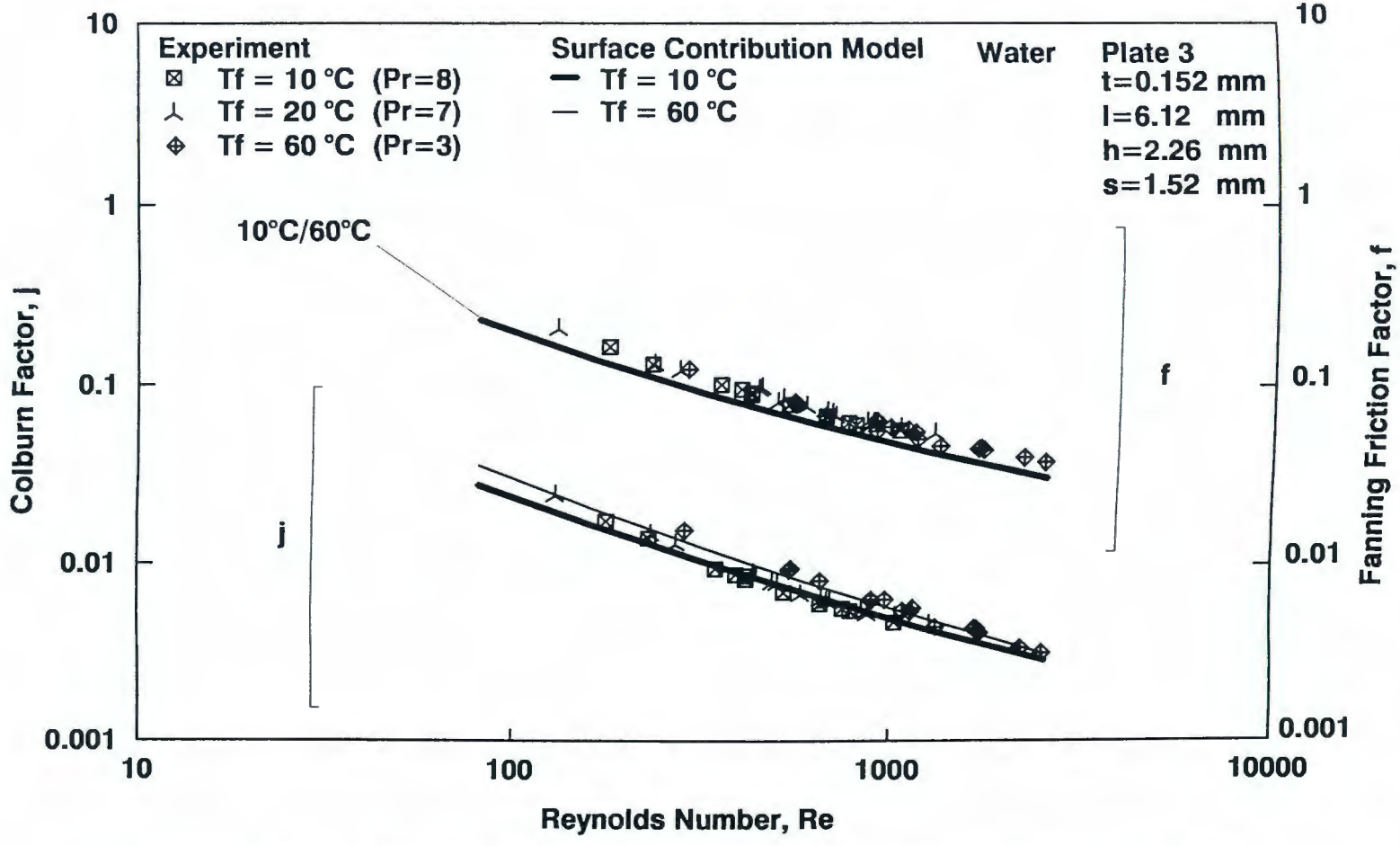

Figure 6-8 Effect of Fluid Temperature on Performance of Plate 3 with Water as Coolant

high Reynolds number because of entry length effects. In Figure 6-8 where water is used as the fluid, the Prandtl number ranges from 10 to 3 as temperature ranges from 10 to 60 °C. Because of the smaller Prandtl number compared to PAO, no crossover is observed in the j curves.

The friction factor includes the surface friction and form drag from the fin geometry, which are influenced by Reynolds number. For a certain fin geometry and Reynolds number, the friction factor for different Prandtl numbers should be the same. There are burrs on the fins, created by the fin manufacturing process. Also by cutting open Plates 1 and 7, it was found that some fins are deformed due to the manufacturing process. Both burrs and deformed fins tend to increase the friction factor. The model is designed to consider the effect of burrs and deformed fin ducts by using a form drag coefficient of 1.0. The model results show no Prandtl effect on friction factor, which is consistent with the experimental results.

Figures 6-9 to 6-20 compare the model results and experimental data for the six other plates. Similar to the results of Plate 3, all plates except Plate 1 show that model results are in good agreement with experimental data. For Plates 2 to 7, the model predicts 94% of the Colburn factor data within $\pm 20\%$, and 90% of the Fanning friction factor data within $\pm 20\%$.

Plate 1 experienced scaling problems in initial testing. Also, when Plate 1 was cut after the tests, the fins were found to be clogged with fibers. These fibers came from filters used in the deionization process of water and were subsequently eliminated from the system by filters. However the data from Plate 1 were affected.

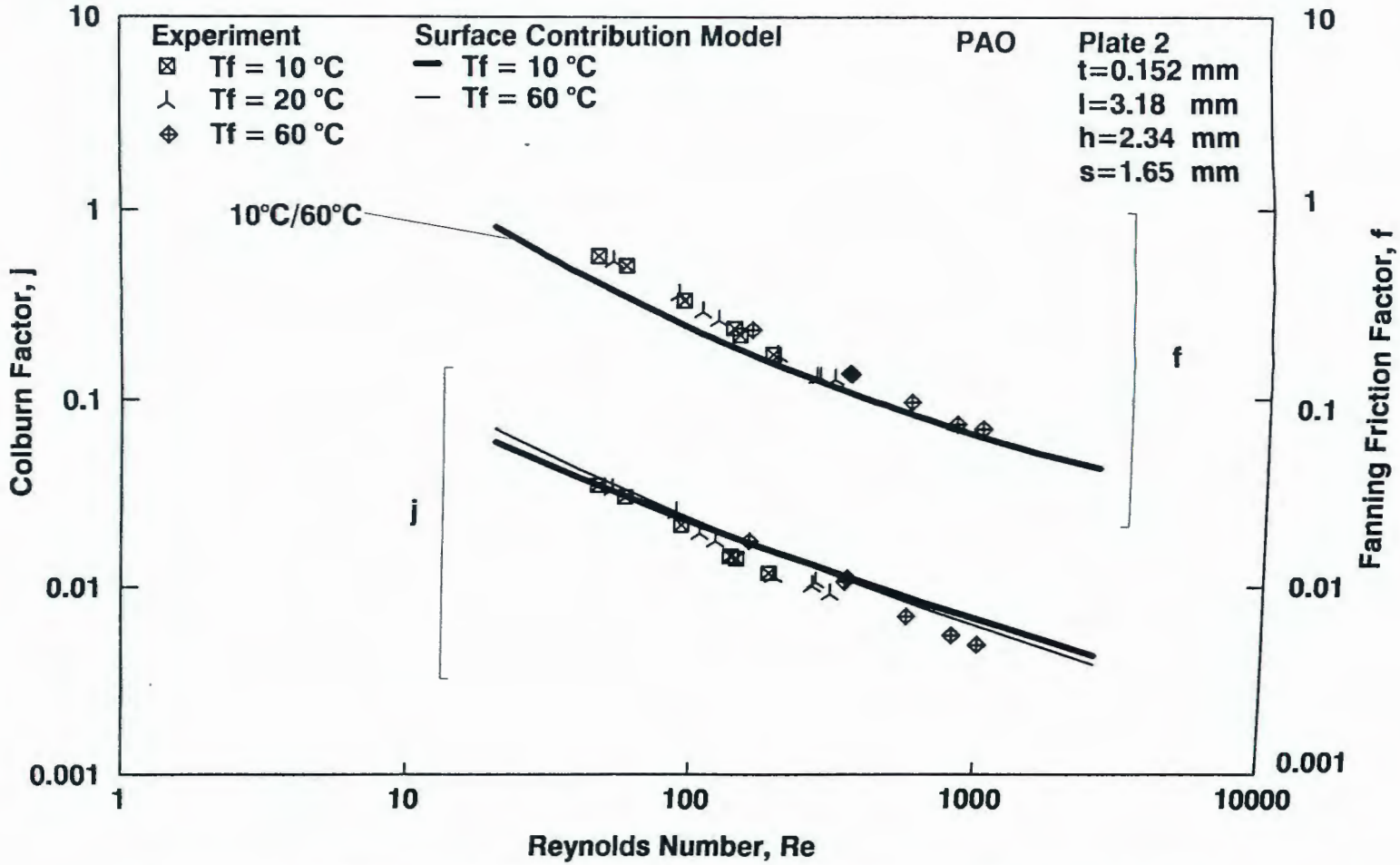

Figure 6-9 Effect of Fluid Temperature on Performance of Plate 2 with PAO as Coolant

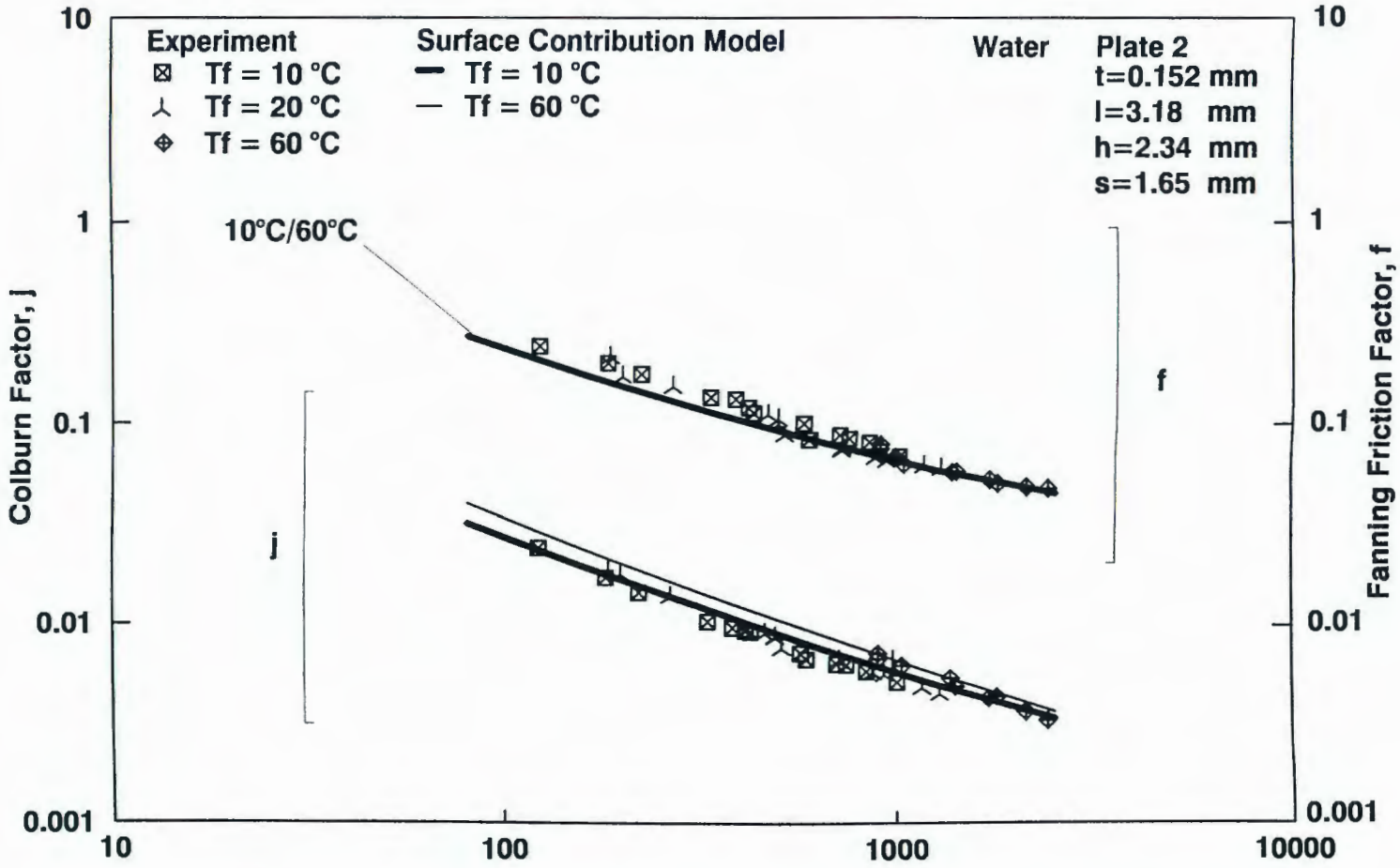

Figure 6-10 Effect of Fluid Temperature on Performance of Plate 2 with Water as Coolant

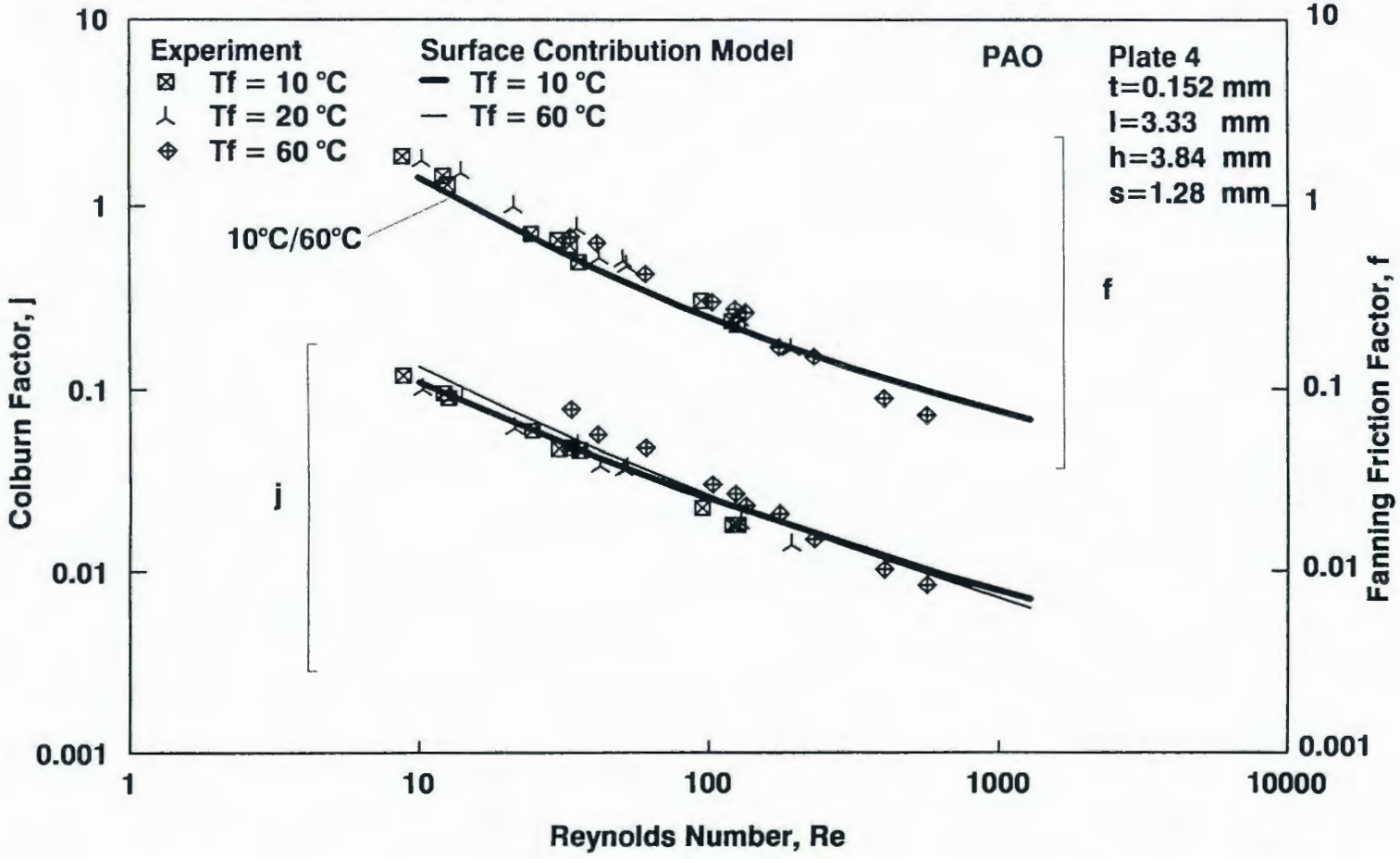

Figure 6-11 Effect of Fluid Temperature on Performance of Plate 4 with PAO as Coolant

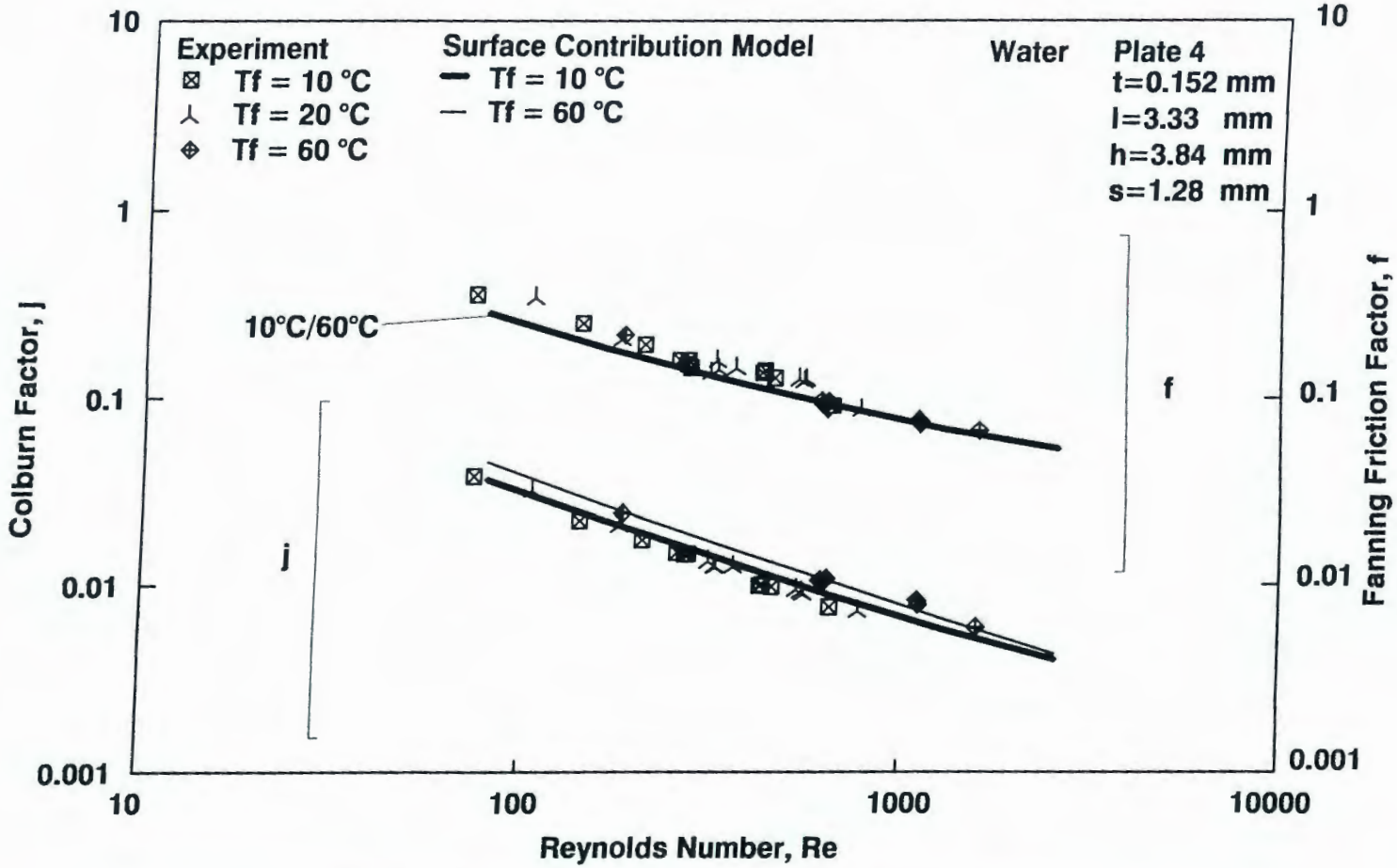

Figure 6-12 Effect of Fluid Temperature on Performance of Plate 4 with Water as Coolant

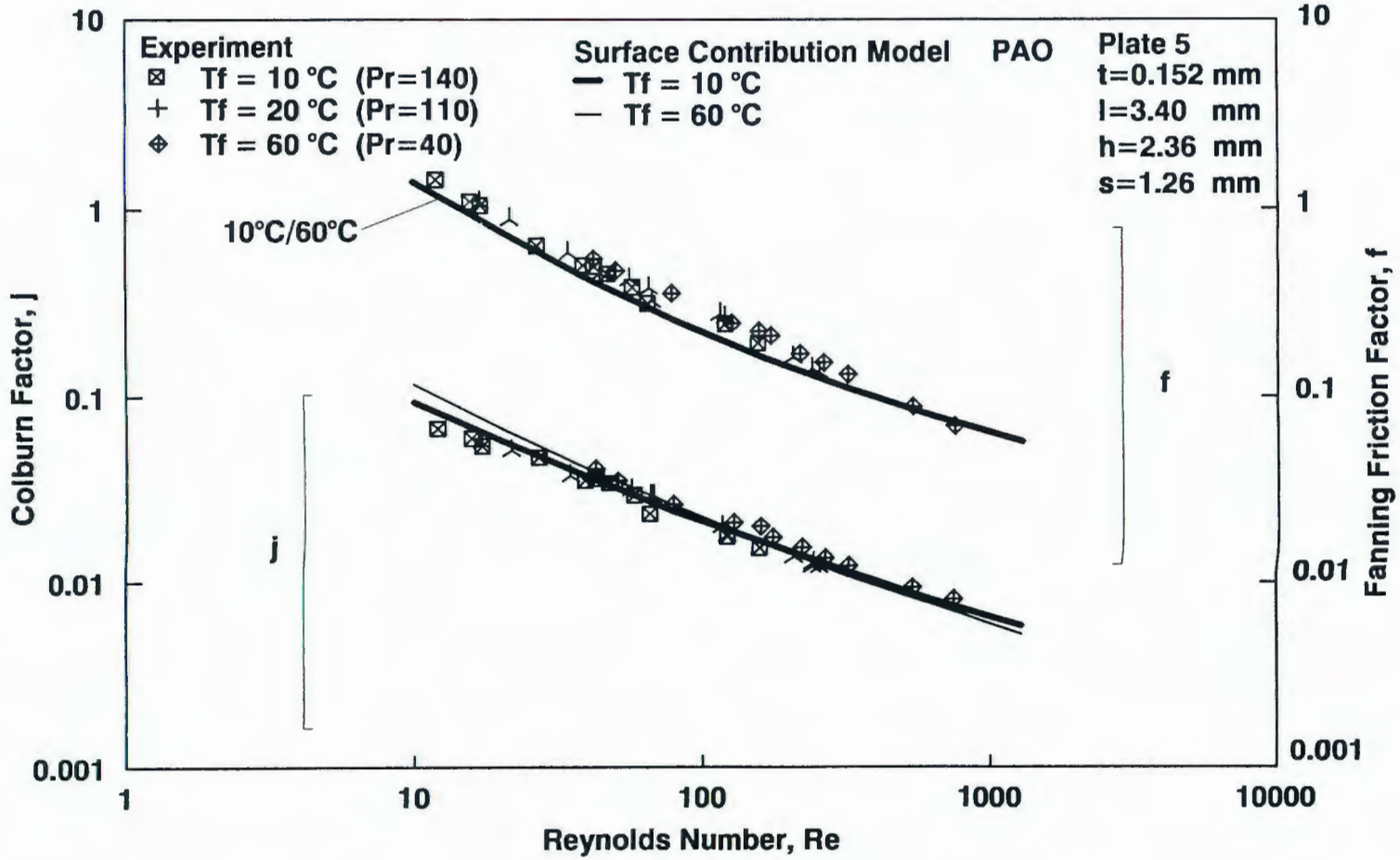

Figure 6-13 Effect of Fluid Temperature on Performance of Plate 5 with PAO as Coolant

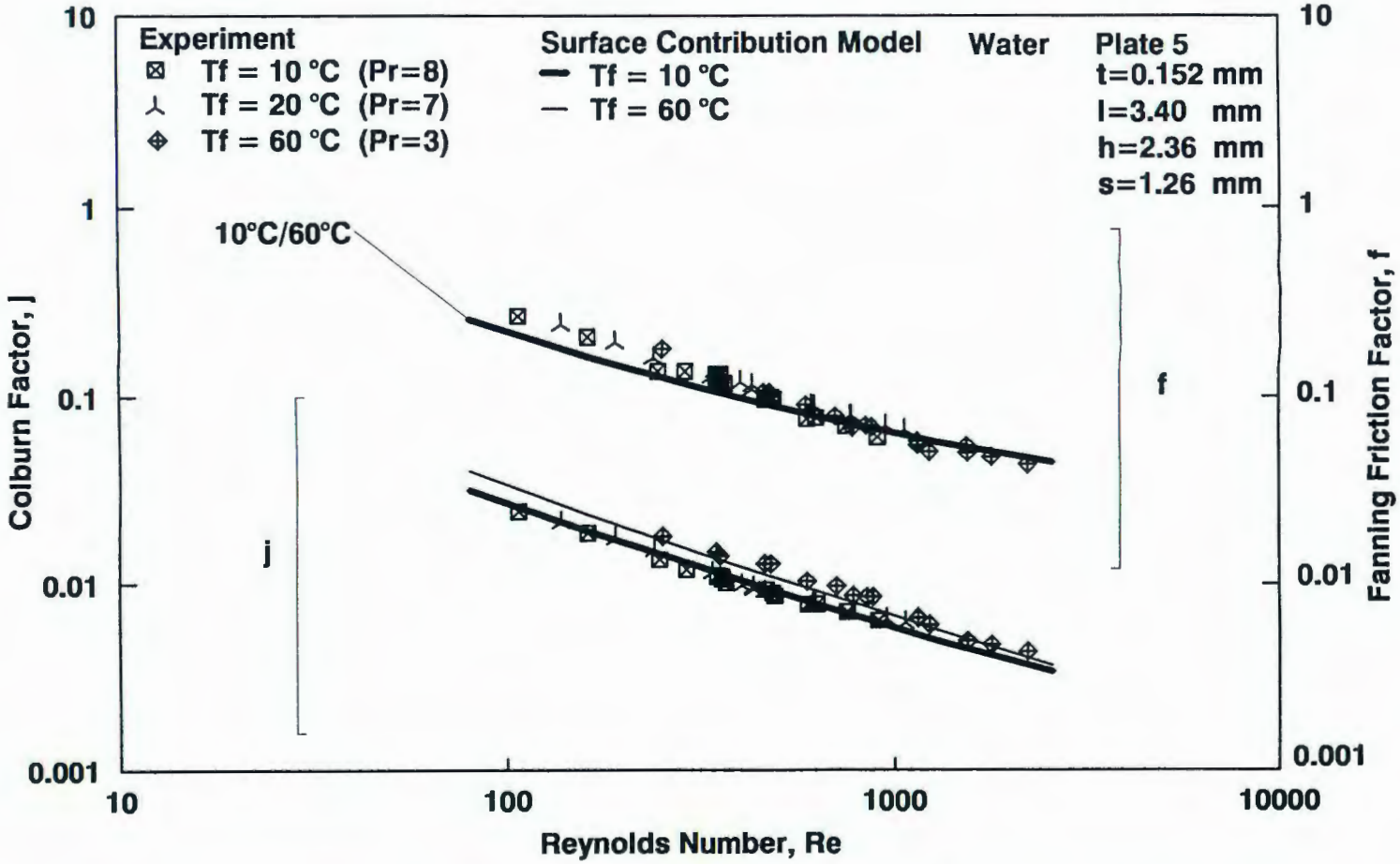

Figure 6-14 Effect of Fluid Temperature on Performance of Plate 5 with Water as Coolant

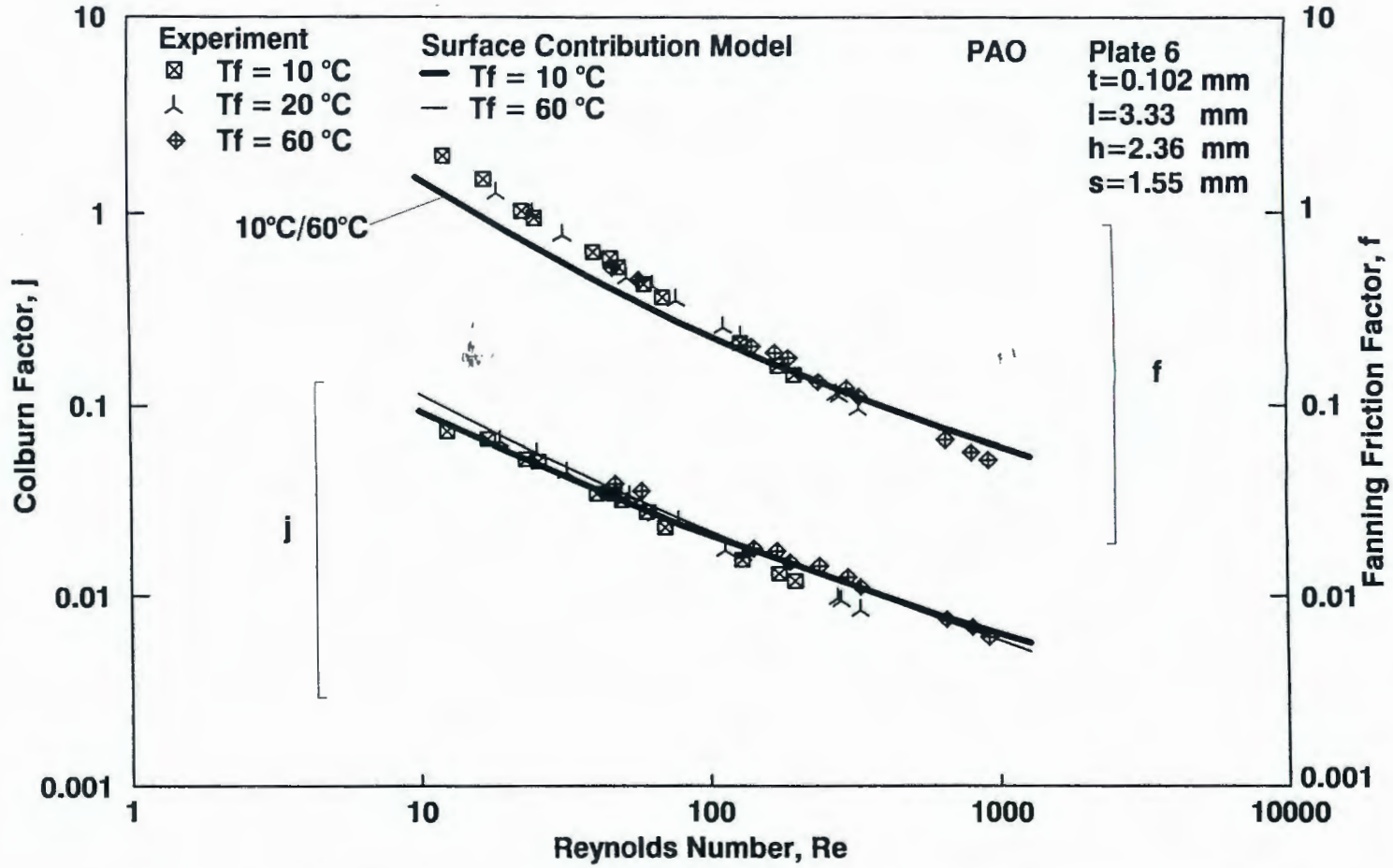

Figure 6-15 Effect of Fluid Temperature on Performance of Plate 6 with PAO as Coolant

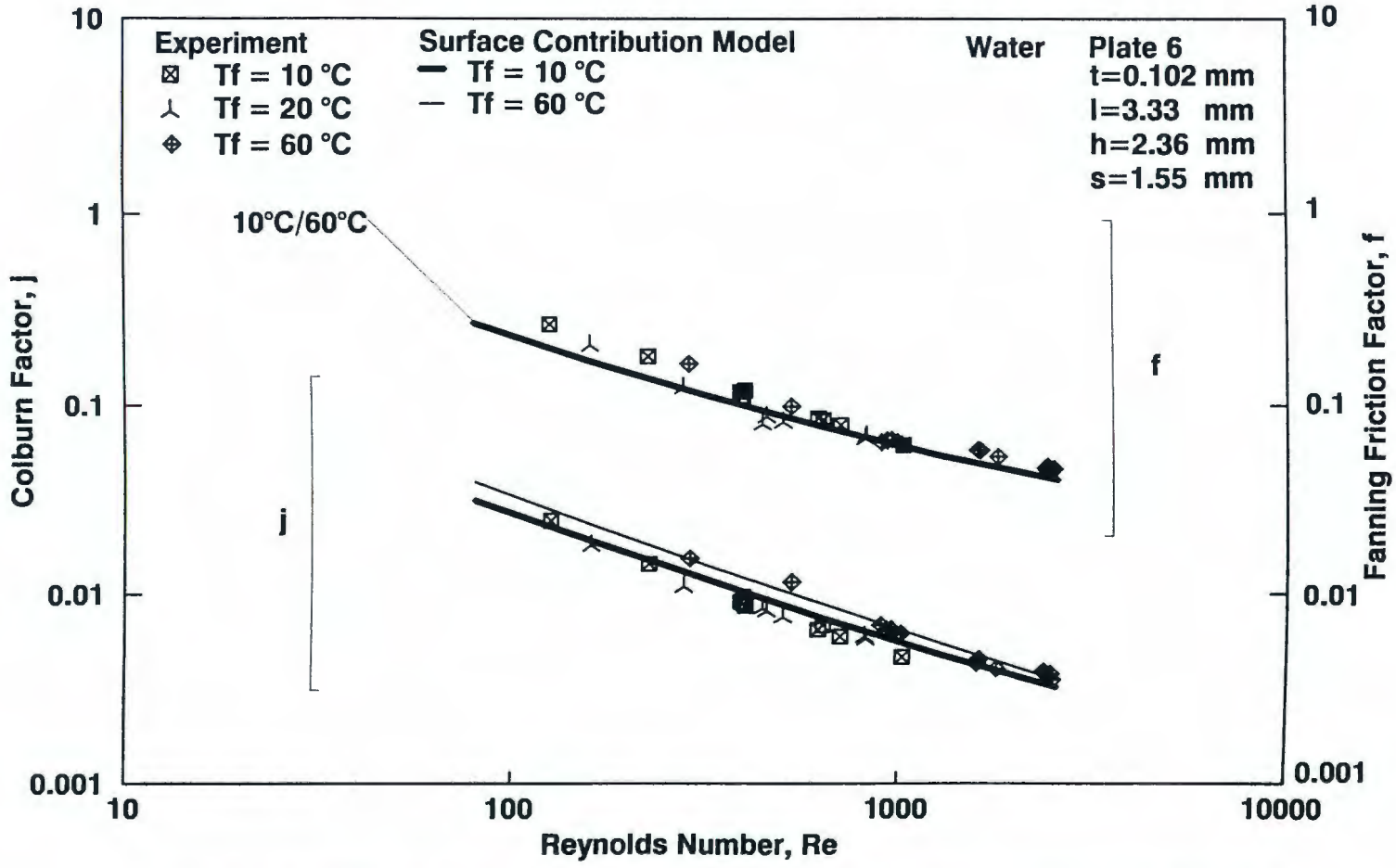

Figure 6-16 Effect of Fluid Temperature on Performance of Plate 6 with Water as Coolant

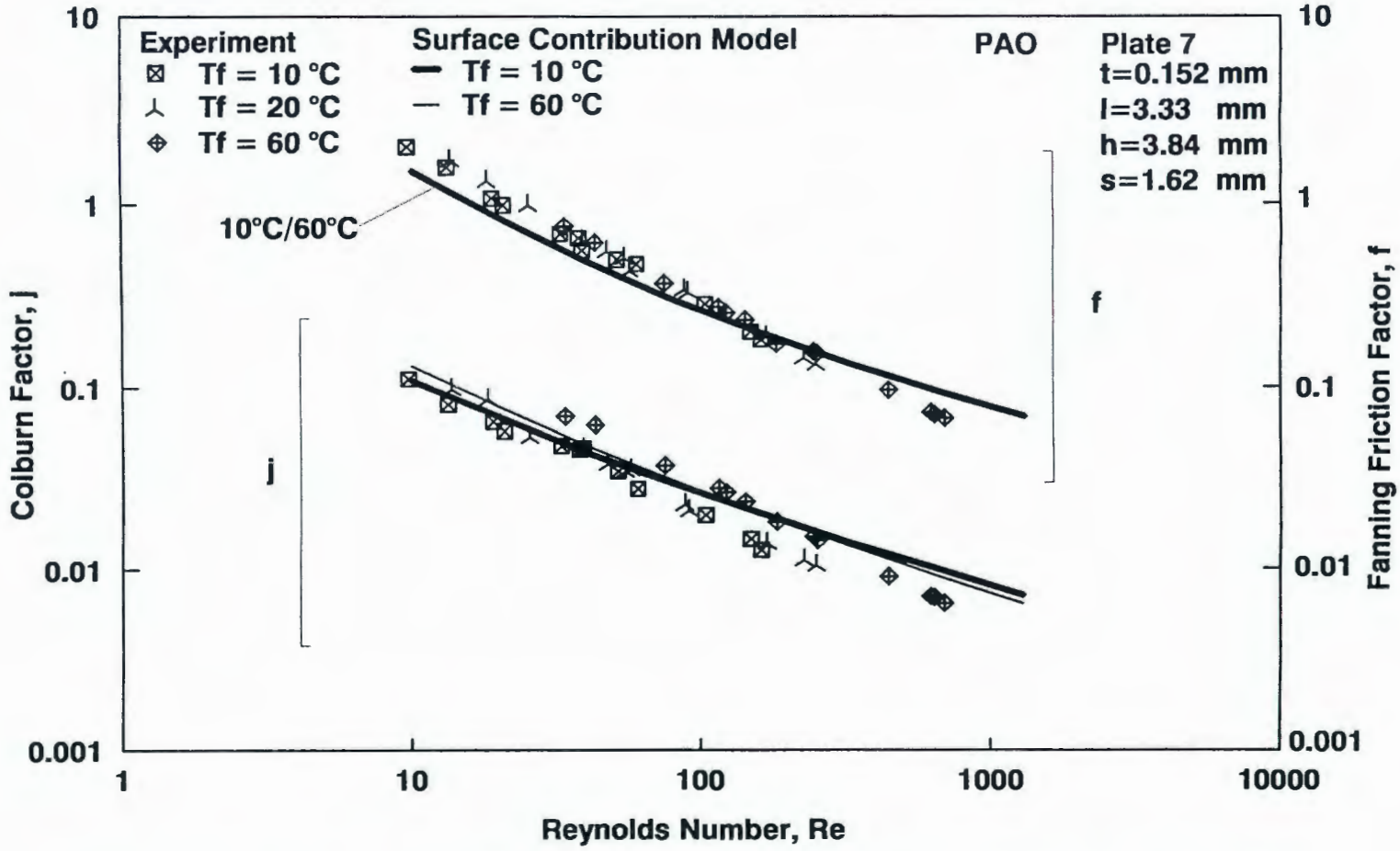

Figure 6-17 Effect of Fluid Temperature on Performance of Plate 7 with PAO as Coolant

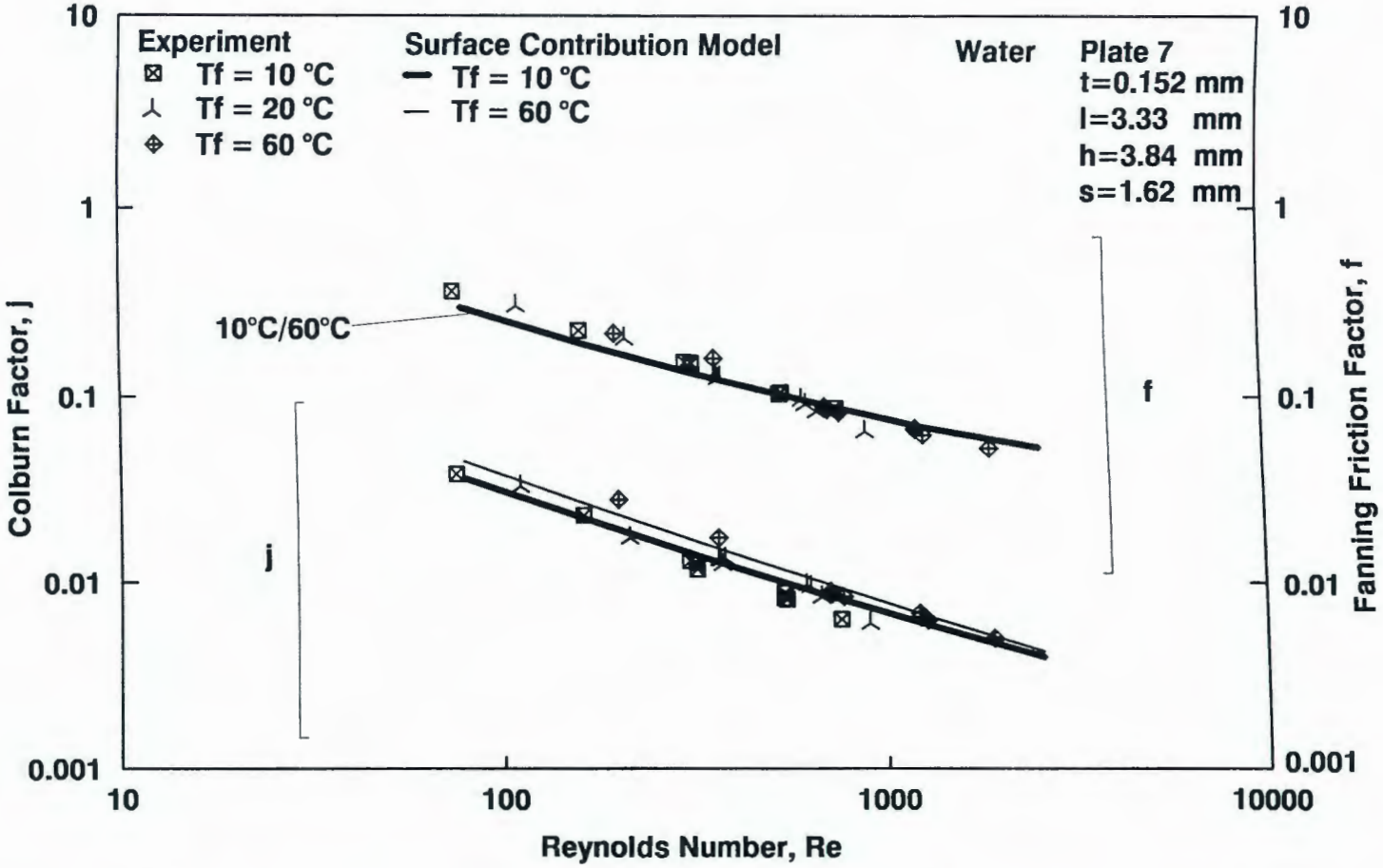

Figure 6-18 Effect of Fluid Temperature on Performance of Plate 7 with Water as Coolant

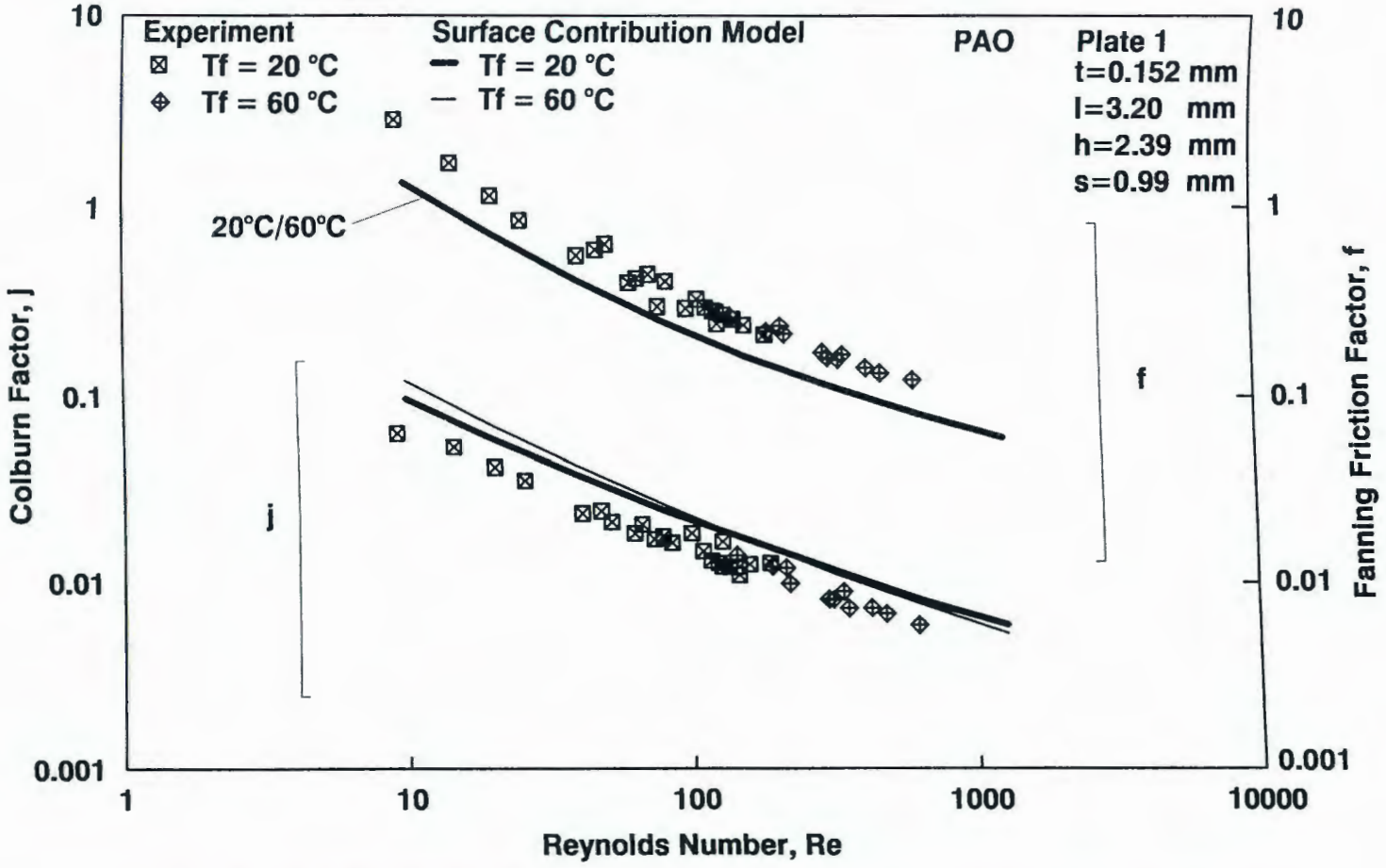

Figure 6-19 Effect of Fluid Temperature on Performance of Plate 1 with PAO as Coolant

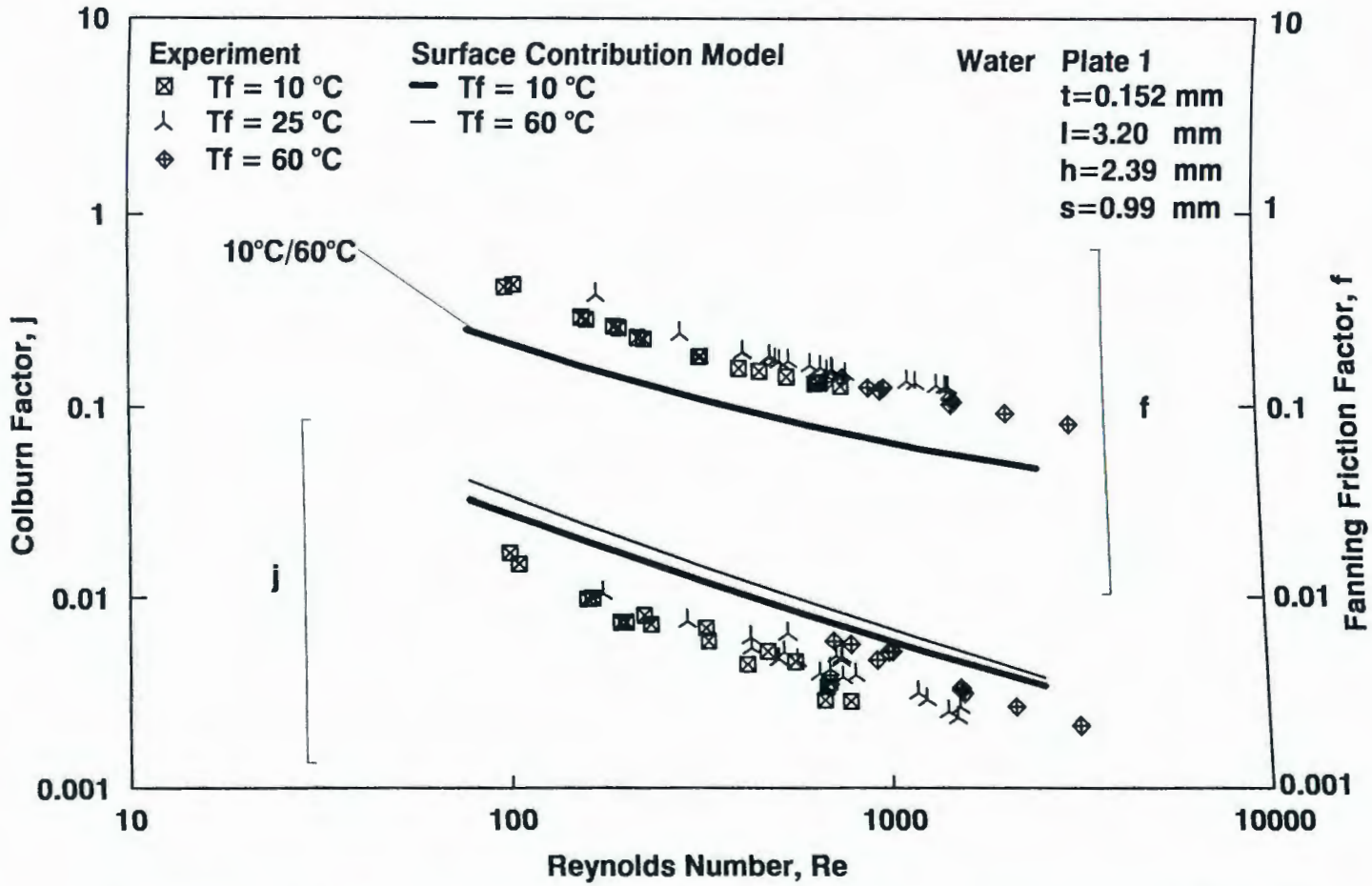

Figure 6-20 Effect of Fluid Temperature on Performance of Plate 1 with Water as Coolant

In Figures 6-19 and 6-20, the test data of Plate 1 show lower Colburn factor and higher friction factor as compared to the model predictions.

6.2.3 Comparison of Experimental Results with the Current Model and Air Correlations

Figure 6-21 shows a comparison of experimental data for Plate 3 against air correlations from Joshi and Webb (1987) and Wieting (1975) (note: correlations were modified to use a Reynolds number consistent with the current study). In the figure, the solid lines represent the surface contribution model results, the thick dashed lines represent the air model of Wieting (1975) and thin dotted lines represent the air model of Joshi and Webb (1987). Both air models are based on experimental data from Kays and London (1950), Kays (1960) and London and Shah (1968), which were obtained from air tests with constant surface temperature. In Figure 6-21, the experimental data and the various model results are for a fluid temperature of 10 °C. The comparison demonstrates that the Colburn factor results for air cannot be accurately applied to liquid applications.

Figure 6-21 shows that the Colburn factor for liquids is lower than for air. The difference is caused by Prandtl number effects. Because of the definition of the Colburn factor, $j = Nu_0/(RePr^{1/3})$, a large Prandtl number would give a lower j at the same Reynolds and Nusselt number if the Nusselt number were independent of Prandtl number. For the offset fin application, it was found that the Nusselt number increases with Prandtl number but at a rate less than $Pr^{1/3}$. Thus the Colburn factor decreases as Prandtl number increases. But it should be realized that lower j does not necessarily

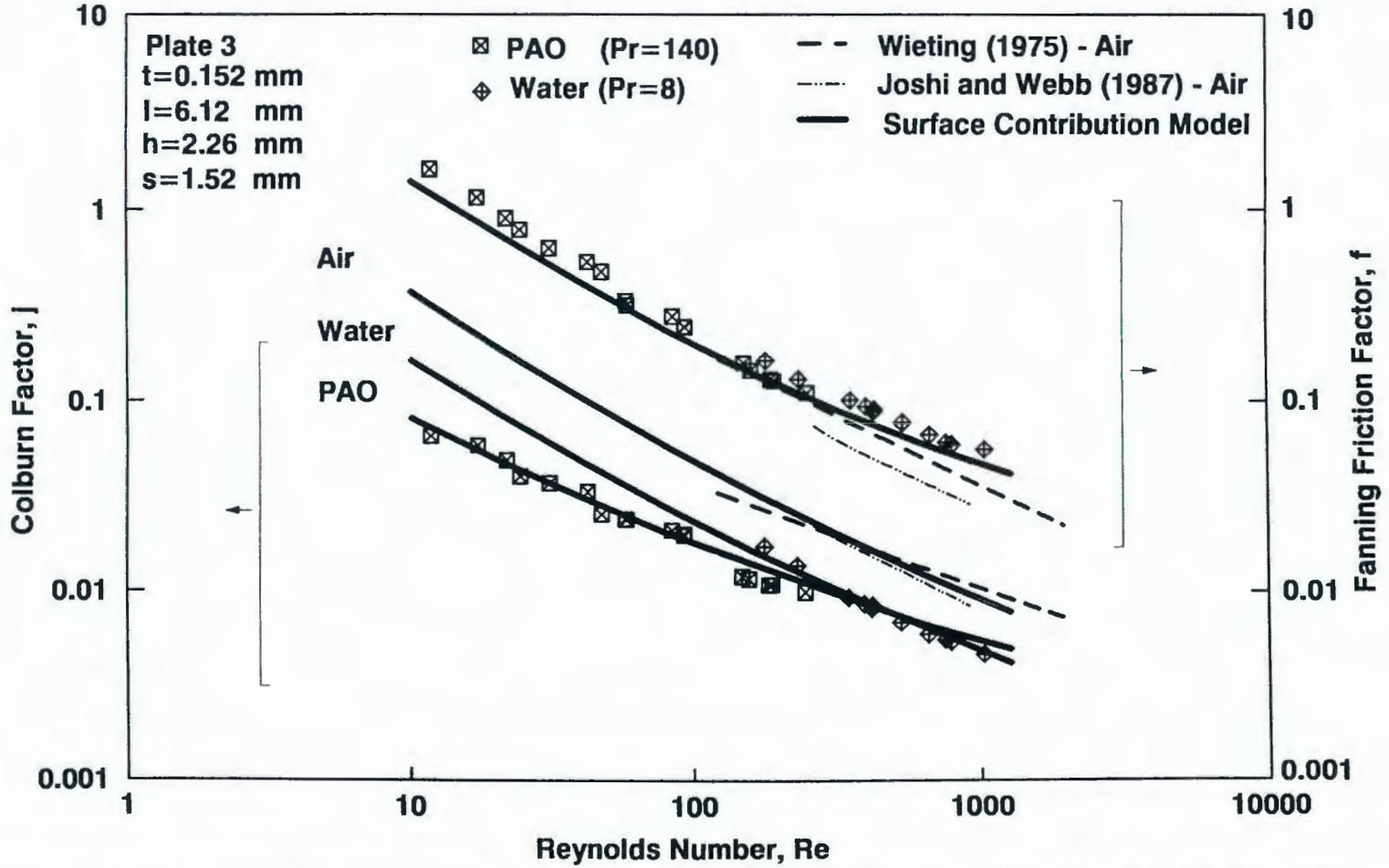

Figure 6-21 Comparison of Air Models and Results From Present Work at 10°C For Plate 3

imply a smaller heat transfer coefficient. In Figure 6-21, the j of PAO is lower than the j for air, but the heat transfer coefficient of PAO is approximately five times larger than that of air.

In Figure 6-21, comparison of the surface contribution model is also made against air models from Wieting (1975) and Joshi and Webb (1987). The choice of fluids has a significant effect on the Colburn factor, as seen in Figure 6-21. Air, with Prandtl number of 0.7, has the smallest thermal entry length effect (array perspective Prandtl number effect). It can be seen that the Colburn factor of PAO is cross over to the Colburn factor of water. This is due to the fact that a higher Prandtl number fluid tends to have a longer developing region (array perspective), which means that PAO has more array perspective effects than water. Besides the Prandtl number, the development length is proportional to the Reynolds number. At low Reynolds number, the array perspective effect is small. At high Reynolds number, the array perspective effect becomes large, which increases the overall heat transfer in the fin array and cause the slope of the j curve to flatten out. This flattening is more pronounced for higher Prandtl number fluids.

Wieting (1975) and Joshi and Webb (1987) considered only air as fluid. Approximate agreement is found between their results and our model with air properties as inputs, as seen in Figure 6-21. It should be noted that the results of Wieting (1975) and Joshi and Webb (1987) were obtained from constant surface temperature boundary conditions and the current results (experiments and model) were obtained based on constant heat flux boundary condition. Because there are no studies

for air with constant heat flux boundary condition, the air models of Wieting (1975) and Joshi and Webb (1987) in the current comparison are used as a reference to compare with the current model for air application.

According to the experimental results, the friction factor is not affected significantly by Prandtl number. This is also reflected in the model predictions in Figure 6-21, where the friction factor curves for different Prandtl numbers are coincident. The current model predictions of friction factor are higher than the results of Wieting (1975) and Joshi and Webb (1987), but these predictions match the liquid data quite closely. It is known that burrs on the fins increase form drag. The burrs are caused by the process of manufacturing the fin stock. In Kays and London (1984), burr effects are shown to increase the friction factor. The fin stock used in the experiments in the present study were manufactured by standard methods which result in significant burrs. The occurrence of the burrs is documented in Chapter 3. The model put forward here is designed to represent real-world offset fin practice.

It has been suggested that air correlations could be used for liquid cooled designs (Kays and London, 1984). From the comparison presented here, it can be seen that the Colburn factor for air is higher than the Colburn factor for the liquids at the same Reynolds number. The air model overpredicts the heat transfer coefficient for liquids. This implies that air models can not be used for liquid applications. The difference in Colburn factor between liquid and air is approximately a factor of two. If the Wieting correlation is used for a liquid application, it will predict the temperature difference between the surface and the fluid two times smaller than the

actual situation. This prediction error can endanger the components being cooled, especially in electronic cooling applications.

Figures 6-22 to 6-27 compare the model results and experimental data and air models for the other six plates. As was found for Plate 3, the model can predict the heat transfer with good agreement for Prandtl number ranging from 0.7 to 150. The poorest agreement is seen for Plate 1 which is due to clogging of the fin structure (as discussed in Section 6.2.2)

Since the model considers the Prandtl number effects on the heat transfer in the fin array as well as the effects from fin height of flow duct, the model is very close to the physics of actual applications. From the comparison of the current model results with liquid test data and air models, the model results are seen to produce good predictions of heat transfer with Prandtl number ranging from 0.7 to 150.

6.2.4 Comparison of the Current Surface Contribution Model with Brinkmann's Experimental Results.

Brinkmann et al. (1987) conducted an experimental study on two small offset fin arrays (25.4 mm long $\times$ 12.7 mm wide) using water as fluid. Uniform heat flux was applied on the base of the fin array and the flow duct around the fin array is thermally insulated. The fin geometry of the two arrays are listed in Table 6-2. Because of the short fin array, entry length considerations are significant for heat transfer. Figure 6-28 shows a comparison between the current model and Brinkmann's experimental results, which are converted to match the hydraulic diameter definition used in the current research. In the figure, the abscissa is Reynolds number and the

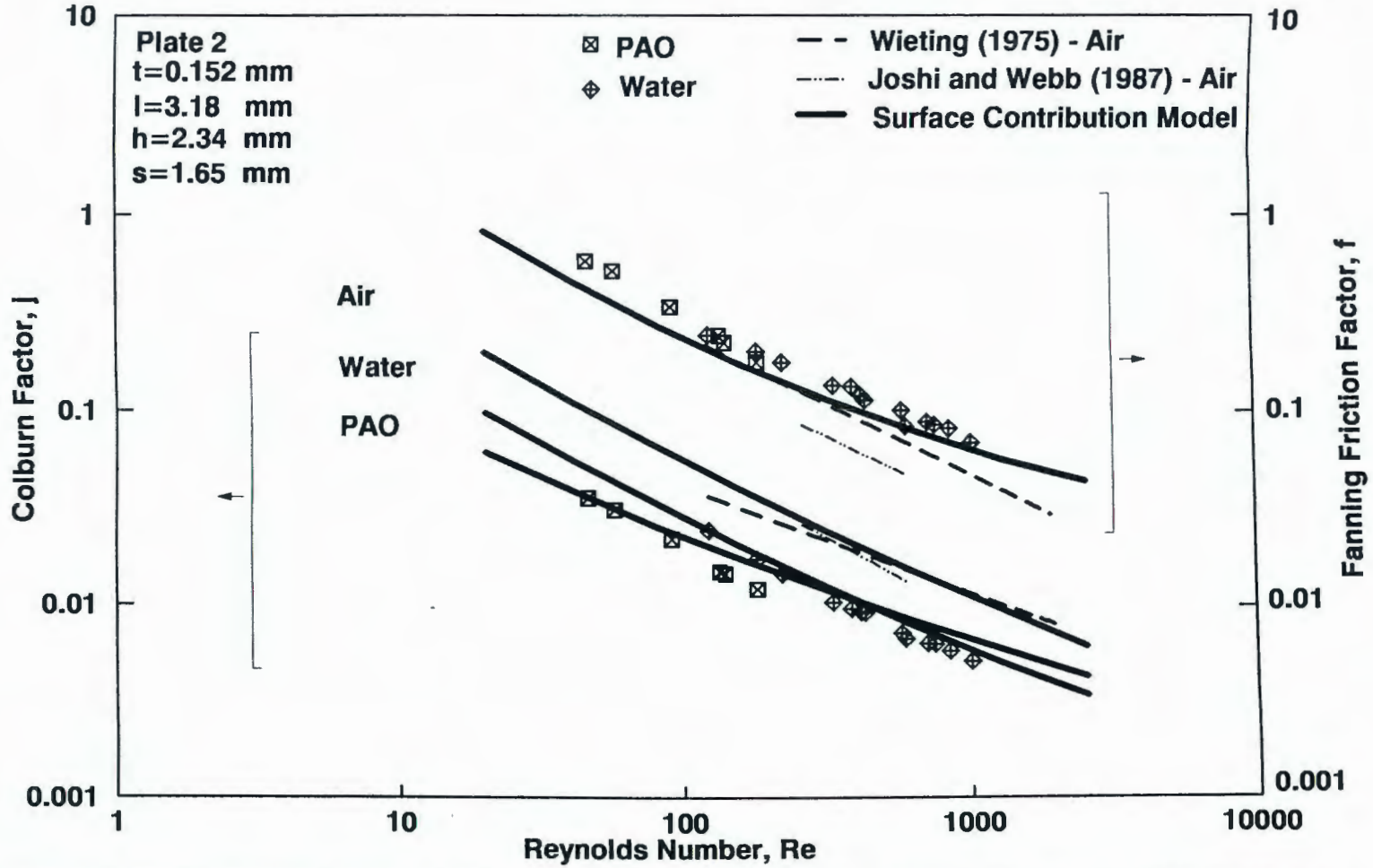

Figure 6-22 Comparison of Air Models and Results From Present Work at 10°C For Plate 2

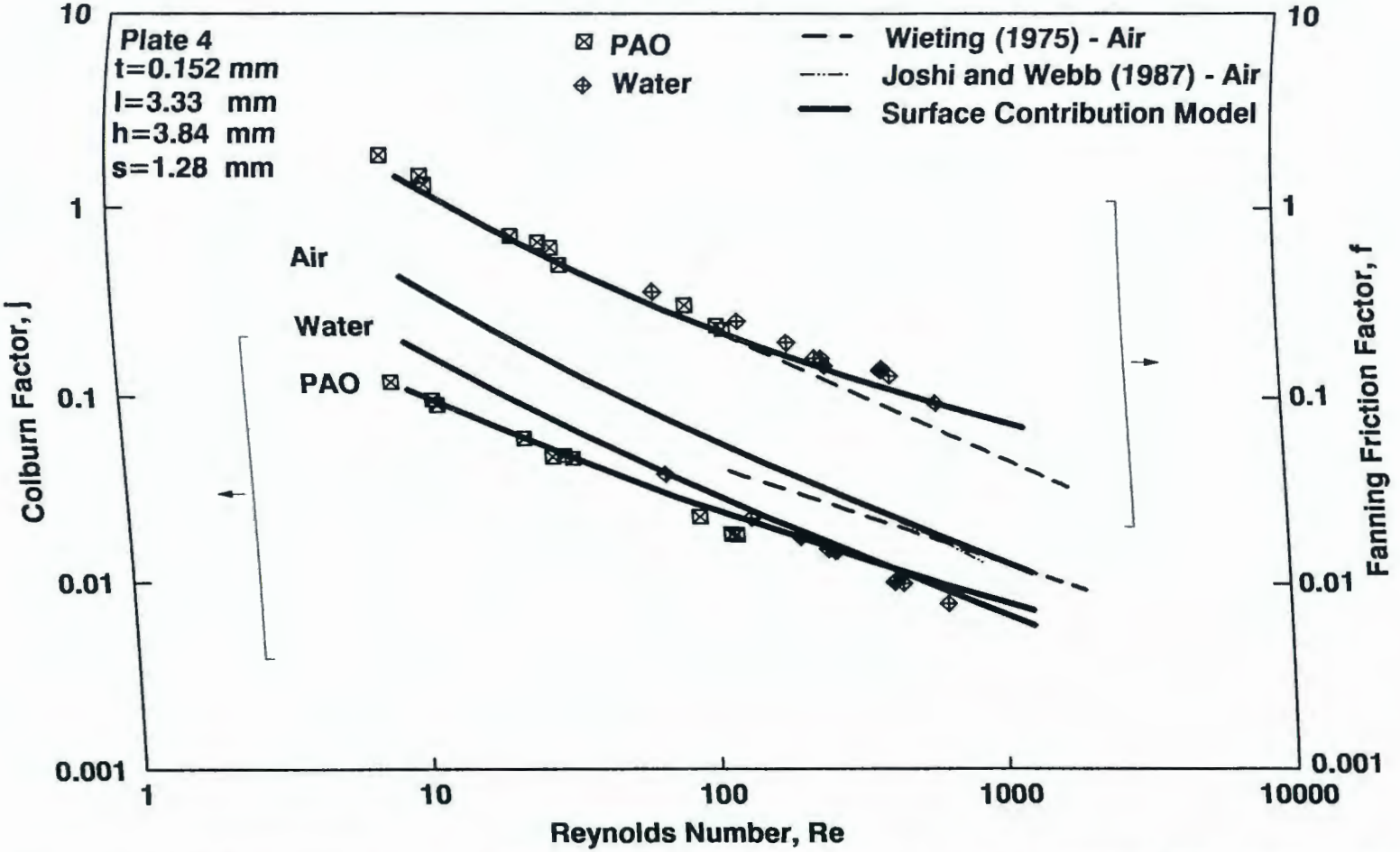

Figure 6-23 Comparison of Air Models and Results From Present Work at 10°C For Plate 4

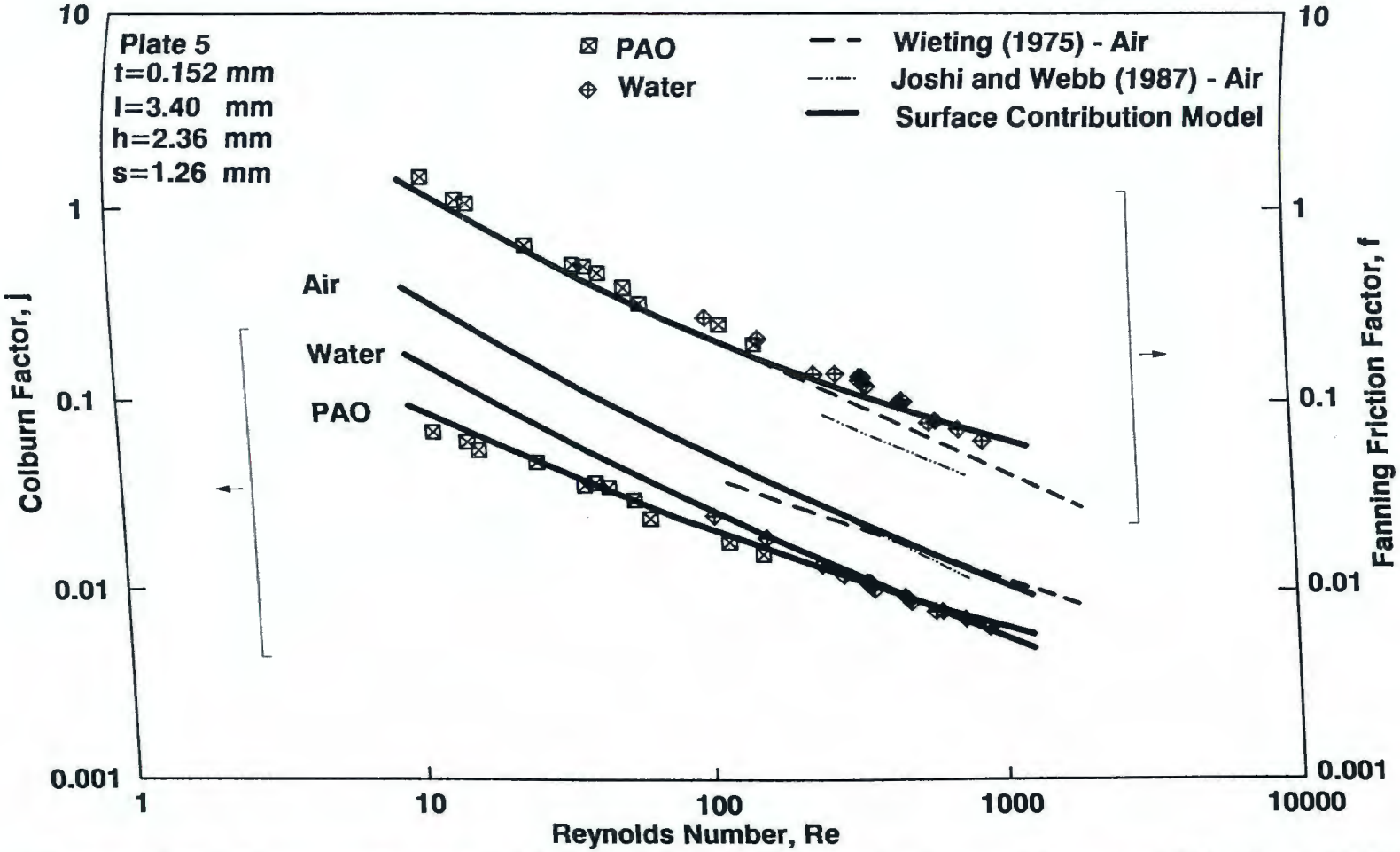

Figure 6-24 Comparison of Air Models and Results From Present Work at 10°C For Plate 5

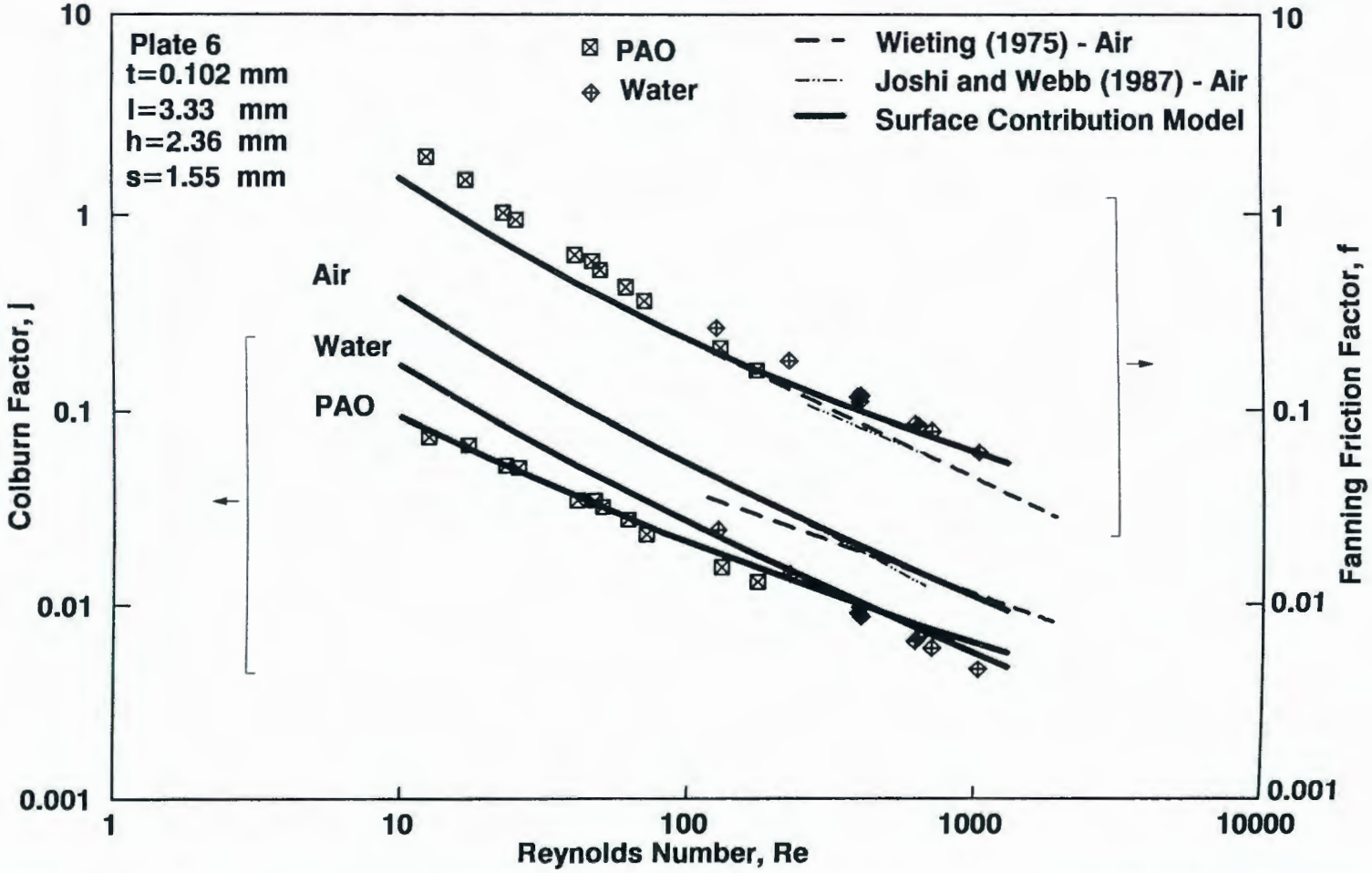

Figure 6-25 Comparison of Air Models and Results From Present Work at 10°C For Plate 6

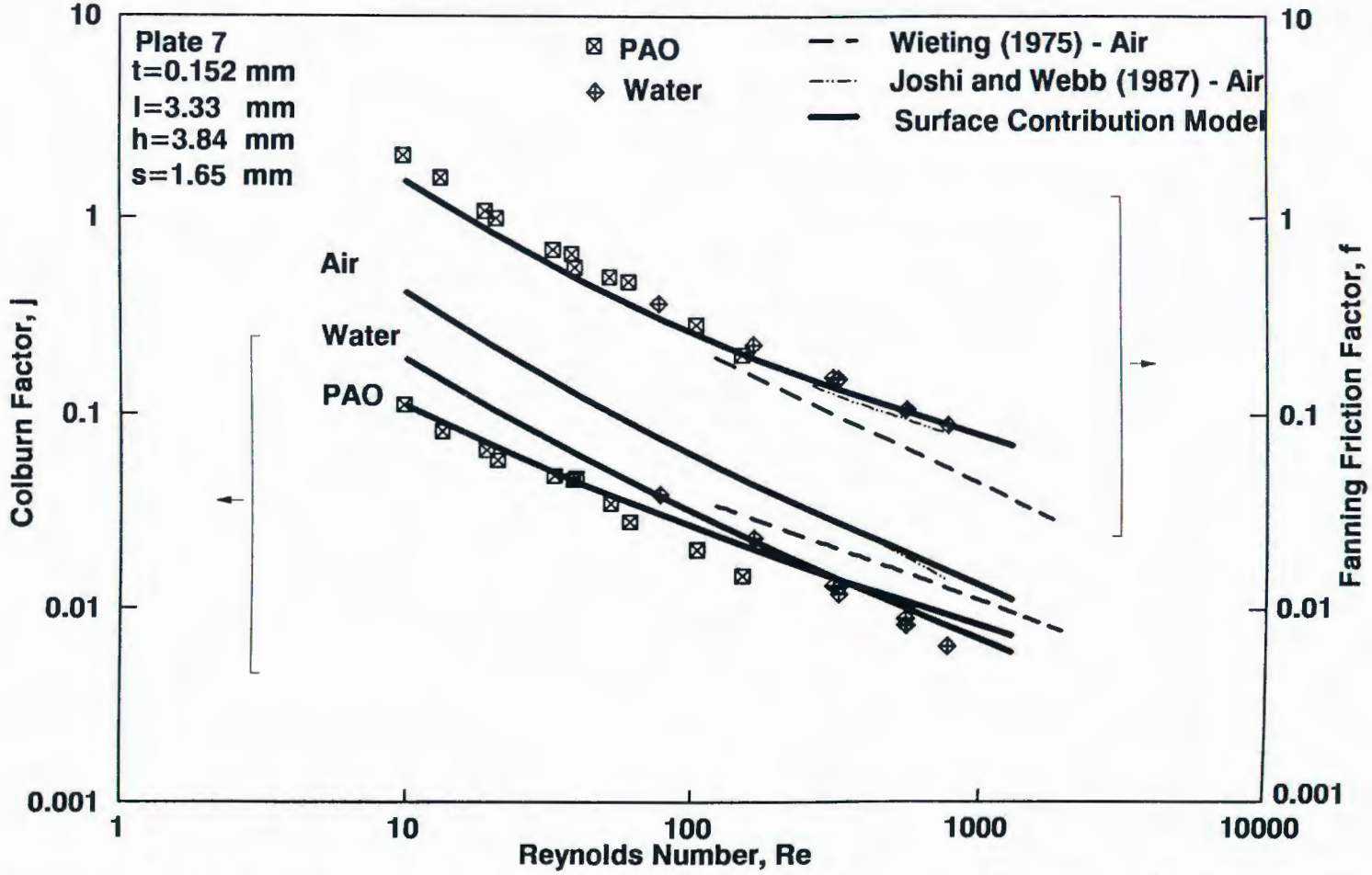

Figure 6-26 Comparison of Air Models and Results From Present Work at 10°C For Plate 7

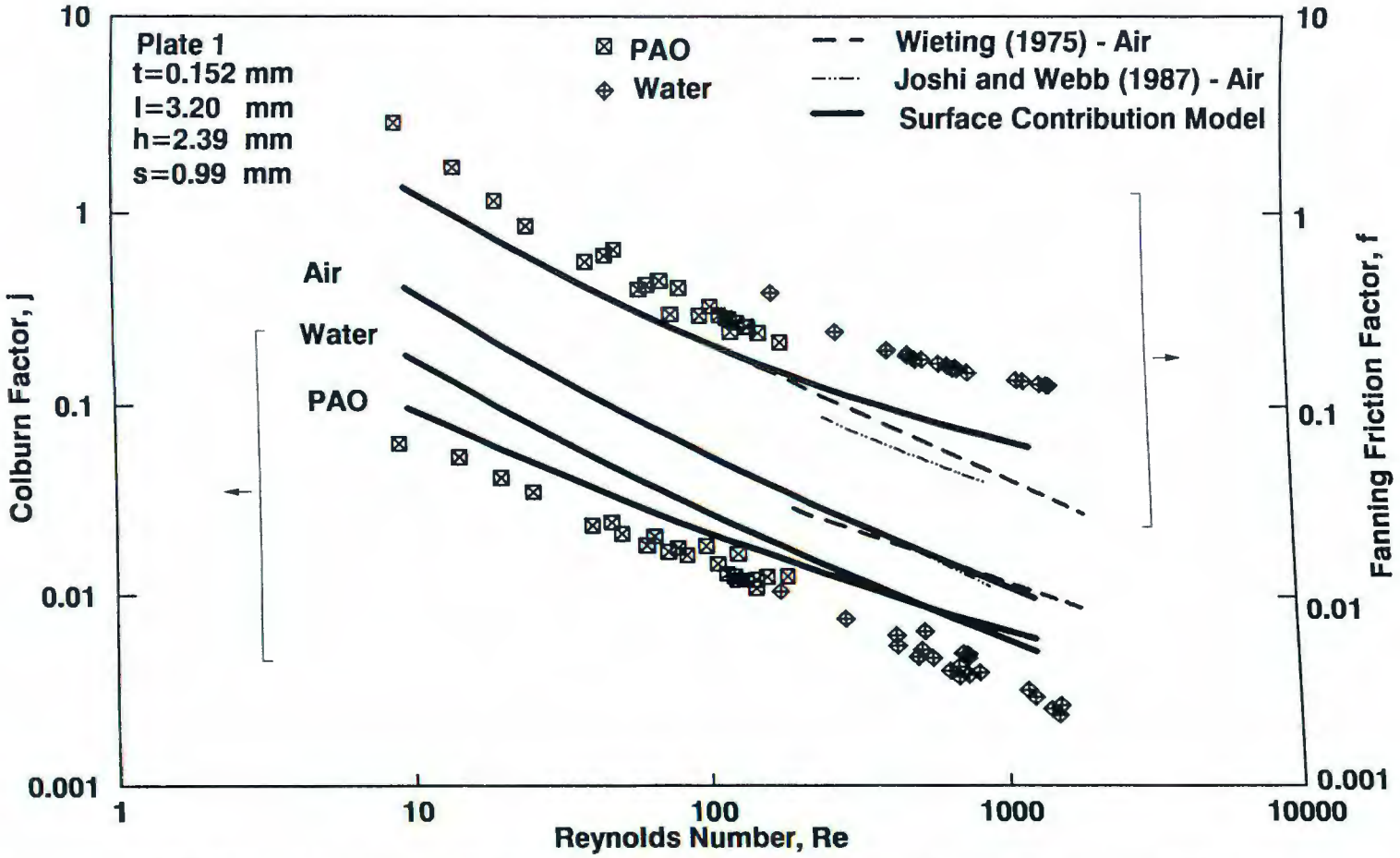

Figure 6-27 Comparison of Air Models and Results From Present Work at 10°C For Plate 3

Table 6-2 Fin Geometry of Experimental Study (Brinkmann et al., 1987)

Fin Array	t (mm)	s (mm)	h (mm)	l (mm)
A	0.76	2.41	8.76	3.18
B	0.38	2.08	5.33	3.30

ordinate is the ratio of j from the current model and the experimental data, j^*, from Brinkmann et al. (1987). With Reynolds number from 1000 to 10000, the current model can predict their experimental data within $\pm 12\%$. Although the surface contribution model was verified to Re of 2000 in the current study, it was tested against the Brinkmann data up to Re=10,000. Compared with air test data, the Colburn factors of Brinkmann's liquid tests are larger, which appears contrary to the current water test data when compared to air. The model explains the apparent contradiction in terms of entry length effects. Since the fin array used by Brinkmann et al. (1987) has only 4 rows of fins in the flow direction, the heat transfer coefficient is very high due to entry effects. In comparison, the fin array used in the current experiments have more than 80 rows of fins in the flow direction and, therefore, the entry effects are weaker. Therefore, with the same Prandtl number, the Colburn factor for a fin array can be different due to the dimension of the fin array. The good agreement between the current model and test data of Brinkmann et al. (1987) indicates that the current model is useful over a wide range of configurations.

From Figure 6-28, it can be seen that for large Reynolds numbers, the current model tends to underpredict the experimental data. This is because turbulence appears

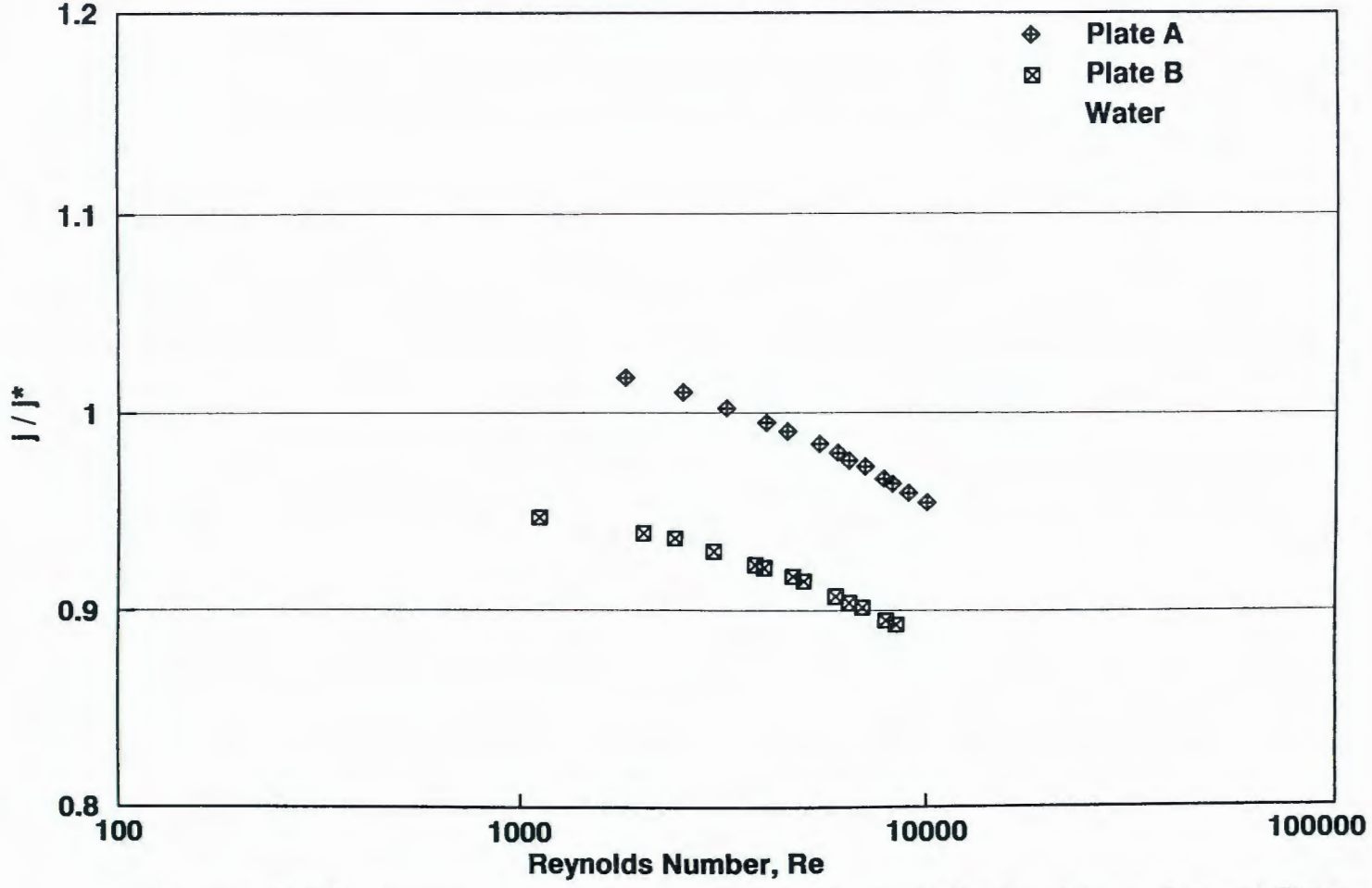

Figure 6-28 Comparison of the Current Model with Experiment Data from Brinkmann et al. (1987)

at high Reynolds number. For Reynolds number above 2300, turbulence was found in the free stream after 4 rows of fins by Mochizuki et al. (1988). The current model is based on laminar flow, which does not model the effects of turbulence.

CHAPTER 7

SUMMARY AND CONCLUSIONS

7.1 Summary

Although a large number of air studies on the offset fin geometry appear in the literature, very few studies were found using liquid coolants. Liquid coolants are of on-going interest for high performance applications such as electronic cooling. The motivation for the present study was to provide detailed design data for liquid cooled applications and to understand the physics of these devices. A total of 511 experiments to measure heat transfer and pressure drop were performed using liquids with Prandtl number from 3 to 150, Reynolds number from 10 to 2000 for seven offset fin cold plates with different fin geometries. Uniform heat flux was ranging from 1 to 8 W/cm^2 applied on the cold plates. From experimental results, Prandtl number was found to influence the Colburn factor significantly. Higher Prandtl number implies a longer developing heat transfer region, which means larger average Nusselt number in the fin array. Prandtl number was found to have little effect on the friction factor.

A series of repeatability tests were performed. For Colburn factor, all the repeatability tests were within $\pm 20\%$ of the original tests while 80% of the repeatability results are within $\pm 10\%$ of the original data. For friction factor, all the repeatability results are within $\pm 20\%$ of the original tests while 85% of the repeatability test results are within $\pm 10\%$ of the original test results. An uncertainty analysis was performed (Appendix B) to interpret these results. The uncertainty values

for low Reynolds number tests are $\pm 25.8\%$ for Colburn factor and $\pm 23.6\%$ for friction factor. For higher Reynolds number tests, the uncertainty values are significantly smaller. This trend can also be seen in the detailed data of the repeatability tests.

During experiments using water without deionizing treatment (tap water), water scaling occurred in the fin array, which caused lower Colburn factor and higher friction factor. This problem occurred only for Plate 1. The experimental data of Plate 1 shows significant effects of water scaling in the initial tests. The scale was cleaned from Plate 1 using an acid wash, but the data were still affected. On Plates 2 to 7, deionized water was used to minimize the water scaling problem. Filters are necessary in the test loop to prevent blocking of the fin ducts by foreign materials. Early tests on Plate 1 were done without filters and subsequent inspection indicated significant clogging of the flow passages with fibers, which came from the deionizing process of water. All tests on Plates 2 to 7 were performed with filters.

Comparison between the current liquid test results and air models (Wieting, 1975; Joshi and Webb, 1987) shows that air models can not accurately predict the Colburn factor in liquid applications. Because liquids have a higher Prandtl number than air, the array perspective effect is larger. In low Reynolds number, the comparison results demonstrate the lower Colburn factor for liquid than that for air, which is due to the Prandtl number effects.

A surface contribution model was constructed to predict the heat transfer and pressure drop for the offset fin arrays, which is modified from a laminar model for

rectangular ducts. The model considers the significant effects of Prandtl number on heat transfer from two perspectives: fin perspective and array perspective. The fin perspective considers the effects of Prandtl number on the periodic fully developed Nusselt number due to interruptions in the fin geometry. The array perspective considers the effects of Prandtl number on the entry length characteristics. The thermal developing length of offset fins is as much as 10 times shorter than the developing length of a rectangular duct. The model also takes account of the effects from Reynolds number and fin geometry, which allows the model to predict the heat transfer and pressure drop of offset fin arrays. Within a deviation of $\pm 20\%$, the model predicts 94% of Colburn factor test data and 90% of friction factor test data.

The model results are also compared with Colburn factor from the water tests done by Brinkmann et al. (1987), which show agreement within $\pm 12\%$. The model explains the high Colburn factor from their four-row fin array in terms of entry length effects. The good agreement of the current model results with test data indicates that the model is applicable to laminar offset fin applications with Prandtl number from 0.7 to 150.

A numerical heat transfer model was built to study the conduction (thermal spreading and end effects) in the cover plate over the finned section. From the heat flux distribution along the plate, the thermal spreading is found to be about 0.2% of the total heating power and the conduction end effects is about 1.9% of the total heating power. From the results, approximately uniform convective heat flux is observed in the middle section of the plate, which is consistent with the constant heat

flux assumption used in the current study. Thermal spreading and end effects can be significant if the thickness of the cover plate is large. The results show that end effects are important in the cold plate design but that conduction effects (thermal spreading) in the central section is not important for typical cold plate design.

7.2 Conclusions

Liquid coolants have higher heat transfer coefficient than air due to their combined properties including higher density, thermal conductivity and specific heat. Even though liquids have higher viscosity than air, they still have better specific heat transfer for a certain specific pumping power. For cooling applications with heat flux between 1 to 8 W/cm^2, liquid coolant are the preferred choice.

In practical cooling applications, water is not a reliable coolant, even though it has higher specific heat transfer with a certain specific pumping power. Water has the problem of scaling, which fouls the surface and reduces the performance significantly. Since PAO is a low viscosity oil (μ=7.229$\times$10^{-3} kg/m-s, at 20 °C), it has no scaling problems and also has reasonable heat transfer without a significant pressure drop. From a practical point of view, PAO is the liquid coolant of choice.

The hydraulic diameter has large effects on the fin performance. The fin arrays with smaller hydraulic diameter have a higher specific heat transfer for a certain specific pumping power. To increase heat transfer with the same pressure drop and fluid, fin arrays with smaller hydraulic diameters should be selected. But it should be noted that the fin array with smaller hydraulic diameter is likely to have the fin burrs

and deformed fins due to the manufacturing process.

Besides the hydraulic diameter, other fin geometry parameters also affect the offset fin performance. From results of the current study, the design of these particular parameters should consider the fluid type. For example, the design of fin height and fin thickness should be modified between air and PAO. Air has low heat transfer coefficient (60 - 170 W/m^2-°C), which tends to have higher surface efficiency (98 - 94%). For air, fin height and fin thickness have little effects on the surface efficiency. With design constraints, such as a certain frontal flow area and more compact fin array, the selection freedom of selecting fin height and fin thickness is important. Different from air, PAO has higher heat transfer coefficient (600 - 1935 W/m^2-°C), which leads to a lower surface efficiency (80 - 60%). From the current analyses, smaller fin height and larger fin thickness can improve the surface efficiency, consequently increase the heat transfer. It should be realized that smaller fin height and larger fin thickness can have larger pressure drop. To select fin height and fin thickness with satisfying the constraints, it is necessary to consider the tradeoff of specific heat transfer and specific pumping power.

Fin length should also be modified depending on different fluids. Due to the low Prandtl number of air, the fin is in the thermal fully developed region, which has the a constant heat transfer coefficient. For air, fin length has no large effect on the heat transfer coefficient. In contrast, PAO with a large Prandtl number, experiences significant entry length effects. Since the heat transfer coefficient is larger in the thermal developing region, short fins can have a higher average heat transfer

coefficient than longer fins. Although the effects of developing heat transfer can be reduced by the nonuniform inlet fluid temperature, the thermal developing effects still exists and increases the heat transfer of the offset fins. For high Prandtl number fluids, it is preferred to select the fin length shorter than the developing length. The fin spacing distance effects on the fin performance is not affect by the fluid type. Since the smaller fin spacing distance can reduce the hydraulic diameter, it is preferred to be reduced, but the size of fin spacing distance is limited by the occurrence of burrs due to the manufacturing process. Since the difference of design objective and constraints, the detailed design method should be based on the particular application. No general design rules can cover all the cases.

Similar to the discussion about the fin length, the design of array length should also depend on the fluid. For air, a large fraction of the array is in thermal periodic fully developed region, which has a constant cell-average heat transfer coefficient. Using air, the array length has no large effect on heat transfer coefficient. Since PAO has a longer thermal developing region, short arrays can have a significantly higher average heat transfer coefficient than longer arrays. To improve heat transfer, it is advisable to choose the array length less than the thermal developing length, which can improve the heat transfer.

CHAPTER 8

FUTURE WORK

The current study has investigated the heat transfer and pressure drop performance of the offset fin array, with Prandtl number ranging from 0.7 - 150 and different fin geometries. To achieve better understanding about the performance of offset fin arrays, the following tasks should be performed.

1. To decrease the uncertainty of experimental data, better control of experimental system is needed.
2. To obtain better understanding of the array perspective effects at the beginning of the fin array, the end effects need to be minimized. Two methods are recommended: 1) Smaller cover plate thickness and 2) Guard heaters at the end sections. The heaters can decrease the surface temperature difference between the finned section and the end sections, which can minimize the end effects.
3. The laminar experiments and model described in this dissertation need to be extended to the turbulent regime. Although most liquid applications employ laminar flows due to the pressure drop considerations, the turbulent characteristics are of interest for a complete understanding of the physics.
4. The reduced entry length of the offset fin geometry as compared to a rectangular duct needs to be more fully documented and understood. This could be achieved through numerical calculations. The effects of Reynolds and Prandtl numbers on entry length are relevant to a more complete understanding.

5. The conclusions about hydraulic diameter are that smaller hydraulic diameter leads to a more effective design. The term micro-channel has been used to describe recent work in even smaller flow ducts. The micro-channel work is very promising. It would be of interest to determine whether or not offset fins are useful in very small fin geometries.

6 The flow perpendicular to the offset fin surfaces is an option to improve the heat transfer, because it can reduce the thickness of boundary layers. With the increased heat transfer, it can also lead to a high pressure drop. It is of interest to compare the heat transfer against pressure drop for this application and understand effects of the flow direction on the performance of the offset fin arrays. The effects of Prandtl number and fin geometry on the fin array performance are also needed to investigate to achieve a complete understanding.

7. An optimization study is needed to help the design of the fin geometry parameters, with consideration of the fluid type. Based on the surface contribution model described in the dissertation, an optimization software is needed to achieve the design objective by satisfying the constraints.

APPENDIX A

CALIBRATION OF THE MEASURING TRANSDUCERS

All the transducers used in the tests were calibrated before the tests. The data processing of experimental data is based on the calibration results. Calibrations were conducted on the thermocouples, the differential pressure transducer, the power transducer, and the flow meters. The data acquisition system is used in the calibration process to prevent the system error induced from data acquisition system.

A.1 Calibration of Thermocouples

All the thermocouples used in the test are type T, but they include different sizes of thermocouple wire. Thermocouples with 0.076 mm diameter, are used to measure the heated surface temperatures. The thermocouples with 0.1 mm diameter are used to measure the unheated top surface temperatures. Sheathed thermocouples with 0.32 mm sheath diameter are used to measure the fluid temperatures. All the thermocouples were calibrated individually against a platinum thermometer with an absolute accuracy of better than 0.01 K. In the calibration system, a water container and temperature control device (HAAKE, 001-4200) provide the constant temperature source. All the thermocouples use an ice bath as the temperature reference, which is also used in the actual experiment. The range of calibration temperature (0 - 82 °C) covers actual experimental temperature range (10 - 70 °C). All thermocouples with diameter of 0.076 mm and 0.1 mm have essentially the same calibration curve.

Table A-1 Thermocouple Calibration Data

Thermocouple Wires (0.076 mm; 0.1 mm)		Sheathed Thermocouple (0.32 mm)	
Temperature (°C)	Thermocouple Voltage (mV)	Temperature (°C)	Thermocouple Voltage (mV)
0	0	0	0
10.24	0.402	10.26	0.395
20.49	0.813	20.47	0.804
30.77	1.234	30.70	1.223
41.07	1.665	40.96	1.654
51.38	2.106	51.23	2.091
61.69	2.557	61.52	2.540
72.02	3.018	71.79	2.999
82.34	3.489	82.08	3.469

However, the sheathed thermocouples have different calibration results. The calibration data of the thermocouples are shown in Table A-1.

A.2 Calibration of the Turbine Flow Meters

The calibration loop for the flow meters was designed in the system, shown in Figure 3-3. Tank A used as a buffer to hold the flowing fluid before and after the calibration. Tank B takes the fluid flowing through the flow meter. The calibration accuracy of flow meters depends on the weight change in Tank B. For the small flow rate, the calibration time is longer than that for the larger flow rate in order to obtain enough fluid weight change in Tank B. During calibration, fluid flows into Tank B after valve H and C or D are shut off and the weight change of fluid in Tank B was

Table A-2 Calibration Results for Flow Meters with PAO

Sponsler: SP-1/2		Sponsler: MF-80	
Frequency (Hz)	Flow Rate (liter/min)	Frequency (Hz)	Flow Rate (liter/min)
43	1.68	40	0.13
81	2.85	80	0.19
102	3.55	111	0.24
146	4.91	221	0.38
199	6.73	403	0.64
241	8.18	632	1.01
323	11.3	784	1.24
452	16.41	972	1.52
		1443	2.25
		1976	3.19
		2558	4.24

measured. In the same period of time, the frequency from the turbine flow meter was recorded and averaged. Then, the correspondence between flow rates and flow meter frequencies, was obtained. With each fluid, both flow meters were calibrated at 20 and 60 °C. Table A-2 and A-3 show the calibration results for both flow meters with each fluid at 20 °C.

In the calibration, the absolute errors of calibration time is ± 0.5 second. The weight measuring maximum absolute error is ± 0.2 kg for the large flow meter (SP-1/2) and ± 0.13 kg for the small flow meter (MF-80). The minimum calibration time is 3 minutes and the minimum weight change is 14 kg. Calibrations of the flow meters at fluid temperature of 60 °C were also performed. It was found that the fluid

Table A-3 Calibration Results for Flow Meters with Water

Sponsler: SP-1/2		Sponsler: MF-80	
Frequency (Hz)	Flow Rate (liter/min)	Frequency (Hz)	Flow Rate (liter/min)
43	1.47	33	0.0568
87	3.01	54	0.0871
103	3.57	55	0.0908
134	4.62	63	0.102
166	5.74	90	0.140
204	7.07	135	0.204
245	8.47	193	0.288
288	9.96	256	0.375
343	11.83	304	0.435
372	12.82	374	0.541
		488	0.712
		626	0.882
		823	1.16
		1042	1.45
		1854	2.50

temperature has little effect on the calibration curve.

A.3 Calibration of the Differential Pressure Transducer

The differential pressure transducer was calibrated with a manometer using mercury and water, where mercury was used for the differential pressure range from 23 to 150 kPa and water was used for the range from 0.4 to 27 kPa. Compressed air

Table A-4 Calibration Results of Differential Pressure Transducer

Differential Pressure Transducer (V)	Differential Pressure (Pa) Water Manometer	Differential Pressure (Pa) Mercury Manometer
0.016	400	
0.05	1701	
0.30	11000	
0.74	26904	
0.64		23402
1.01		37404
1.62		57690
2.07		73148
2.33		83930
2.61		92107
3.01		105850
3.22		112991
3.71		133411
4.01		142457
4.22		150143

was used as the pressure source for the calibration. Table A-4 shows the calibration results of the differential pressure transducer.

In the manometers, the maximum error of height measurement is 0.5 mm and the minimum height difference between the two tubes is 40 mm. Based on this calibration, the pressure transducer has an accuracy of ± 8 Pa.

Table A-5 Calibration Results of the Power Transducer

Power Transducer (V)	Power (W)
0.64	256
1.02	410
1.62	640
2.11	859
2.42	970
2.61	1040
3.05	1230
3.23	1303
3.75	1510
4.11	1639
4.24	1695
5.03	2012

A.4 Calibration of the Power Transducer

The power transducer is calibrated with two autoranging microvolt DMMs (KEITHLEY) used as an ammeter and a voltmeter. The calibration range is from 256 to 2012 W, which covers the power range in the application. Table A-5 shows the calibration results of the power transducer.

Since the accuracy of the ammeter and voltmeter is $\pm 1\%$ and $\pm 1.5\%$ of the reading, they have the measuring error of ± 100 mA for 10 A and ± 3 V for the voltmeter at the 200 V. The power transducer has accuracy of $\pm 1.8\%$ which has the error of ± 4 W.

APPENDIX B

UNCERTAINTY ANALYSIS

The uncertainty in the measurement of Colburn factor and friction factor are calculated based on the maximum errors from each of measuring transducers. Kline (1985) described the method of uncertainty evaluation, which is outlined briefly as follows.

If R is the result computed from n measurement quantities x_1, x_2,..., x_n, the absolute uncertainty of R, which is denoted by W_R, has the form

$$W_R = \sqrt{\left(\frac{\partial R}{\partial x_1}\delta x_1\right)^2 + \left(\frac{\partial R}{\partial x_2}\delta x_2\right)^2 + \ldots + \left(\frac{\partial R}{\partial x_n}\delta x_n\right)^2} \qquad \textbf{(B.1)}$$

The relative uncertainty can be obtained by

$$w_R = \frac{W_R}{R} \qquad \textbf{(B.2)}$$

If a quantity R has the form

$$R = x_1^a x_2^b x_3^c \ldots x_n^m \qquad \textbf{(B.3)}$$

then relative uncertainty of R is (Moffat, 1988)

$$w_R = \frac{\delta R}{R} = \sqrt{\left(a\frac{\delta x_1}{x_1}\right)^2 + \left(b\frac{\delta x_2}{x_2}\right)^2 + \ldots + \left(m\frac{\delta x_n}{x_n}\right)^2} \qquad \textbf{(B.4)}$$

The uncertainty of the reported results is caused by uncertainties in fin geometry, temperatures, pressure drop and flow rate. The measuring transducers for temperature, pressure drop and flow rate are calibrated, which have the accuracy as

Temperature: ± 0.1 °C

Pressure drop: ± 8 Pa

Flow Rate: ± 0.016 liter/min (for MF-80 flow meter)

± 0.067 liter/min (for SP-1/2 flow meter)

The accuracy of fin geometry (t, l, h, s) measurement is $\pm 2.54 \times 10^{-5}$ m.

The experimental parameters can be expressed in terms of the above quantities. For example, the heat transfer area A, can be expressed as a function of fin geometry

$$A = f(s, h, l, t) \tag{B.5}$$

and so can the velocity and other parameters. By using the above uncertainty of basic parameters and Equations B.1 to B.4, the uncertainty of each experimental data point can estimated. The following sample uncertainty calculation on Run P3-10-2 for Plate 3 demonstrates the uncertainty estimation methods in the current study.

Fin geometry parameters for Plate 3 are listed in Table 3-1, which has the measurement uncertainty of $\pm 2.54 \times 10^{-5}$ m. The flow meter SP-1/2 is used in the run, which has the uncertainty of ± 0.067 liter/min.

w_G	=	$\pm 1.54\%$	-----	relative uncertainty of flow rate
w_A	=	$\pm 2.01\%$	-----	relative uncertainty of surface area
w_{Dh}	=	$\pm 2.09\%$	-----	relative uncertainty of hydraulic diameter
$w_{\Delta Tlm}$	=	$\pm 5.73\%$	-----	relative uncertainty of log mean temperature difference
w_q	=	$\pm 2.50\%$	-----	relative uncertainty of heating power

where the physical properties are assumed to have zero uncertainty.

The Colburn factor can be expressed in the form

$$j = \left(\frac{q}{A\ T_{lm}}\right)\left(\frac{1}{\rho\ c_p\ G/A}\right) Pr^{2/3} \qquad \textbf{(B.6)}$$

From Equations B.1 to B.4, the relative uncertainty of Colburn factor can be calculated with

$$\frac{\delta j}{j} = \sqrt{\left(\frac{\delta q}{q}\right)^2 + \left(-\frac{\delta(\Delta T_{lm})}{\Delta T_{lm}}\right)^2 + \left(-\frac{\delta G}{G}\right)^2} \qquad \textbf{(B.7)}$$

which yields the relative uncertainty of Colburn factor as $\pm 6.25\%$. From Equation 6.10, the relative uncertainty of friction factor can be calculated with

$$\frac{\delta f}{f} = \sqrt{\left(\frac{\delta \Delta P_L}{\Delta P_L}\right)^2 + 2\left(\frac{\delta u}{u}\right)^2 + \left(\frac{\delta D_h}{D_h}\right)^2 + \left(\frac{\delta L}{L}\right)^2} \qquad \textbf{(B.8)}$$

which gives the relative uncertainty of friction factor as $\pm 3.67\%$. The results give the uncertainty values for experimental parameters for Run P3-10-2 with Re=245. The uncertainty estimation for other test runs follows the same method. For example, for Run P3-10-6 with Re=92, the relative uncertainty for Colburn factor and friction factor are $\pm 7.2\%$ and $\pm 6.52\%$. For Run P3-10-15 with Re=12, the relative uncertainty for Colburn factor and friction factor are $\pm 25.8\%$ and $\pm 23.6\%$. It can be found that tests with low Reynolds number have higher uncertainty of Colburn factor and friction factor due to the higher uncertainty of flow rate.

APPENDIX C

COOLANT PHYSICAL PROPERTIES

The physical properties of interest in the current study are specific heat, thermal conductivity, density and viscosity. Among the three coolants (air, water and PAO) considered in the current study, the physical properties of water and air can be found in standard reference sources. The properties of PAO were obtained from the manufacturer (Chevron Chemical Company). Data regression equations were formulated to predict the coolant physical properties in the temperature range of 0 - 80 °C, which covers the fluid temperature range in the study. In the following formula, T_f indicates the fluid temperature in °C.

C.1 Air Properties

The property data for air were obtained from Incropera and Dewitt (1990). In the temperature range 0 - 80 °C, the data regression formula of physical properties are listed as following.

Thermal Conductivity (W/m-°C):

$$k = 0.02882 - 5.2452\times10^{-4} T_f + 2.8408\times10^{-5} T_f^2 - 5.5\times10^{-7} T_f^3 + 3.6\times10^{-9} T_f^4 \quad \textbf{(C.1)}$$

Density (kg/m^3):

$$\rho = 1.4594 - 0.02241 T_f + 6.66\times10^{2} T_f^2 - 9.9\times10^{6} T_f^3 + 5.3\times10^{-8} T_f^4 \quad \textbf{(C.2)}$$

Dynamic viscosity (kg/m-s):

$$\mu = 1.7\times10^{-5} + 2.2\times10^{-8} T_f + 1.6\times10^{-9} T_f^2 - 3.4\times10^{-11} T_f^3 + 2.4\times10^{-13} T_f^4 \quad \textbf{(C.3)}$$

Specific heat (J/kg-°C):

$$c_p = 1005 \tag{C.4}$$

C.2 Water Properties

The property data for water were obtained from Incropera and Dewitt (1990). In the temperature range 0 - 80 °C, the data regression formula of physical properties are listed as following.

Thermal Conductivity (W/m-°C):

$$k = 0.5604 + 2.359\times10^{-3}T_f + 1.3\times10^{-5}T_f^2 \tag{C.5}$$

Density (kg/m^3):

$$\rho = 999.62 - 0.02161T_f - 4.17\times10^{-3}T_f^2 \tag{C.6}$$

Dynamic viscosity (kg/m-s):

$$\mu = 1.498\times10^{-3} - 2.9\times10^{-5}T_f + 2\times10^{-7}T_f^2 \tag{C.7}$$

Specific heat (J/kg-°C):

$$c_p = 4178 \tag{C.8}$$

C.3 PAO Properties

The property data for PAO were obtained from the manufacturer (Chevron Chemical Company). In the temperature range 0 - 80 °C, the data regression formula of physical properties are listed as following.

Thermal Conductivity (W/m-°C):

$$k = 0.145 + 9.786\times10^{-5}(T_f + 10) \tag{C.9}$$

Density (kg/m^3):

$$\rho = 805 - 0.66667\ T_f \qquad \textbf{(C.10)}$$

Dynamic viscosity (kg/m-s):

$$\log_{10}\mu = 1.2037\times10^{-3} - 1.995\times10^{-5}T_f + 1.5\times10^{-7}T_f^2 - 7\times10^{-10}T_f^3 \qquad \textbf{(C.11)}$$

Specific heat (J/kg-°C):

$$c_p = 2090 + 3.463(T_f + 10) \qquad \textbf{(C.12)}$$

APPENDIX D

DATA REGRESSION RESULTS

Table D-1. Empirical Form of Surface Friction Factor of Fin Sides

$x^+_F \leq 0.001$	$\log_{10}(Re^r f_p) = a_{1,1} + a_{1,2} \log_{10} x^+_F$			
	$a_{1,1}$	0.6401	$a_{1,2}$	-0.4683
$x^+_F > 0.001$	$Re^r f_P = A_2 + A_3 \log_{10} x^+_F + A_4 \log^2_{10} x^+_F + A_5 \log^3_{10} x^+_F$			
	$A_2 = a_{2,1} + a_{2,2} \log_{10} (1/\alpha)$			
	$A_3 = a_{3,1} + a_{3,2} \log_{10} (1/\alpha)$			
	$A_4 = a_{4,1} + a_{4,2} \log_{10} (1/\alpha)$			
	$A_5 = a_{5,1} + a_{5,2} \log_{10} (1/\alpha)$			
	$a_{2,1}$	9.92122	$a_{2,2}$	-2.92464
	$a_{3,1}$	-17.0381	$a_{3,2}$	1.08256
	$a_{4,1}$	-14.4094	$a_{4,2}$	2.35842
	$a_{5,1}$	-6.49488	$a_{5,2}$	-0.616856

The multiple correlation coefficient R^2 is 0.9999.

Table D-2 Surface Friction Factor on Top / Bottom Surfaces (Shah and London, 1978)

$$f_E Re^r = 24 (1 - 1.3553\alpha + 1.9467\alpha^2 - 1.7012\alpha^3 + 0.9564\alpha^4 - 0.2537\alpha^5)$$

Table D-3 Empirical Form for Nusselt Number on the Fin Sides

$x^*_F \le 0.005/X_{rl}$	$\log_{10}Nu_F = B_1(Pr)+B_2(Pr)\log_{10}(x^*_F X_{rl})+\log_{10}F_\alpha$			
	$B_1(Pr) = b_{1,1} + b_{1,2}\log_{10}(1/Pr + 0.02)$			
	$B_2(Pr) = b_{2,1} + b_{2,2}\log_{10}(1/Pr + 0.02)$			
	$b_{1,1}$	0.41752	$b_{1,2}$	0.048235
	$b_{2,1}$	-0.31915	$b_{2,2}$	-0.013015
$0.005/X_{rl} \le x^*_F \le 4/X_{rl}$	$Nu_F = (B_3(Pr)+B_4(Pr)\log_{10}(x^*_F X_{rl})+B_5(Pr)\log^2_{10}(x^*_F X_{rl}) +B_6(Pr)\log_{10}{}^3(x^*_F X_{rl}))\ F_\alpha$			
	$B_3(Pr) = b_{3,1} + b_{3,2}\log_{10}(1/Pr + 0.02)$			
	$B_4(Pr) = b_{4,1} + b_{4,2}\log_{10}(1/Pr + 0.02)$			
	$B_5(Pr) = b_{5,1} + b_{5,2}\log_{10}(1/Pr + 0.02)$			
	$B_6(Pr) = b_{6,1} + b_{6,2}\log(1/Pr + 0.02)$			
	$b_{3,1}$	4.2326	$b_{3,2}$	0.058957
	$b_{4,1}$	-0.43881	$b_{4,2}$	-0.16341
	$b_{5,1}$	0.25764	$b_{5,2}$	0.13332
	$b_{6,1}$	-0.61898	$b_{6,2}$	-0.082139
$x^*_F > 4/X_{rl}$	$Nu_F = 4.11\ F_\alpha$			
$F_\alpha = 1.12995-0.446876\alpha+0.450324\alpha^2-0.155325\alpha^3$				

The multiple correlation coefficient R^2 is 0.9961. The empirical formula of the modification factor for aspect ratio, F_α, is obtained by data regression from Shah and London (1978). When $\alpha=0.5$, the modification factor F_α equals 1.

Table D-4. Empirical Form for Thermal Field Development of Fin Array

$x^* \le 0.01/X_{r2}$	$\log_{10} Nu_x^m = C_1(Pr)+C_2(Pr)\log_{10}(x^*X_{r2})+\log_{10}F_\alpha$		
	$C_1(Pr) = c_{1,1} + c_{1,2}\log_{10}(1/Pr)$		
	$C_2(Pr) = c_{2,1} + c_{2,2}\log_{10}(1/Pr)$		
	$c_{1,1}$	0.17773	$c_{1,2}$	-0.01096
	$c_{2,1}$	-0.034447	$c_{2,2}$	-0.02854
$0.01/X_{r2} \le x^* \le 4/X_{r2}$	$Nu_x^m = (C_3(Pr)+C_4(Pr)\log_{10}(x^*X_{r2})+C_5(Pr)\log_{10}^2(x^*X_{r2})$ $+C_6(Pr)\log_{10}^3(x^*X_{r2}))\ F_\alpha$		
	$C_3(Pr) = c_{3,1} + c_{3,2}\log_{10}(1/Pr)$		
	$C_4(Pr) = c_{4,1} + c_{4,2}\log_{10}(1/Pr)$		
	$C_5(Pr) = c_{5,1} + c_{5,2}\log_{10}(1/Pr)$		
	$C_6(Pr) = c_{6,1} + c_{6,2}\log_{10}(1/Pr)$		
	$c_{3,1}$	4.1641	$c_{3,2}$	0.049146
	$c_{4,1}$	-0.076964	$c_{4,2}$	-0.021481
	$c_{5,1}$	-0.24932	$c_{5,2}$	-0.041330
	$c_{6,1}$	-0.49395	$c_{6,2}$	-0.099595
$x^* \ge 4/X_{r2}$	$Nu_x^m = 4.11\ F_\alpha$		

where F_α has the same definition as that in Table D-3. The multiple correlation coefficient R^2 is 0.9961.

Table D-5. Empirical Correlations of Developing Heat Transfer in Parallel Plates (Shah and London, 1978)

If $x^{P*} \leq 0.001$	$Nu_x^p = 1.233\ x^{P*-1/3} + 0.4$
If $x^{P*} > 0.001$	$Nu_x^p = 7.541 + 6.874(10^3\ x^{P*})^{-0.488} e^{-245\ x^{P*}}$

APPENDIX E

SUMMARY OF EXPERIMENTAL RESULTS

The experiments on seven plates were performed with different fluids and fluid temperatures. Total 511 experimental data are reported according to the fluid type and fluid temperature as following.

Table E.1 Experimental Data for Plate 1

Run No.	Fluid Type	Aver. Fluid Temp. (°C)	Prandtl Number	Reynolds Number	Heat Flux (W/cm^2)	LMTD (°C)	Colburn Factor	Pressure Drop (kPa)	Friction Factor
P1-20-1	PAO	22.3	104	147	6.84	15.2	0.0121	77.9	0.257
P1-20-2	PAO	21.1	108	80	4.71	18.0	0.0118	57.9	0.600
P1-20-3	PAO	23.4	100	159	7.60	15.6	0.0125	79.7	0.240
P1-20-4	PAO	25.1	95	110	7.24	17.9	0.0147	46.6	0.330
P1-20-5	PAO	28.0	88	86	7.08	20.4	0.0163	29.5	0.410
P1-20-6	PAO	24.3	98	135	7.09	17.3	0.0120	61.3	0.271
P1-20-7	PAO	22.8	102	128	5.51	13.9	0.0121	62.4	0.282
P1-20-8	PAO	22.3	104	146	5.52	13.4	0.0109	77.8	0.259
P1-20-9	PAO	25.8	93	74	5.48	16.9	0.0170	27.5	0.446
P1-20-10	PAO	27.6	89	52	5.35	19.0	0.0210	17.7	0.647
P1-20-11	PAO	26.3	92	188	3.45	6.2	0.0126	82.3	0.214
P1-20-12	PAO	27.3	89	129	3.23	5.5	0.0199	41.4	0.244
P1-20-13	PAO	28.9	85	100	3.13	6.1	0.0219	27.5	0.293
P1-20-14	PAO	29.5	84	63	3.05	7.4	0.0275	14.4	0.403

Run No.	Fluid Type	Aver. Fluid Temp. (°C)	Prandtl Number	Reynolds Number	Heat Flux (W/cm^2)	LMTD (°C)	Colburn Factor	Pressure Drop (kPa)	Friction Factor
P1-20-15	PAO	32.3	78	41	3.11	9.0	0.0352	7.3	0.562
P1-20-16	PAO	26.9	90	118	2.99	7.8	0.0130	43.2	0.296
P1-20-17	PAO	26.8	91	124	2.99	7.7	0.0126	46.9	0.286
P1-20-18	PAO	29.0	85	67	3.30	9.7	0.0204	17.6	0.424
P1-20-19	PAO	30.5	82	48	3.21	11.1	0.0242	11.8	0.603
P1-20-20	PAO	38.1	67	26	3.10	12.0	0.0422	3.2	0.858
P1-20-21	PAO	43.7	59	20	3.12	14.7	0.0458	2.0	1.15
P1-20-22	PAO	31.3	80	15	1.06	7.2	0.0381	3.0	1.70
P1-20-23	PAO	35.7	71	9	1.13	10.6	0.0450	1.6	2.87
P1-60-1	PAO	62.3	40	477	7.29	13.2	0.00679	55.2	0.133
P1-60-2	PAO	63.2	39	310	7.01	15.7	0.00808	27.1	0.161
P1-60-3	PAO	63.2	39	299	7.00	16.1	0.00812	27.0	0.172
P1-60-4	PAO	66.6	37	219	6.86	17.9	0.00983	15.7	0.215
P1-60-5	PAO	59.0	43	425	5.82	10.6	0.00732	53.9	0.142
P1-60-6	PAO	59.0	43	338	6.00	11.2	0.00895	37.4	0.157

Run No.	Fluid Type	Aver. Fluid Temp. (°C)	Prandtl Number	Reynolds Number	Heat Flux (W/cm^2)	LMTD (°C)	Colburn Factor	Pressure Drop (kPa)	Friction Factor
P1-60-7	PAO	64.6	38	144	5.86	15.9	0.0140	9.0	0.264
P1-60-8	PAO	62.3	40	191	5.79	13.8	0.0121	14.6	0.221
P1-60-9	PAO	27.2	90	82	6.87	16.6	0.0206	111.8	1.59
P1-60-10	PAO	26.0	93	92	3.09	5.3	0.0274	146.2	1.56
P1-60-11	PAO	65.3	38	624	8.06	9.4	0.00942	76.8	0.123
P1-60-12	PAO	66.1	37	352	7.34	11.8	0.0109	32.1	0.167
P1-60-13	PAO	63.1	39	213	3.55	4.5	0.0238	19.0	0.238
P1-60-14	PAO	67.9	36	77	3.36	8.8	0.0279	5.0	0.591
P1-60-15	PAO	64.5	38	42	1.25	1.8	0.1040	4.3	1.45
P1-60-16	PAO	70.3	34	21	1.22	6.7	0.0462	2.6	4.73
W1-10-1	WATER	16.1	8	38	1.06	1.4	0.0476	0.4	1.00
W1-10-2	WATER	12.5	8	101	1.10	1.5	0.0172	1.5	0.426
W1-10-3	WATER	11.6	8	167	1.07	1.5	0.0100	2.8	0.289
W1-10-4	WATER	11.1	9	237	1.07	1.5	0.00726	4.6	0.228
W1-10-5	WATER	11.9	8	227	2.97	4.0	0.00807	4.1	0.232

Run No.	Fluid Type	Aver. Fluid Temp. (°C)	Prandtl Number	Reynolds Number	Heat Flux (W/cm^2)	LMTD (°C)	Colburn Factor	Pressure Drop (kPa)	Friction Factor
W1-10-6	WATER	20.5	7	61	2.93	4.1	0.0297	0.7	0.729
W1-10-7	WATER	15.0	8	107	2.94	4.4	0.0151	1.5	0.437
W1-10-8	WATER	12.8	8	162	2.90	4.4	0.00990	2.6	0.296
W1-10-9	WATER	12.2	8	197	2.67	4.3	0.00746	3.5	0.266
W1-10-10	WATER	11.6	8	203	2.69	4.2	0.00747	3.8	0.260
W1-10-11	WATER	10.0	9	424	2.52	3.3	0.00448	10.8	0.161
W1-10-12	WATER	9.2	9	671	1.96	2.5	0.00290	23.3	0.134
W1-10-13	WATER	13.8	8	332	5.58	6.5	0.00693	6.5	0.184
W1-10-14	WATER	11.9	8	565	5.69	6.0	0.00463	16.1	0.145
W1-10-15	WATER	10.8	9	682	5.58	6.4	0.00342	22.9	0.136
W1-10-16	WATER	12.4	8	480	5.72	6.2	0.00524	12.1	0.155
W1-10-17	WATER	11.5	8	693	6.73	7.4	0.00359	22.7	0.135
W1-10-18	WATER	13.7	8	336	6.75	8.7	0.00592	6.7	0.185
W1-10-19	WATER	9.5	9	784	6.34	7.4	0.00285	30.5	0.130
W1-25-1	WATER	30.4	5	177	2.69	3.9	0.0105	1.9	0.386

Run No.	Fluid Type	Aver. Fluid Temp. (°C)	Prandtl Number	Reynolds Number	Heat Flux (W/cm^2)	LMTD (°C)	Colburn Factor	Pressure Drop (kPa)	Friction Factor
W1-25-2	WATER	26.9	6	542	3.45	3.1	0.00650	9.5	0.174
W1-25-3	WATER	26.1	6	813	3.69	3.5	0.00394	18.9	0.149
W1-25-4	WATER	29.2	6	295	3.08	3.9	0.00755	3.6	0.243
W1-25-5	WATER	27.9	6	435	3.37	3.7	0.00619	6.5	0.194
W1-25-6	WATER	27.0	6	725	3.61	3.2	0.00497	15.1	0.156
W1-25-7	WATER	26.4	6	750	3.66	3.2	0.00490	16.5	0.155
W1-25-8	WATER	29.8	5	436	6.04	7.3	0.00545	6.1	0.196
W1-25-9	WATER	28.5	6	573	6.23	6.8	0.00468	10.0	0.175
W1-25-10	WATER	27.4	6	746	6.40	5.8	0.00471	16.0	0.159
W1-25-11	WATER	30.2	5	513	7.42	8.8	0.00476	7.9	0.186
W1-25-12	WATER	28.6	6	653	7.66	8.6	0.00402	12.3	0.166
W1-25-13	WATER	27.1	6	698	7.73	8.6	0.00376	14.5	0.163
W1-25-14	WATER	30.0	5	530	7.40	8.0	0.00520	8.2	0.179
W1-25-15	WATER	28.7	6	698	7.67	7.9	0.00423	13.5	0.162
W1-25-16	WATER	27.6	6	1185	8.05	7.0	0.00319	34.4	0.136

Run No.	Fluid Type	Aver. Fluid Temp. (°C)	Prandtl Number	Reynolds Number	Heat Flux (W/cm^2)	LMTD (°C)	Colburn Factor	Pressure Drop (kPa)	Friction Factor
W1-25-17	WATER	26.5	6	1417	8.01	7.2	0.00253	49.1	0.130
W1-25-18	WATER	26.4	6	1493	7.95	7.2	0.00235	54.1	0.128
W1-25-19	WATER	27.3	6	1520	6.65	5.5	0.00265	53.8	0.128
W1-25-20	WATER	26.3	6	1249	6.55	5.8	0.00292	39.7	0.134
W1-25-21	WATER	27.3	6	752	6.16	6.4	0.00383	16.2	0.157
W1-25-22	WATER	28.3	6	511	5.99	7.0	0.00476	8.3	0.183
W1-60-1	WATER	61.2	3	3140	7.12	4.8	0.00213	45.6	0.0824
W1-60-2	WATER	61.4	3	2139	6.88	5.1	0.00267	24.0	0.0935
W1-60-3	WATER	62.0	3	1537	6.72	5.3	0.00337	13.6	0.103
W1-60-4	WATER	63.3	3	997	6.77	5.3	0.00520	6.6	0.122
W1-60-5	WATER	64.7	3	717	6.55	5.9	0.00592	3.7	0.136
W1-60-6	WATER	61.9	3	1535	5.51	4.4	0.00327	14.5	0.111
W1-60-7	WATER	62.5	3	1025	5.34	4.1	0.00523	7.4	0.127
W1-60-8	WATER	63.9	3	794	5.15	4.4	0.00572	4.9	0.143
W1-60-9	WATER	59.7	3	1560	2.33	1.9	0.00315	15.1	0.107

Run No.	Fluid Type	Aver. Fluid Temp. (°C)	Prandtl Number	Reynolds Number	Heat Flux (W/cm^2)	LMTD (°C)	Colburn Factor	Pressure Drop (kPa)	Friction Factor
W1-60-10	WATER	61.4	3	930	2.46	2.1	0.00472	6.1	0.127

Table E.2 Experimental Data for Plate 2

Run No.	Fluid Type	Aver. Fluid Temp. (°C)	Prandtl Number	Reynolds Number	Heat Flux (W/cm^2)	LMTD (°C)	Colburn Factor	Pressure Drop (kPa)	Friction Factor
P2-10-1	PAO	11.9	147	183	5.03	15.1	0.0119	63.4	0.174
P2-10-2	PAO	11.9	147	222	6.96	19.6	0.0105	80.6	0.150
P2-10-3	PAO	11.6	148	141	4.21	13.5	0.0142	48.4	0.220
P2-10-4	PAO	14.0	136	90	5.14	17.5	0.0214	25.3	0.335
P2-10-5	PAO	17.9	119	57	5.86	23.0	0.0303	11.4	0.510
P2-10-6	PAO	11.5	149	46	2.40	9.4	0.0349	13.2	0.572
P2-10-7	PAO	10.9	152	135	2.28	7.4	0.0146	50.4	0.239
P2-20-1	PAO	20.9	108	266	6.35	16.8	0.0106	52.6	0.130
P2-20-2	PAO	20.4	110	306	6.54	18.1	0.00866	69.2	0.125
P2-20-3	PAO	20.1	111	259	5.66	15.8	0.0101	52.7	0.130
P2-20-4	PAO	20.2	111	191	5.60	18.4	0.0113	37.0	0.170
P2-20-5	PAO	21.8	105	119	5.95	20.5	0.0175	19.9	0.262
P2-20-6	PAO	27.9	88	86	6.27	22.2	0.0249	9.8	0.358
P2-20-7	PAO	25.8	94	51	2.73	11.6	0.0331	5.9	0.537

Run No.	Fluid Type	Aver. Fluid Temp. (°C)	Prandtl Number	Reynolds Number	Heat Flux (W/cm^2)	LMTD (°C)	Colburn Factor	Pressure Drop (kPa)	Friction Factor
P2-20-8	PAO	20.6	109	105	1.93	6.7	0.0192	18.6	0.290
P2-60-1	PAO	62.7	40	814	4.86	11.9	0.00550	32.3	0.0739
P2-60-2	PAO	63.1	39	954	6.56	15.4	0.00495	41.3	0.0700
P2-60-3	PAO	64.3	39	564	5.76	15.8	0.00696	18.9	0.0967
P2-60-4	PAO	64.1	39	344	6.39	17.8	0.0112	10.0	0.136
P2-60-5	PAO	64.1	39	156	2.92	10.8	0.0176	3.6	0.234
P2-60-6	PAO	61.5	41	339	2.52	7.2	0.0107	11.0	0.138
W2-10-1	WATER	12.6	8	1015	7.68	8.4	0.00513	8.7	0.0682
W2-10-2	WATER	13.0	8	850	7.58	8.6	0.00579	7.1	0.0803
W2-10-3	WATER	13.3	8	755	7.50	8.8	0.00626	5.8	0.0837
W2-10-4	WATER	13.9	8	598	7.22	9.5	0.00667	3.5	0.0826
W2-10-5	WATER	15.0	8	432	7.01	9.4	0.00908	2.4	0.112
W2-10-6	WATER	13.7	8	420	5.70	7.7	0.00918	2.5	0.118
W2-10-7	WATER	11.7	8	714	5.87	7.0	0.00634	5.7	0.0869
W2-10-8	WATER	11.3	9	579	3.26	4.2	0.00713	4.4	0.0992

Run No.	Fluid Type	Aver. Fluid Temp. (°C)	Prandtl Number	Reynolds Number	Heat Flux (W/cm^2)	LMTD (°C)	Colburn Factor	Pressure Drop (kPa)	Friction Factor
W2-10-9	WATER	12.1	8	388	3.18	4.4	0.00953	2.5	0.131
W2-10-10	WATER	12.2	8	334	3.02	4.4	0.0102	1.9	0.133
W2-10-11	WATER	13.5	8	223	2.99	4.6	0.0142	1.0	0.174
W2-10-12	WATER	14.3	8	183	2.99	4.7	0.0169	0.8	0.199
W2-10-13	WATER	16.8	7	123	2.97	5.0	0.0237	0.4	0.240
W2-20-1	WATER	22.2	7	1302	7.51	7.9	0.00444	8.3	0.0588
W2-20-2	WATER	22.4	7	1175	7.49	8.1	0.00478	6.9	0.0607
W2-20-3	WATER	22.8	6	941	7.38	8.3	0.00556	4.6	0.0645
W2-20-4	WATER	23.6	6	725	7.15	8.6	0.00658	3.1	0.0741
W2-20-5	WATER	25.0	6	498	7.02	9.2	0.00856	1.8	0.0977
W2-20-6	WATER	22.0	7	880	5.84	6.8	0.00567	4.4	0.0670
W2-20-7	WATER	21.5	7	724	3.16	3.8	0.00650	3.3	0.0726
W2-20-8	WATER	21.9	7	470	3.09	4.0	0.00890	2.0	0.109
W2-20-9	WATER	22.0	7	518	2.79	3.9	0.00746	1.9	0.0862
W2-20-10	WATER	23.9	6	268	2.98	4.3	0.0135	0.8	0.150

Run No.	Fluid Type	Aver. Fluid Temp. (°C)	Prandtl Number	Reynolds Number	Heat Flux (W/cm^2)	LMTD (°C)	Colburn Factor	Pressure Drop (kPa)	Friction Factor
W2-20-11	WATER	25.4	6	185	2.96	4.5	0.0185	0.5	0.211
W2-20-12	WATER	24.9	6	199	2.97	4.5	0.0175	0.5	0.168
W2-20-13	WATER	23.7	6	498	5.67	7.4	0.00848	2.0	0.103
W2-60-1	WATER	62.9	3	2446	6.87	6.6	0.00328	5.7	0.0473
W2-60-2	WATER	63.3	3	2153	6.81	6.7	0.00363	4.5	0.0482
W2-60-3	WATER	64.0	3	1728	6.84	7.0	0.00426	3.1	0.0523
W2-60-4	WATER	64.8	3	1426	6.78	7.1	0.00490	2.3	0.0574
W2-60-5	WATER	66.2	3	908	6.51	7.5	0.00672	1.3	0.0784
W2-60-6	WATER	64.9	3	907	5.08	5.6	0.00712	1.2	0.0746
W2-60-7	WATER	63.1	3	1814	5.32	5.2	0.00434	3.3	0.0500
W2-60-8	WATER	62.7	3	1388	2.84	2.8	0.00537	2.2	0.0570
W2-60-9	WATER	62.9	3	990	2.81	3.0	0.00669	1.3	0.0675
W2-60-10	WATER	62.5	3	1043	2.72	3.0	0.00621	1.4	0.0623

Table E.3 Experimental Data for Plate 3

Run No.	Fluid Type	Aver. Fluid Temp. (°C)	Prandtl Number	Reynolds Number	Heat Flux (W/cm^2)	LMTD (°C)	Colburn Factor	Pressure Drop (kPa)	Friction Factor
P3-10-1	PAO	13.5	138	188	7.61	23.3	0.0107	49.2	0.126
P3-10-2	PAO	12.8	142	245	7.60	19.8	0.00993	76.9	0.109
P3-10-3	PAO	13.4	139	147	7.27	25.2	0.0119	37.8	0.156
P3-10-4	PAO	12.5	143	156	6.81	22.8	0.0116	41.4	0.143
P3-10-5	PAO	14.5	134	91	6.40	21.9	0.0197	20.9	0.243
P3-10-6	PAO	14.7	133	92	6.36	22.0	0.0194	20.7	0.241
P3-10-7	PAO	18.8	116	57	6.46	29.9	0.0235	7.8	0.315
P3-10-8	PAO	14.2	135	47	2.51	12.5	0.0252	10.8	0.470
P3-10-9	PAO	11.8	147	83	2.13	7.4	0.0206	23.9	0.276
P3-10-10	PAO	16.1	127	42	2.94	13.0	0.0329	8.5	0.528
P3-10-11	PAO	14.4	134	57	3.46	15.3	0.0237	11.1	0.330
P3-10-12	PAO	17.9	119	31	3.19	17.2	0.0366	4.8	0.626
P3-10-13	PAO	23.0	102	22	3.06	18.6	0.0485	2.4	0.896
P3-10-14	PAO	29.5	84	17	2.95	20.1	0.0578	1.3	1.15

Run No.	Fluid Type	Aver. Fluid Temp. (°C)	Prandtl Number	Reynolds Number	Heat Flux (W/cm^2)	LMTD (°C)	Colburn Factor	Pressure Drop (kPa)	Friction Factor
P3-10-15	PAO	17.4	121	12	1.06	8.3	0.0647	1.8	1.61
P3-10-16	PAO	12.7	142	24	1.08	6.3	0.0397	5.4	0.784
P3-10-17	PAO	10.8	152	183	6.70	20.4	0.0107	58.3	0.128
P3-20-1	PAO	21.0	108	264	6.46	19.1	0.00873	39.5	0.0868
P3-20-2	PAO	20.8	109	309	7.54	21.9	0.00761	48.5	0.0764
P3-20-3	PAO	21.8	105	191	6.07	20.5	0.0104	27.1	0.119
P3-20-4	PAO	23.5	100	126	6.24	22.6	0.0148	15.5	0.173
P3-20-5	PAO	28.1	88	76	6.54	26.3	0.0230	6.8	0.281
P3-20-6	PAO	21.8	105	63	2.28	9.7	0.0243	8.0	0.323
P3-20-7	PAO	19.5	113	117	1.29	4.2	0.0174	18.8	0.189
P3-20-8	PAO	23.1	101	75	2.23	8.9	0.0222	9.7	0.300
P3-20-9	PAO	25.6	94	50	2.52	12.1	0.0281	4.7	0.390
P3-20-10	PAO	45.9	56	23	3.08	21.1	0.0506	0.8	1.01
P3-20-11	PAO	30.3	82	16	1.10	7.8	0.0586	1.4	1.44
P3-20-12	PAO	25.7	94	39	1.19	5.4	0.0377	4.0	0.534

Run No.	Fluid Type	Aver. Fluid Temp. (°C)	Prandtl Number	Reynolds Number	Heat Flux (W/cm^2)	LMTD (°C)	Colburn Factor	Pressure Drop (kPa)	Friction Factor
P3-60-1	PAO	63.8	39	778	7.10	18.2	0.00508	19.8	0.0449
P3-60-2	PAO	61.1	41	942	7.16	17.0	0.00453	30.3	0.0418
P3-60-3	PAO	64.1	39	496	6.92	20.0	0.00692	11.3	0.0638
P3-60-4	PAO	65.5	38	342	6.92	21.9	0.00910	7.0	0.0875
P3-60-5	PAO	68.7	35	220	7.12	25.2	0.0127	3.2	0.111
P3-60-6	PAO	63.4	39	200	3.27	11.1	0.0141	3.7	0.123
P3-60-7	PAO	61.7	41	341	3.01	9.3	0.00913	8.1	0.0869
P3-60-8	PAO	63.3	39	237	3.57	12.0	0.0120	4.5	0.107
P3-60-9	PAO	68.6	35	109	3.23	14.2	0.0201	1.5	0.204
W3-10-1	WATER	12.4	8	1035	7.08	7.7	0.00467	8.7	0.0555
W3-10-2	WATER	13.2	8	795	7.09	8.3	0.00543	5.3	0.0593
W3-10-3	WATER	13.4	8	757	7.08	8.5	0.00559	4.9	0.0610
W3-10-4	WATER	15.6	8	421	7.01	9.5	0.00848	2.0	0.0897
W3-10-5	WATER	14.0	8	395	5.60	7.8	0.00862	2.0	0.0934
W3-10-6	WATER	12.3	8	662	5.78	7.2	0.00595	4.3	0.0666

Run No.	Fluid Type	Aver. Fluid Temp. (°C)	Prandtl Number	Reynolds Number	Heat Flux (W/cm^2)	LMTD (°C)	Colburn Factor	Pressure Drop (kPa)	Friction Factor
W3-10-7	WATER	11.3	9	529	3.05	4.0	0.00688	3.3	0.0772
W3-10-8	WATER	12.0	8	347	2.93	4.2	0.00930	2.0	0.109
W3-10-9	WATER	11.4	9	420	2.89	4.0	0.00813	2.3	0.0872
W3-10-10	WATER	13.4	8	229	2.95	4.3	0.0136	1.1	0.154
W3-10-11	WATER	14.7	8	176	2.95	4.5	0.0171	0.8	0.193
W3-20-1	WATER	23.1	6	1282	7.42	7.4	0.00449	8.1	0.0531
W3-20-2	WATER	23.4	6	1043	7.15	7.7	0.00497	5.7	0.0567
W3-20-3	WATER	23.3	6	851	7.01	8.1	0.00551	4.1	0.0610
W3-20-4	WATER	23.9	6	702	6.95	8.6	0.00607	2.9	0.0659
W3-20-5	WATER	25.2	6	508	6.94	9.2	0.00763	1.8	0.0822
W3-20-6	WATER	24.1	6	492	5.61	7.5	0.00774	1.7	0.0789
W3-20-7	WATER	23.2	6	664	5.61	7.0	0.00622	2.8	0.0698
W3-20-8	WATER	22.6	7	884	5.64	6.4	0.00539	4.5	0.0609
W3-20-9	WATER	22.3	7	881	3.02	3.5	0.00514	4.5	0.0596
W3-20-10	WATER	22.8	6	686	2.94	3.6	0.00606	3.0	0.0685

Run No.	Fluid Type	Aver. Fluid Temp. (°C)	Prandtl Number	Reynolds Number	Heat Flux (W/cm^2)	LMTD (°C)	Colburn Factor	Pressure Drop (kPa)	Friction Factor
W3-20-11	WATER	23.5	6	448	2.91	3.9	0.00827	1.7	0.0949
W3-20-12	WATER	23.0	6	586	2.84	3.7	0.00666	2.4	0.0749
W3-20-13	WATER	23.6	6	440	3.02	4.0	0.00870	1.6	0.0931
W3-20-14	WATER	25.0	6	270	3.00	4.3	0.0126	0.9	0.142
W3-20-15	WATER	25.5	6	231	2.96	4.4	0.0143	0.8	0.166
W3-20-16	WATER	29.5	6	128	2.89	4.6	0.0235	0.4	0.325
W3-60-1	WATER	62.6	3	2529	6.88	6.3	0.00314	5.6	0.0369
W3-60-2	WATER	63.4	3	1735	6.88	6.8	0.00406	3.0	0.0430
W3-60-3	WATER	62.9	3	2220	6.89	6.5	0.00336	4.5	0.0393
W3-60-4	WATER	65.2	3	900	6.75	7.8	0.00624	1.2	0.0628
W3-60-5	WATER	64.2	3	1145	6.83	7.4	0.00536	1.6	0.0542
W3-60-6	WATER	63.7	3	1700	6.61	6.3	0.00433	3.0	0.0444
W3-60-7	WATER	64.0	3	1161	5.50	5.7	0.00566	1.5	0.0495
W3-60-8	WATER	64.4	3	977	5.42	5.9	0.00628	1.3	0.0581
W3-60-9	WATER	63.0	3	1675	5.45	5.3	0.00431	2.9	0.0439

Run No.	Fluid Type	Aver. Fluid Temp. (°C)	Prandtl Number	Reynolds Number	Heat Flux (W/cm^2)	LMTD (°C)	Colburn Factor	Pressure Drop (kPa)	Friction Factor
W3-60-10	WATER	62.3	3	1330	2.93	3.2	0.00439	1.9	0.0454
W3-60-11	WATER	62.9	3	901	2.95	3.4	0.00626	1.2	0.0622
W3-60-12	WATER	63.0	3	903	3.01	3.4	0.00621	1.1	0.0601
W3-60-13	WATER	62.8	3	1092	2.92	3.2	0.00547	1.6	0.0562
W3-60-14	WATER	64.3	3	550	3.05	3.7	0.00933	0.5	0.0773
W3-60-15	WATER	64.5	3	545	3.07	3.8	0.00915	0.5	0.0799
W3-60-16	WATER	63.8	3	658	3.02	3.6	0.00801	0.7	0.0668
W3-60-17	WATER	67.1	3	285	3.04	4.2	0.0152	0.2	0.133

Table E.4 Experimental Data for Plate 4

Run No.	Fluid Type	Aver. Fluid Temp. (°C)	Prandtl Number	Reynolds Number	Heat Flux (W/cm^2)	LMTD (°C)	Colburn Factor	Pressure Drop (kPa)	Friction Factor
P4-10-1	PAO	12.1	146	138	7.38	15.7	0.0156	40.2	0.188
P4-10-2	PAO	12.4	144	120	7.13	15.1	0.0181	37.5	0.239
P4-10-3	PAO	12.4	144	125	7.30	15.1	0.0180	39.3	0.228
P4-10-4	PAO	13.0	141	94	7.06	15.3	0.0225	28.5	0.307
P4-10-5	PAO	19.0	115	33	6.73	19.1	0.0483	4.7	0.618
P4-10-6	PAO	15.9	128	30	3.11	9.3	0.0476	5.1	0.659
P4-10-7	PAO	15.5	129	36	3.48	9.3	0.0466	5.5	0.500
P4-10-8	PAO	17.3	122	24	3.31	10.0	0.0596	3.2	0.717
P4-10-9	PAO	26.3	92	12	3.07	12.2	0.0963	0.9	1.45
P4-10-10	PAO	16.6	124	9	1.10	4.3	0.119	1.2	1.85
P4-10-11	PAO	14.0	136	13	1.09	3.9	0.0903	2.0	1.31
P4-20-1	PAO	23.5	100	191	7.36	14.7	0.0140	30.7	0.166
P4-20-2	PAO	24.0	98	212	7.36	14.7	0.0127	33.7	0.153
P4-20-3	PAO	32.4	78	52	6.86	18.8	0.0370	3.8	0.475

Run No.	Fluid Type	Aver. Fluid Temp. (°C)	Prandtl Number	Reynolds Number	Heat Flux (W/cm^2)	LMTD (°C)	Colburn Factor	Pressure Drop (kPa)	Friction Factor
P4-20-4	PAO	23.6	100	128	7.00	15.4	0.0184	20.0	0.243
P4-20-5	PAO	25.1	95	42	2.92	8.7	0.0382	4.3	0.527
P4-20-6	PAO	24.4	97	51	3.26	8.7	0.0364	6.3	0.507
P4-20-7	PAO	40.9	63	14	3.03	12.5	0.0906	0.6	1.52
P4-20-8	PAO	27.3	89	35	3.22	9.2	0.0494	3.7	0.759
P4-20-9	PAO	29.1	85	10	1.09	4.9	0.100	0.7	1.76
P4-20-10	PAO	25.2	95	21	1.09	3.9	0.0613	2.0	0.993
P4-60-1	PAO	64.1	39	561	7.27	12.3	0.00848	16.9	0.0820
P4-60-2	PAO	65.8	37	401	7.04	13.3	0.0102	10.0	0.102
P4-60-3	PAO	66.0	37	634	7.26	11.5	0.00842	18.4	0.0759
P4-60-4	PAO	67.6	36	230	6.87	14.9	0.0151	4.6	0.152
P4-60-5	PAO	71.1	34	133	6.95	16.8	0.0230	2.3	0.265
P4-60-6	PAO	68.3	36	123	3.06	6.9	0.0269	2.3	0.277
P4-60-7	PAO	68.1	36	174	3.59	7.5	0.0209	2.9	0.171
P4-60-8	PAO	69.9	35	103	3.34	8.0	0.0302	1.6	0.302

Run No.	Fluid Type	Aver. Fluid Temp. (°C)	Prandtl Number	Reynolds Number	Heat Flux (W/cm^2)	LMTD (°C)	Colburn Factor	Pressure Drop (kPa)	Friction Factor
P4-60-9	PAO	77.2	30	41	3.14	9.7	0.0569	0.4	0.635
P4-60-10	PAO	67.1	37	34	1.14	3.0	0.0782	0.4	0.681
P4-60-11	PAO	66.5	37	60	1.14	2.8	0.0481	0.9	0.430
W4-10-1	WATER	12.4	8	649	7.95	7.3	0.00765	5.1	0.0922
W4-10-2	WATER	13.6	8	457	7.92	7.7	0.00984	3.4	0.129
W4-10-3	WATER	16.0	8	269	7.76	8.2	0.0146	1.7	0.208
W4-10-4	WATER	14.5	8	255	6.22	6.6	0.0150	1.7	0.210
W4-10-5	WATER	12.4	8	431	6.42	6.3	0.0101	3.5	0.141
W4-10-6	WATER	11.0	9	426	3.32	3.3	0.00996	3.5	0.137
W4-10-7	WATER	11.6	8	268	3.32	3.5	0.0145	1.9	0.199
W4-10-8	WATER	11.4	9	274	3.16	3.2	0.0147	2.1	0.205
W4-10-9	WATER	11.9	8	207	3.19	3.5	0.0174	1.5	0.253
W4-10-10	WATER	13.2	8	141	3.22	3.9	0.0220	0.8	0.329
W4-10-11	WATER	17.3	7	74	3.20	4.2	0.0381	0.3	0.541
W4-20-1	WATER	22.0	7	773	6.94	6.1	0.00722	4.6	0.0864

Run No.	Fluid Type	Aver. Fluid Temp. (°C)	Prandtl Number	Reynolds Number	Heat Flux (W/cm^2)	LMTD (°C)	Colburn Factor	Pressure Drop (kPa)	Friction Factor
W4-20-2	WATER	23.1	6	552	6.93	6.5	0.00893	3.2	0.125
W4-20-3	WATER	24.9	6	362	7.31	7.3	0.0125	1.8	0.174
W4-20-4	WATER	23.8	6	320	5.45	5.8	0.0125	1.6	0.190
W4-20-5	WATER	22.1	7	546	5.89	5.5	0.00914	3.2	0.123
W4-20-6	WATER	22.1	7	530	3.25	3.0	0.00942	3.1	0.126
W4-20-7	WATER	23.0	6	310	3.31	3.4	0.0133	1.4	0.178
W4-20-8	WATER	22.8	6	324	3.22	3.4	0.0124	1.5	0.172
W4-20-9	WATER	24.5	6	180	3.29	3.7	0.0207	0.7	0.270
W4-20-10	WATER	27.5	6	105	3.25	3.9	0.0318	0.4	0.481
W4-60-1	WATER	62.1	3	1587	7.36	5.3	0.00597	3.6	0.0672
W4-60-2	WATER	62.8	3	1113	7.14	5.4	0.00787	2.0	0.0753
W4-60-3	WATER	64.7	3	608	6.60	5.9	0.0105	0.8	0.0981
W4-60-4	WATER	64.2	3	611	5.42	4.8	0.0106	0.7	0.0936
W4-60-5	WATER	63.1	3	1103	5.80	4.3	0.00830	2.0	0.0768
W4-60-6	WATER	61.9	3	1110	3.40	2.5	0.00823	1.9	0.0727

Run No.	Fluid Type	Aver. Fluid Temp. (°C)	Prandtl Number	Reynolds Number	Heat Flux (W/cm^2)	LMTD (°C)	Colburn Factor	Pressure Drop (kPa)	Friction Factor
W4-60-7	WATER	62.8	3	630	3.20	2.8	0.0106	0.7	0.0882
W4-60-8	WATER	63.0	3	634	3.24	2.8	0.0109	0.8	0.0973
W4-60-9	WATER	66.8	3	183	3.01	3.4	0.0243	0.2	0.307

Table E.5 Experimental Data for Plate 5

Run No.	Fluid Type	Aver. Fluid Temp. (°C)	Prandtl Number	Reynolds' Number	Heat Flux (W/cm^2)	LMTD (°C)	Colburn Factor	Pressure Drop (kPa)	Friction Factor
P5-10-1	PAO	12.6	143	157	7.11	14.9	0.0153	80.6	0.196
P5-10-2	PAO	11.2	150	120	6.90	15.7	0.0177	66.9	0.248
P5-10-3	PAO	15.3	130	57	6.71	19.3	0.0296	17.5	0.389
P5-10-4	PAO	17.8	120	47	6.87	21.1	0.0345	11.7	0.460
P5-10-5	PAO	12.8	142	39	2.98	10.0	0.0354	12.7	0.511
P5-10-6	PAO	10.3	155	65	2.82	8.4	0.0235	26.6	0.319
P5-10-7	PAO	12.3	145	42	3.27	9.9	0.0364	15.5	0.500
P5-10-8	PAO	15.2	130	27	3.12	11.6	0.0471	6.4	0.647
P5-10-9	PAO	22.9	102	16	2.97	15.6	0.0601	2.2	1.11
P5-10-10	PAO	14.9	132	12	1.12	6.1	0.0679	3.0	1.45
P5-10-11	PAO	12.3	145	17	1.10	5.2	0.0545	5.3	1.06
P5-20-1	PAO	24.5	97	242	7.53	14.4	0.0127	61.7	0.142
P5-20-2	PAO	24.9	96	255	7.53	14.4	0.0121	64.1	0.136
P5-20-3	PAO	24.5	97	207	7.22	14.8	0.0136	52.0	0.163

Run No.	Fluid Type	Aver. Fluid Temp. (°C)	Prandtl Number	Reynolds Number	Heat Flux (W/cm^2)	LMTD (°C)	Colburn Factor	Pressure Drop (kPa)	Friction Factor
P5-20-4	PAO	26.6	91	116	6.91	17.1	0.0199	24.1	0.279
P5-20-5	PAO	31.9	79	65	6.88	20.8	0.0294	7.8	0.384
P5-20-6	PAO	23.4	100	242	7.05	13.9	0.0121	65.5	0.141
P5-20-7	PAO	26.2	92	56	3.10	9.6	0.0314	8.9	0.427
P5-20-8	PAO	22.8	102	120	2.97	7.5	0.0179	31.9	0.269
P5-20-9	PAO	24.5	97	67	3.34	9.2	0.0295	11.0	0.329
P5-20-10	PAO	26.4	92	45	3.21	10.5	0.0371	6.0	0.458
P5-20-11	PAO	36.0	71	22	3.07	15.6	0.0516	1.6	0.895
P5-20-12	PAO	27.4	89	17	1.10	5.8	0.0570	2.0	1.10
P5-20-13	PAO	24.1	98	35	1.07	4.2	0.0377	5.4	0.594
P5-60-1	PAO	64.6	38	746	7.53	11.0	0.00819	39.0	0.0701
P5-60-2	PAO	64.1	39	537	7.20	12.1	0.00943	26.2	0.0893
P5-60-3	PAO	65.8	37	321	6.98	14.4	0.0123	13.0	0.133
P5-60-4	PAO	70.6	34	174	6.98	18.4	0.0175	5.0	0.214
P5-60-5	PAO	65.8	37	158	2.98	7.4	0.0200	5.4	0.227

Run No.	Fluid Type	Aver. Fluid Temp. (°C)	Prandtl Number	Reynolds Number	Heat Flux (W/cm^2)	LMTD (°C)	Colburn Factor	Pressure Drop (kPa)	Friction Factor
P5-60-6	PAO	64.5	38	265	2.86	6.3	0.0135	10.8	0.154
P5-60-7	PAO	65.5	38	220	3.40	7.9	0.0155	8.0	0.171
P5-60-8	PAO	67.5	36	127	3.19	9.2	0.0211	3.6	0.250
P5-60-9	PAO	75.3	31	51	3.09	13.4	0.0355	0.8	0.477
P5-60-10	PAO	67.2	36	43	1.08	4.5	0.0412	0.9	0.550
P5-60-11	PAO	65.4	38	79	1.05	3.7	0.0264	2.2	0.362
W5-10-1	WATER	12.8	8	906	7.24	5.8	0.00637	10.2	0.0612
W5-10-2	WATER	13.0	8	752	7.25	6.1	0.00710	8.0	0.0707
W5-10-3	WATER	14.2	8	470	6.94	6.7	0.00935	4.1	0.0972
W5-10-4	WATER	13.3	8	631	7.05	6.3	0.00779	6.2	0.0781
W5-10-5	WATER	15.0	8	359	6.77	7.0	0.0109	3.2	0.133
W5-10-6	WATER	15.1	8	359	6.89	7.1	0.0109	3.1	0.131
W5-10-7	WATER	13.8	8	350	5.50	5.8	0.0109	3.0	0.127
W5-10-8	WATER	12.3	8	597	5.64	5.2	0.00779	5.6	0.0767
W5-10-9	WATER	12.7	8	492	5.54	5.4	0.00866	4.9	0.0989

Run No.	Fluid Type	Aver. Fluid Temp. (°C)	Prandtl Number	Reynolds Number	Heat Flux (W/cm^2)	LMTD (°C)	Colburn Factor	Pressure Drop (kPa)	Friction Factor
W5-10-10	WATER	11.9	8	485	3.02	2.9	0.00894	5.0	0.100
W5-10-11	WATER	12.4	8	350	2.94	3.0	0.0111	3.4	0.133
W5-10-12	WATER	12.2	8	360	2.90	3.0	0.0106	3.3	0.121
W5-10-13	WATER	12.7	8	291	3.07	3.4	0.0119	2.4	0.138
W5-10-14	WATER	13.3	8	247	3.07	3.5	0.0135	1.7	0.137
W5-10-15	WATER	14.8	8	162	3.03	3.7	0.0187	1.0	0.209
W5-10-16	WATER	17.3	7	107	2.96	4.1	0.0244	0.5	0.270
W5-10-17	WATER	12.1	8	368	3.03	3.2	0.0101	3.4	0.119
W5-20-1	WATER	22.6	7	1063	7.47	5.7	0.00616	10.1	0.0667
W5-20-2	WATER	23.1	6	951	7.40	5.9	0.00647	8.4	0.0704
W5-20-3	WATER	24.2	6	625	7.09	6.5	0.00791	4.4	0.0902
W5-20-4	WATER	23.8	6	776	7.19	6.2	0.00709	6.1	0.0794
W5-20-5	WATER	25.6	6	436	6.76	7.1	0.00936	2.6	0.116
W5-20-6	WATER	24.8	6	435	5.51	5.7	0.00955	2.6	0.110
W5-20-7	WATER	23.0	6	772	5.70	4.9	0.00695	6.2	0.0794

Run No.	Fluid Type	Aver. Fluid Temp. (°C)	Prandtl Number	Reynolds Number	Heat Flux (W/cm^2)	LMTD (°C)	Colburn Factor	Pressure Drop (kPa)	Friction Factor
W5-20-8	WATER	23.3	6	615	5.59	5.2	0.00777	4.5	0.0910
W5-20-9	WATER	23.3	6	616	3.13	2.8	0.00805	4.4	0.0893
W5-20-10	WATER	23.4	6	406	3.00	3.1	0.00986	2.6	0.120
W5-20-11	WATER	22.7	6	466	3.04	3.0	0.00917	2.9	0.101
W5-20-12	WATER	23.6	6	339	3.07	3.3	0.0114	1.9	0.128
W5-20-13	WATER	24.9	6	239	3.09	3.5	0.0151	1.1	0.162
W5-20-14	WATER	26.1	6	191	3.08	3.7	0.0175	0.8	0.196
W5-20-15	WATER	28.3	6	137	3.06	4.1	0.0213	0.5	0.244
W5-60-1	WATER	63.3	3	2212	6.96	4.7	0.00437	7.1	0.0439
W5-60-2	WATER	63.5	3	1783	6.92	5.1	0.00475	5.0	0.0479
W5-60-3	WATER	63.7	3	1552	6.85	5.3	0.00497	4.0	0.0507
W5-60-4	WATER	64.5	3	1235	6.83	5.4	0.00607	2.5	0.0514
W5-60-5	WATER	63.5	3	1150	5.41	4.2	0.00665	2.5	0.0584
W5-60-6	WATER	62.8	3	1546	5.50	4.3	0.00496	4.4	0.0551
W5-60-7	WATER	62.6	3	1152	3.03	2.4	0.00656	2.5	0.0558

Run No.	Fluid Type	Aver. Fluid Temp. (°C)	Prandtl Number	Reynolds Number	Heat Flux (W/cm^2)	LMTD (°C)	Colburn Factor	Pressure Drop (kPa)	Friction Factor
W5-60-8	WATER	63.0	3	780	2.99	2.5	0.00868	1.4	0.0692
W5-60-9	WATER	62.5	3	846	2.81	2.2	0.00853	1.7	0.0707
W5-60-10	WATER	62.9	3	707	2.81	2.3	0.00979	1.3	0.0795
W5-60-11	WATER	63.8	3	481	2.78	2.5	0.01278	0.8	0.106
W5-60-12	WATER	65.0	3	347	2.79	2.8	0.0149	0.5	0.129
W5-60-13	WATER	66.5	3	251	2.82	3.1	0.0180	0.4	0.181
W5-60-14	WATER	61.1	3	876	3.13	2.4	0.00855	1.8	0.0695
W5-60-15	WATER	63.6	3	596	3.17	2.8	0.0103	1.1	0.0915
W5-60-16	WATER	64.1	3	466	3.10	2.8	0.0129	0.8	0.106
W5-60-17	WATER	64.9	3	355	3.11	3.2	0.0141	0.5	0.120

Table E.6 Experimental Data for Plate 6

Run No.	Fluid Type	Aver. Fluid Temp. (°C)	Prandtl Number	Reynolds Number	Heat Flux (W/cm^2)	LMTD (°C)	Colburn Factor	Pressure Drop (kPa)	Friction Factor
P6-10-1	PAO	12.2	145	173	7.77	22.0	0.0131	55.1	0.162
P6-10-2	PAO	10.2	156	194	7.66	20.6	0.0121	70.6	0.141
P6-10-3	PAO	11.4	149	130	7.44	22.9	0.0156	43.4	0.212
P6-10-4	PAO	16.0	127	61	7.05	26.6	0.0276	13.7	0.431
P6-10-5	PAO	18.5	117	50	6.97	28.2	0.0321	9.4	0.526
P6-10-6	PAO	13.0	141	41	3.06	13.0	0.0346	11.0	0.628
P6-10-7	PAO	10.7	153	71	3.20	11.7	0.0231	23.5	0.368
P6-10-8	PAO	12.4	144	47	3.42	12.8	0.0346	14.3	0.585
P6-10-9	PAO	17.0	123	26	3.10	14.6	0.0511	5.0	0.948
P6-10-10	PAO	24.3	98	17	2.96	16.9	0.0669	2.2	1.50
P6-10-11	PAO	14.8	132	12	1.10	6.9	0.0735	2.8	1.96
P6-10-12	PAO	11.4	149	23	1.16	5.5	0.0526	6.6	1.03
P6-20-1	PAO	24.3	98	274	7.37	20.6	0.00972	42.3	0.114
P6-20-2	PAO	23.9	99	319	7.35	20.0	0.00862	50.2	0.0976

Run No.	Fluid Type	Aver. Fluid Temp. (°C)	Prandtl Number	Reynolds Number	Heat Flux (W/cm^2)	LMTD (°C)	Colburn Factor	Pressure Drop (kPa)	Friction Factor
P6-20-3	PAO	24.3	98	281	7.34	20.6	0.00944	43.6	0.112
P6-20-4	PAO	27.1	90	130	6.89	23.4	0.0165	16.0	0.229
P6-20-5	PAO	30.8	81	79	6.88	26.2	0.0248	7.3	0.354
P6-20-6	PAO	25.3	95	65	3.04	12.1	0.0266	8.3	0.421
P6-20-7	PAO	23.0	102	113	3.08	10.8	0.0174	17.6	0.256
P6-20-8	PAO	26.2	92	53	3.29	13.1	0.0335	5.7	0.464
P6-20-9	PAO	34.9	73	25	3.13	16.2	0.0561	1.7	0.994
P6-20-10	PAO	25.1	95	19	1.15	6.2	0.0652	2.1	1.26
P6-20-11	PAO	22.3	104	32	1.17	5.4	0.0446	4.4	0.768
P6-60-1	PAO	62.2	40	895	7.11	14.0	0.00649	29.9	0.0515
P6-60-2	PAO	62.8	40	804	6.24	12.7	0.00688	26.0	0.0570
P6-60-3	PAO	65.5	38	655	6.51	14.7	0.00753	18.0	0.0665
P6-60-4	PAO	66.6	37	297	6.64	18.7	0.0126	6.5	0.123
P6-60-5	PAO	69.7	35	189	6.75	24.2	0.0151	3.3	0.178
P6-60-6	PAO	64.1	39	170	3.00	10.1	0.0173	3.7	0.190

Run No.	Fluid Type	Aver. Fluid Temp. (°C)	Prandtl Number	Reynolds Number	Heat Flux (W/cm^2)	LMTD (°C)	Colburn Factor	Pressure Drop (kPa)	Friction Factor
P6-60-7	PAO	62.5	40	329	2.99	8.3	0.0111	8.7	0.111
P6-60-8	PAO	63.7	39	237	3.49	10.4	0.0145	5.1	0.133
P6-60-9	PAO	65.5	38	142	3.27	12.7	0.0177	2.6	0.203
P6-60-10	PAO	74.5	32	58	3.19	15.4	0.0358	0.7	0.453
P6-60-11	PAO	65.1	38	47	1.14	5.7	0.0391	0.7	0.524
W6-10-1	WATER	12.4	8	1015	7.90	9.4	0.00465	8.5	0.0615
W6-10-2	WATER	13.1	8	700	7.65	9.9	0.00597	5.1	0.0792
W6-10-3	WATER	14.9	8	394	7.18	10.5	0.00889	2.2	0.117
W6-10-4	WATER	13.5	8	394	6.08	8.3	0.00975	2.3	0.112
W6-10-5	WATER	12.1	8	632	6.11	7.7	0.00685	4.6	0.0843
W6-10-6	WATER	10.8	9	614	3.40	4.5	0.00648	4.6	0.0858
W6-10-7	WATER	12.4	8	388	3.24	4.7	0.00910	2.4	0.118
W6-10-8	WATER	12.6	8	398	3.15	4.6	0.00866	2.5	0.120
W6-10-9	WATER	14.6	8	225	3.20	4.9	0.0144	1.1	0.181
W6-10-10	WATER	18.2	7	126	3.25	5.3	0.0244	0.4	0.268

Run No.	Fluid Type	Aver. Fluid Temp. (°C)	Prandtl Number	Reynolds Number	Heat Flux (W/cm^2)	LMTD (°C)	Colburn Factor	Pressure Drop (kPa)	Friction Factor
W6-20-1	WATER	24.0	6	442	6.08	8.9	0.00840	1.3	0.0795
W6-20-2	WATER	21.8	7	814	6.10	7.5	0.00577	4.2	0.0689
W6-20-3	WATER	24.0	6	442	6.08	8.9	0.00840	1.3	0.0795
W6-20-4	WATER	21.8	7	814	6.10	7.5	0.00577	4.2	0.0689
W6-20-5	WATER	21.0	7	810	3.33	4.0	0.00594	4.1	0.0667
W6-20-6	WATER	23.7	6	454	4.44	6.5	0.00813	1.5	0.0866
W6-20-7	WATER	22.7	6	500	3.22	4.6	0.00755	1.8	0.0814
W6-20-8	WATER	24.5	6	277	3.27	5.5	0.0109	0.8	0.123
W6-20-9	WATER	28.0	6	159	3.30	5.8	0.0180	0.4	0.206
W6-60-1	WATER	62.8	3	2416	6.46	5.9	0.00375	6.0	0.0474
W6-60-2	WATER	62.8	3	2474	6.37	5.7	0.00379	6.1	0.0457
W6-60-3	WATER	62.5	3	2505	6.41	6.0	0.00351	6.3	0.0459
W6-60-4	WATER	63.4	3	1790	6.64	7.0	0.00402	3.7	0.0533
W6-60-5	WATER	65.2	3	925	6.25	7.4	0.00651	1.2	0.0651
W6-60-6	WATER	61.9	3	2373	7.16	6.4	0.00391	5.8	0.0465

Run No.	Fluid Type	Aver. Fluid Temp. (°C)	Prandtl Number	Reynolds Number	Heat Flux (W/cm^2)	LMTD (°C)	Colburn Factor	Pressure Drop (kPa)	Friction Factor
W6-60-7	WATER	61.7	3	2386	6.81	6.2	0.00386	5.9	0.0465
W6-60-8	WATER	63.5	3	1006	5.45	6.3	0.00621	1.4	0.0625
W6-60-9	WATER	63.3	3	948	5.14	6.0	0.00655	1.3	0.0660
W6-60-10	WATER	62.7	3	1615	5.27	5.5	0.00452	3.3	0.0575
W6-60-11	WATER	61.5	3	1590	2.68	2.9	0.00430	3.3	0.0581
W6-60-12	WATER	61.9	3	893	2.83	3.3	0.00689	1.1	0.0640
W6-60-13	WATER	61.4	3	981	2.90	3.4	0.00612	1.4	0.0642
W6-60-14	WATER	63.9	3	525	3.09	3.6	0.0116	0.6	0.0992
W6-60-15	WATER	67.3	3	286	3.24	4.7	0.0153	0.3	0.165

Table E.7 Experimental Data for Plate 7

Run No.	Fluid Type	Aver. Fluid Temp. (°C)	Prandtl Number	Reynolds Number	Heat Flux (W/cm^2)	LMTD (°C)	Colburn Factor	Pressure Drop (kPa)	Friction Factor
P7-10-1	PAO	12.3	144	148	7.35	20.8	0.0147	28.4	0.201
P7-10-2	PAO	12.0	146	158	7.31	21.1	0.0133	30.7	0.185
P7-10-3	PAO	13.0	141	103	6.97	20.7	0.0199	18.7	0.286
P7-10-4	PAO	15.7	129	51	6.69	23.0	0.0345	6.6	0.500
P7-10-5	PAO	19.0	115	38	6.69	24.3	0.0457	3.7	0.656
P7-10-6	PAO	14.7	133	33	2.95	11.1	0.0480	3.9	0.689
P7-10-7	PAO	12.2	145	60	2.92	10.2	0.0277	11.1	0.473
P7-10-8	PAO	13.9	137	39	3.31	11.0	0.0467	4.8	0.560
P7-10-9	PAO	18.2	118	21	3.09	15.1	0.0576	1.8	0.998
P7-10-10	PAO	25.7	94	13	2.95	17.0	0.0810	0.7	1.58
P7-10-11	PAO	16.4	125	10	1.07	5.5	0.111	0.9	2.04
P7-10-12	PAO	12.8	142	19	1.09	4.9	0.0648	2.4	1.07
P7-20-1	PAO	23.2	101	223	7.33	20.6	0.0111	21.9	0.145
P7-20-2	PAO	22.9	102	236	7.34	21.0	0.0103	22.3	0.130

Run No.	Fluid Type	Aver. Fluid Temp. (°C)	Prandtl Number	Reynolds Number	Heat Flux (W/cm^2)	LMTD (°C)	Colburn Factor	Pressure Drop (kPa)	Friction Factor
P7-20-3	PAO	26.6	91	87	6.90	23.9	0.0227	6.4	0.343
P7-20-4	PAO	23.7	99	167	7.17	21.5	0.0138	15.4	0.189
P7-20-5	PAO	31.0	81	54	6.87	25.6	0.0347	2.8	0.510
P7-20-6	PAO	24.9	96	47	3.10	11.5	0.0378	3.3	0.553
P7-20-7	PAO	22.4	104	90	3.00	10.4	0.0210	8.6	0.331
P7-20-8	PAO	24.0	99	57	3.34	11.2	0.0353	4.0	0.439
P7-20-9	PAO	25.7	94	39	3.20	11.9	0.0463	2.5	0.633
P7-20-10	PAO	36.0	71	18	3.07	14.0	0.0857	0.6	1.33
P7-20-11	PAO	26.0	93	14	1.13	5.4	0.0979	0.8	1.72
P7-20-12	PAO	22.4	104	25	1.07	4.9	0.0533	2.0	0.989
P7-60-1	PAO	62.5	40	614	7.06	16.8	0.00708	11.3	0.0729
P7-60-2	PAO	62.3	40	655	7.25	17.3	0.00660	11.9	0.0669
P7-60-3	PAO	61.9	40	632	7.11	16.7	0.00699	11.9	0.0710
P7-60-4	PAO	64.1	39	437	6.98	17.9	0.00911	7.1	0.0968
P7-60-5	PAO	66.8	37	241	6.84	19.0	0.0151	3.1	0.158

Run No.	Fluid Type	Aver. Fluid Temp. (°C)	Prandtl Number	Reynolds Number	Heat Flux (W/cm^2)	LMTD (°C)	Colburn Factor	Pressure Drop (kPa)	Friction Factor
P7-60-6	PAO	71.4	34	142	7.03	21.4	0.0236	1.3	0.234
P7-60-7	PAO	64.5	38	121	3.05	9.2	0.0265	1.4	0.257
P7-60-8	PAO	62.2	40	249	2.88	7.9	0.0144	4.0	0.154
P7-60-9	PAO	63.0	39	180	3.48	10.2	0.0182	2.3	0.173
P7-60-10	PAO	67.1	37	115	3.30	10.1	0.0280	1.2	0.274
P7-60-11	PAO	77.0	30	43	3.18	12.0	0.0625	0.3	0.621
P7-60-12	PAO	65.3	38	34	1.16	4.5	0.0695	0.3	0.758
P7-60-13	PAO	63.1	39	75	1.10	3.6	0.0374	0.8	0.371
W7-10-1	WATER	14.5	8	321	6.95	9.7	0.0118	1.1	0.151
W7-10-2	WATER	12.8	8	549	7.13	8.9	0.00811	2.4	0.106
W7-10-3	WATER	12.2	8	759	7.20	8.5	0.00636	3.9	0.0876
W7-10-4	WATER	12.0	8	543	5.76	7.2	0.00820	2.4	0.104
W7-10-5	WATER	13.5	8	319	5.69	7.5	0.0128	1.2	0.153
W7-10-6	WATER	12.1	8	307	3.12	4.1	0.0130	1.1	0.154
W7-10-7	WATER	11.5	8	543	3.25	3.8	0.00882	2.5	0.104

Run No.	Fluid Type	Aver. Fluid Temp. (°C)	Prandtl Number	Reynolds Number	Heat Flux (W/cm^2)	LMTD (°C)	Colburn Factor	Pressure Drop (kPa)	Friction Factor
W7-10-8	WATER	13.4	8	76	1.11	1.8	0.0385	0.2	0.366
W7-10-9	WATER	14.4	8	163	3.11	4.3	0.0229	0.4	0.227
W7-20-1	WATER	25.0	6	366	6.82	8.4	0.0132	0.8	0.134
W7-20-2	WATER	23.0	6	676	7.26	8.1	0.00835	1.9	0.0834
W7-20-3	WATER	22.3	7	903	7.35	8.4	0.00599	2.7	0.0654
W7-20-4	WATER	22.7	6	631	5.70	6.1	0.00946	1.8	0.0916
W7-20-5	WATER	24.3	6	370	5.52	6.7	0.0131	0.9	0.132
W7-20-6	WATER	22.6	6	374	3.14	3.9	0.0125	0.9	0.126
W7-20-7	WATER	21.5	7	617	3.21	3.4	0.00970	1.9	0.0965
W7-20-8	WATER	28.0	6	111	3.11	4.6	0.0329	0.2	0.306
W7-20-9	WATER	24.5	6	214	3.13	4.5	0.0173	0.4	0.205
W7-20-10	WATER	22.6	6	380	3.07	3.6	0.0134	0.9	0.128
W7-60-1	WATER	63.1	3	1912	6.87	6.2	0.00500	2.4	0.0531
W7-60-2	WATER	63.8	3	1284	6.83	6.8	0.00628	1.3	0.0626
W7-60-3	WATER	65.4	3	719	6.63	7.8	0.00870	0.5	0.0855

Run No.	Fluid Type	Aver. Fluid Temp. (°C)	Prandtl Number	Reynolds Number	Heat Flux (W/cm^2)	LMTD (°C)	Colburn Factor	Pressure Drop (kPa)	Friction Factor
W7-60-4	WATER	63.8	3	714	5.37	6.2	0.00892	0.5	0.0871
W7-60-5	WATER	62.4	3	1231	5.48	5.5	0.00654	1.3	0.0681
W7-60-6	WATER	61.5	3	1223	2.92	2.8	0.00685	1.3	0.0669
W7-60-7	WATER	62.4	3	710	2.86	3.4	0.00859	0.6	0.0892
W7-60-8	WATER	62.4	3	773	3.01	3.4	0.00841	0.6	0.0829
W7-60-9	WATER	64.2	3	368	3.11	3.6	0.0174	0.3	0.161

REFERENCES

Bar-Cohen, A. 1985. "Thermal Management of Air and Liquid-Cooled Multi-Chip Modules." *Proceeding of Twenty-Third ACME/AIChE National Heat Transfer Conference*. Denver, Colorado, August 4-7, pp. 1-36.

Bergles, A.E. 1974. "Recent Developments in Convective Heat-Transfer Augmentation." *Applied Mechanics Reviews*. pp. 675-686.

Bergles, A.E., Blumenkrantz, R.R. and Taborek, J. 1974. "Performance Evaluation Criteria for Enhanced Heat Transfer Surfaces." *Proceeding of Fifth International Heat Transfer Conference*. Vol. 2, Paper FC6.3, pp. 239-243.

Blevins, R.D. 1984. *Applied Fluid Dynamics Handbook*, Van Nostrand Reinhold Co.

Briggs, D.C., and London, A. L. 1961. "The Heat Transfer and Flow Friction Characteristics of Five Offset Rectangular Duct and Six Plain Triangular Plate-fin Heat Transfer Surfaces." *International Developments in Heat Transfer*, ASME, New York, pp. 122-134.

Brinkmann, R., Ramadhyani, S. and Incropera, F.P. 1987. "Enhancement of Convective Heat Transfer From Small Heat Sources to Liquid Coolants Using Strip Fins." *Experimental Heat Transfer*, Vol. 1, pp. 315-330.

Chen, C.C., Loh, J.V. and Westwater, J.W. 1981. "Prediction of Boiling Heat Transfer Duty in a Compact Plate-Fin Heat Exchanger Using the Improved Local Assumption." *International Journal of Heat and Mass Transfer*, Vol. 24, No. 12, pp. 1907-1912.

Chen, C.C. and Westwater, J.W. 1983. "Application of the Local Assumption for the Design of Compact Heat Exchangers for Boiling Heat Transfer." *Proceeding of ASME-JSME Thermal Engineering Joint Conference*, Vol. 1, pp. 471-477.

Cowell, T.A. 1990. "A General Methods for the Comparison of Compact Heat Transfer Surfaces." *Transaction of ASME*, Vol. 112, pp. 288-294.

Curr, R.M., Sharma, D. and Tatchell, D.G. 1972. "Numerical Predictions of Some Three Dimensional Boundary Layers in Ducts." *Computer Methods in Applied Mechanics and Engineering*. Vol. 1, pp. 143-158.

Dubrovsky, E.V. and Vasiliev, V. YA. 1987. "Enhancement of Convective Heat Transfer in Rectangular Duct of Interrupted Surface." *International Journal of Heat and Mass Transfer.* Vol. 31, No.4, pp. 807-818.

Haselder, G.G. 1971. *Cryogenic Fundamentals*, Academic Press.

Hoerner S.F. 1965. *Fluid-Dynamic Drag*. Published by the author.

Hou, K.S. 1988. *Thermal Performance of Offset Strip Fins Under Unsymmetrical Heating Condition For Various Fluids*. Master Thesis. California State University.

Hu, S. and Herold, K.E. 1993. "Prandtl Number Effect on Offset Fin Heat Exchanger Performance: Experimental Results." Submitted to *International Journal of Heat and Mass Transfer.*

Hu, S. and Herold, K.E. 1993. "Prandtl Number Effect on Offset Fin Heat Exchanger Performance: Predictive Model for Heat Transfer and Pressure Drop." Submitted to *International Journal of Heat and Mass Transfer.*

Incropera F.P. and DeWitt D.P. 1990. *Fundamentals of Heat and Mass Transfer.* Third Edition. John Wiley & Sons.

Joshi, H.M. and Webb, R.L. 1987. "Heat Transfer and Friction in the Offset Strip-fin Heat Exchanger." *International Journal of Heat and Mass Transfer.* Vol. 30, No.1, pp. 69-84.

Joshi, H.M. 1984. *A Theoretical and Experimental Study of the Offset Strip-fin Heat Exchanger.* Ph.D Dissertation, University of Pennsylvania.

Kays, W.M. and London, A.L. 1950. "Heat Transfer and Flow Friction Characteristics of Some Compact Heat-Exchanger Surfaces, Part I, Test System and Procedure." *Transaction of ASME. Journal of Heat Transfer.* Vol. 72, pp. 1075-1085.

Kays, W.M. 1960. "The Basic Heat Transfer and Flow Friction Characteristics of Six Compact High-Performance Heat Transfer Surfaces." *Journal of Engineering for Power.* pp. 27-34.

Kays, W.M. 1972. *Compact Heat Exchanger.* AGRARD Lecture Series #57 on Heat Exchanger. AGRARD-LS-57-72.

Kays, W.M. and London, A.L. 1984. *Compact Heat Exchangers*. Third Edition, McGraw-Hill, New York.

Kelkar, K.M. and Patankar, S.V. 1989. "Numerical Prediction of Heat Transfer and Fluid in Rectangular Offset-fin Arrays." *Numerical Heat Transfer*. Part A, Vol. 15, pp. 149-164.

Kern, D.Q. and Kraus, A.D. 1972. *Extended Surface Heat Transfer*. McGraw-Hill, Inc. pp. 593-645.

Kline, S.L. 1985. "The Purposes of Uncertainty Analysis." *Journal of Fluid Engineering,* Vol. 107, pp. 153-164.

Kotz, J. 1991. *Chemistry & Chemical Reactivity*. Second Edition, Saunders College Publishing, Philadelphia.

Larkin, B.S. 1968. *ASME paper No. 68-WA/HT-23.*

LeVasseur, R. 1991. "Liquid Cooled Approaches For High Density Avionics." *Proceeding of IEEE/AIAA Tenth Digital Avionics Systems Conference*, pp. 147-152.

London, A.L. and Ferguson, C.K. 1949. "Test Results of High-Performance Heat-Exchanger Surfaces Used in Aircraft Intercooler and Their Significance for Gas-Turbine Regenerator Design" *Transaction of ASME*, Vol. 71, pp. 17-26.

London, A.L and Shah, R.K. 1968. "Offset Rectangular Plate-fin Surfaces - Heat Transfer and Flow Friction Characteristics." *Transaction of ASME*. July, pp. 218-228.

London, A.L. 1980. "A Brief History of Compact Heat Exchanger Technology." *Compact Heat Exchanger-History, Technological Advancement and Mechanical Design Problems, ASME, HTD-10,* New York, pp. 1-4.

Manglik, R.M. and Bergles, A.E. 1990. "The Thermal-Hydraulic Design of the Rectangular Offset-strip-fin Compact Heat Exchanger." *Compact Heat Exchangers*. Shah, R.K etc, pp. 123-149, Hemisphere Publishing Corporation.

Manson, S.V. 1950. "Correlations of Heat Transfer Data and of Friction Data for Interrupted Plane Fins Staggered in Successive Rows." *NACA Technical Note 2237.* National Advisory Committee for Aeronautics, Washington,D.C, December.

Marr, Y.N. 1990. "Correlating Data on Heat Transfer in Plate-Fin Heat Exchangers with Short Offset Fins." *Thermal Engineering*, Vol. 37, No. 5, pp. 249-252.

Mochizuki, S., Yagi, Y., Yang, W.J. 1988. "Flow Pattern and Turbulence Intensity in Stacks of Interrupted Parallel-plate Surfaces." *Experimental Thermal and Fluid Science.* Vol. 1, pp. 51-57.

Mochizuki, S., Yagi, Y. 1977. "Heat Transfer and Friction Characteristics of Strip Fins." *Japanese Research.* Vol. 6,, pp. 36-59.

Mochizuki, S., Yagi, Y. and Yang, W.J. 1987. "Transport Phenomena in Stacks of Interrupted Parallel-plate Surfaces." *Experimental Heat Transfer.* Vol. 1, pp. 127-140.

Moffat, R.J. 1988. "Describing the Uncertainties in Experiment Results." *Experimental Thermal and Fluid Science.* Vol. 1, pp. 257-271.

Montgomery, S.R. and Wilbulswas, P. 1967. "Laminar Flow Heat Transfer for Simultaneously Developing Velocity and Temperature Profiles in Ducts of Rectangular Cross Section." *Applied Science Research.* Vol. 18, pp. 247-259.

Mullisen, R.S. 1983. *Heat Transfer, Pressure Drop and Flow in Interrupted Wall Passages.* Ph.D Dissertation, Colorado State University.

Mullisen, R.S. and Loehrke, R.I. 1986. "A Study of the Flow Mechanism Responsible for Heat Transfer Enhancement in Interrupted-plate Heat Exchangers." *Transaction of ASME. Journal of Heat Transfer.* Vol. 108, pp. 375-385.

Norris, R.H. and Spofford, W.A. 1942. "High-Performance Fins for Heat Transfer." *Transaction of ASME. Journal of Heat Transfer.* Vol. 64, pp. 489-496.

Panitsidis, H., Gresham, R.D. and Westwater, J.W. 1975. "Boiling of Liquids in a Compact Plate-Fin Heat Exchanger." *International Journal of Heat and Mass Transfer*, Vol. 18, pp. 37-42.

Patankar, S.V. and Prakash, C. 1981. "An Analysis of the Effect of Plate Thickness on Laminar Flow and Heat Transfer in Interrupted-plate Passages." *International Journal of Heat Transfer*. Vol. 24, pp. 1801-1810.

Patankar, S.V. 1990. "Numerical Prediction of Flow and Heat Transfer in Compact Heat Exchanger Passages." *Compact Heat Exchangers*. Shah, R.K., Kraus, A.D., Metzger, D., Hemisphere Publishing Corporation, pp. 191-204.

Philips, R.J. 1988. " Forced-convection, Liquid-cooled, Microchannel Heat Sinks." *TR-787. Massachusetts Institute of Technology*.

Phillips, R.J., Glickman, L.R. and Larson, R. 1988. "Forced-convection, Liquid-cooled, Microchannel Heat Sinks for High-power-density Microelectronics." *Cooling Technology for Electronic Equipment*. Aung, W., Hemisphere Publishing.

Robertson, J.M. 1979. "Boiling Heat Transfer with Liquid Nitrogen in Brazed-Aluminum Plate-Fin Heat Exchangers." *AIChE. Symposium Series*, No. 189, pp. 151-164.

Robertson, J.M. 1982. "The Correlation of Boiling Coefficient in Plate-Fin Heat Exchanger Passages with a Film-Flow Model." *Proceeding of Seventh International Heat Transfer Conference*.

Robertson, J.M. 1983. "Boiling Heat Transfer with Freon 11 (R11) in Brazed-Aluminum Plate-Fin Heat Exchangers." *Journal of Heat Transfer*, Vol. 105, pp. 605-610.

Shah, R.K. 1964. "Data Reduction Procedures for the Determination of Convective Surfaces Heat Transfer and Flow Friction Characteristics-- Steam-to-Air Test Cores." *TR-64*. Department of Mechanical Engineering, Stanford University.

Shah, R.K. 1978. "Compact Heat Exchanger Surface Selection Methods." *Proceeding of Sixth International Heat Transfer Conference*. Toronto, Vol. 4, pp. 193-199.

Shah, R.K. and London, A.L. 1978. *Laminar Flow Forced Convection in Ducts - A Source Book for Compact Heat Exchanger Analytical Data*. Academic Press, Inc.

Shah, R.K. and London, A.L. 1980. "Effects of Nonuniform Passages on Compact Heat Exchanger Performance." *Journal of Engineering for Power*. Vol. 102, pp. 653-659.

Shah, R.K. 1990. "Brazing of Compact Heat Exchangers." *Compact Heat Exchangers*. Shah, R.K., Kraus, A.D., Metzger, D., Hemisphere Publishing Corporation, pp. 491-529.

Shah, R.K. and Webb, R.L. 1983. *Compact and Enhanced Heat Exchangers, Heat Exchangers - Theory and Practice*. Hemisphere Publishing Co.,1983.

Shih, T.M. 1990. "Literature Survey on Numerical Heat Transfer." *Numerical Heat Transfer*. Vol. 18, pp. 387-425.

Siebers, D.L., Schwind, R.G. and Moffat, R.J. 1982. "Experimental Mixed Convection from a Large, Vertical Plate in a Horizontal Flow." *Heat Transfer 1982*. Vol. 3, Hemisphere Publishing, Washington, D.C, pp. 447-482.

Sparrow, E.M., Baliga, B.R. and Patankar, S.V. 1977. "Heat Transfer and Fluid Flow Analysis of Interrupted-wall Channels with Application to Heat Exchangers." *Transaction of ASME. Journal of Heat Transfer*. Vol. 22, pp. 1613-1625.

Sparrow, E.M. and Liu,C.H. 1979. "Heat-transfer, Pressure-drop and Performance Relationships for In-line Staggered and Continuous Plate Heat Exchangers." *International Journal of Heat and Mass Transfer*. Vol. 22, pp. 1613-1625.

Sparrow, E.M. and Hajiloo, A. 1980. "Measurements of Heat Transfer and Pressure-drop for an Array of Staggered and Continuous Plate Heat Exchangers." *Transaction of ASME. Journal of Heat Transfer*, Vol. 102, pp. 426-432.

Suzuki, K., Hirai, E., Sato, T. and Kieda, S. 1982. "Numerical and Experimental Studies on a Two-dimensional Model of an Offset Strip-fin Type Compact Heat Exchanger Used at Low Reynolds Number." *International Journal of Heat and Mass Transfer*. Vol. 28, pp. 823-836.

Suzuki, K., Haira, E., Sato, T. and Mayake, T. 1985. "Numerical and

Experimental Studies on a Two-dimensional Model of an Offset-strip-fin Type Compact Heat Exchanger Used at Low Reynolds Number." *International Journal of Heat and Mass Transfer*, Vol. 28, No. 4, pp. 823-836.

Tuckerman, D.B. 1984. *Heat-Transfer Microstructures for Integrated Circuits*. Ph.D dissertation, Stanford University.

Walter, F.M. 1969. "Hypersonic Research Engine Project - Phase IIA, Catalog I Test Report on Fin Heat Exchanger and Pressure Drop Testing." *Data Item No.63.02*. AirResearch Manufacturing Co., Document No.AP-69-5348.

Wieting, A.R. 1975. "Empirical Correlations for Heat Transfer and Flow Friction Characteristics of Rectangular Offset-fin Plate-fin Heat Exchangers." *Transaction of ASME. Journal of Heat Transfer*. Vol. 97, pp. 488-490.

Xi, G.N. and Suzuki, M. 1988. "A Flow Visualization Experiment on the Instability of Wakes for Performance Study of Compact Heat Exchangers." *Second International Symposium on Heat Transfer*. Beijing, pp. 651-656.

Xi, G., Futagami, S. and Hegira, Y. 1991. "Flow and Heat Transfer Characteristics of Offset-fin Array in the Middle Reynolds Number Range." *ASME/JSME Thermal Engineering Proceedings*. Vol. 3, pp. 151-156.

Yung, D., Lorenz, J.J. and Panchal, C. 1980. "Convective Vaporization and Condensation in Serrated-Fin Channels." *Heat Transfer in Ocean Thermal Energy Conversion (OTEC) Systems*, ASME, HTD-Vol.12, pp. 29-37.

Related Literature

Adarkar, D.B. and Kays, W.M. 1963. "Heat Transfer in Wakes." *Technical Report No.55*. Dept. of Mechanical Engineering, Stanford University.

Barrow, H. 1986. "On Average Heat Transfer Coefficient." *International Journal of Heat and Fluid Flow*. Vol.7, No. 3, pp. 162-163.

Baker, E. 1972. "Liquid Cooling of Microelectronic Devices by Free and Forced Convection." *Microelectronic and Reliability*. Vol. 11, pp. 213-222.

Chung, B.T.F. , Pang, Y. , Thomas, L.C. 1982. "Viscous Dissipation Effects on Heat Transfer from Turbulent Flow with High Prandtl Number Fluids." *Heat Transfer 1982*. Vol. 3, Hemisphere Publishing, Washington D.C., pp. 235-240.

Cur, N. and Sparrow, E.M. 1979. "Measurements of Developing and Fully Developed Heat Transfer Coefficients along a Periodically Interrupted Surface." *Transaction of ASME Journal of Heat Transfer*. Vol. 101, pp. 211-216.

Kottke, V. 1982. "Influence of Temperature and Concentration Boundary Layers at Separation on Heat and Mass Transfer In Separated Flows." *Heat Transfer 1982*. Vol. 3, Hemisphere Publishing, Washington D.C.

Kraus, A.D., Snider, A.D. and Landis, F. 1982. "The Reciprocity of Extended Surface and the Node Analysis of Finned Arrays." *Heat Transfer 1982*. Vol. 6, Hemisphere Publishing, Washington D.C.

Loehrke, R.I. and Lane, J.C. 1982. "Flow Through an Array of Interrupted Parallel Plates." *Heat Transfer 1982*. Vol. 3, Hemisphere Publishing, Washington D.C.

Mercer, W.E., Pearce, W.M. and Hitchcock, J.E. 1967. "Laminar Forced Convection in the Entrance Region between Parallel Plates." *Journal of Heat Transfer*, Vol. 89C, pp. 251-257.

Metzger, D.E., Fan, C.S. and Yu, Y. 1990. "Effect of Rib Angle and Orientation on Local Heat Transfer in Square Channels with Angled Roughness Ribs." *Compact Heat Exchangers*. Shah, R.K., Kraus, A.D., Metzger, D., Hemisphere Publishing Corporation, Washington D.C.

Metzger, D.E., Cummings, K.N. and Ruby, W.A. 1982. "Effect of Prandtl Number on Heat Transfer Characteristics of Impinging Liquid Jets." *Heat Transfer 1982*. Vol. 3, Hemisphere Publishing, Washington D.C..

Metzger, D.E., Berry, R.A. and Bronson, J.P. 1982. "Developing Heat Transfer in Rectangular Ducts with Staggered Arrays of Short Pin Fins." *Transaction of ASME*. Vol. 104, pp. 700-706.

Mullisen, R.S. and Loehrke, R.I. 1986. "A Transient Heat Exchanger Evaluation Test for Arbitrary Fluid Inlet Temperature Variation and Longitudinal Core Conduction." *Transaction of ASME. Journal of Heat Transfer*, Vol. 108, pp. 370-376.

Nho, K.M. and Yovanovich, M.M. 1990."Effect of Oxide Layers on Measured and Theoretical Contact Conductances in Finned-tube Heat Exchangers." *Compact Heat Exchangers*. Shah, R.K., Kraus, A.D., Metzger, D., Hemisphere Publishing, Washington D.C.

Prasad, B.S.V. 1991. "The Performance Prediction of Multistream Plate-fin Heat Exchangers Based on Stacking Pattern." *Heat Transfer Engineering*, Vol. 12, No.4, pp. 58-70.

Rannasinghe, J. and Rreistad, G.M. 1990. "Irreversibility in Heat Exchangers-Design and Optimization." *Compact Heat Exchangers*. Shah, R.K., Kraus, A.D., Metzger, D., Hemisphere Publishing Corporation.

Schmidt, F.W. and Newell, M.E. 1967. "Heat Transfer in Fully Developed Laminar Flow Through Rectangular and Isosceles Triangular Ducts." *International Journal of Heat Transfer*. Vol. 10, pp. 1121-1123.

Snider, A.D. and Kraus, A.D. 1982. "Correcting for the Variability of the Heat Transfer Coefficient in Extended Surface Analysis." *Heat Transfer 1982*. Vol. 6, Hemisphere Publishing, Washington D.C.

Webb, R.L. and Joshi, H.M. 1982. "A Friction Factor Correlation for the Offset Strip-fin Matrix." *Heat Transfer 1982*. Vol. 6, Hemisphere Publishing, Washington,D.C.

Webb, R.L. and Jung, S.H. 1992. "Air-side Performance of Enhanced Brazed Aluminum Heat Exchangers." paper from *ASHRAE annual meeting*, Baltimore, June-July, 1992.

Witte, L.C. 1990. "Characterization of Heat Exchangers Using Second Law Concepts." *Compact Heat Exchangers*. Shah, R.K. etc, Hemisphere Publishing.

Xin, R.C. and Tao, W.Q. 1988. "Experimental Study of Heat Transfer and Pressure Drop in Developing and Developed Regions of Wavy Channels." *Second International Symposium on Heat Transfer*. Beijing, pp. 657-663.

Yang, W.J. 1983. "Forced Convective Heat Transfer in Interrupted Compact Surfaces." *Proceeding of 1983 ASME-JSME Thermal Engineering Joint Conference.*, pp. 105-111.

Zariffeh, E.K., Soliman, H.M. and Trupp, A.C. 1982. "The Combined Effects of Wall and Fluid Axial Conduction on Laminar Heat Transfer in Circular Tubes." *Heat Transfer 1982*. Vol. 3, Hemisphere Publishing, Washington D.C., pp. 131-136.

Zelenka, R.L. and Loehrke, R.I. 1982. "Heat Transfer from Interrupted Plates." *Transaction of ASME. Journal of Heat Transfer*. Vol. 105, pp. 172-177.

Zhang, H.Y.,Ebadian, M.A. and Campo, A. 1991. "An Analytical/numerical Solution of Convective Heat Transfer in the Thermal Entrance Region of Irregular Ducts." *International Communication of Heat and Mass Transfer*. Vol. 18, pp. 273-291.